UNIVERSITY OF ALBERTA

Climatology of sounding parameters identifying the potential for convective storm development over central Alberta

by

Neil Michael Taylor ©

A thesis submitted to the Faculty of Graduate Studies and Research in partial fulfillment of the requirements for the degree of Master of Science

Department of Earth and Atmospheric Sciences

Edmonton, Alberta

Fall 1999

National Library of Canada
Acquisitions and Bibliographic Services
395 Wellington Street
Ottawa ON K1A 0N4
Canada

Bibliothèque nationale du Canada
Acquisitions et services bibliographiques
395, rue Wellington
Ottawa ON K1A 0N4
Canada

Your file Votre référence

Our file Notre référence

The author has granted a non-exclusive licence allowing the National Library of Canada to reproduce, loan, distribute or sell copies of this thesis in microform, paper or electronic formats.

L'auteur a accordé une licence non exclusive permettant à la Bibliothèque nationale du Canada de reproduire, prêter, distribuer ou vendre des copies de cette thèse sous la forme de microfiche/film, de reproduction sur papier ou sur format électronique.

The author retains ownership of the copyright in this thesis. Neither the thesis nor substantial extracts from it may be printed or otherwise reproduced without the author's permission.

L'auteur conserve la propriété du droit d'auteur qui protège cette thèse. Ni la thèse ni des extraits substantiels de celle-ci ne doivent être imprimés ou autrement reproduits sans son autorisation.

0-612-47105-5

Canada

UNIVERSITY OF ALBERTA

LIBRARY RELEASE FORM

Name of Author: Neil Michael Taylor

Title of Thesis: Climatology of sounding parameters identifying the potential for convective storm development over central Alberta

Degree: Master of Science

Year this degree granted: 1999

Permission is hereby granted to the University of Alberta Library to reproduce single copies of this thesis and to lend or sell such copies for private, scholarly, or scientific research purposes only.

The author reserves all other publication and other rights in association with the copyright in the thesis, and except as hereinbefore provided, neither the thesis nor any substantial portion thereof may be printed or otherwise reproduced in any material form whatever without the author's prior written permission.

Neil Taylor

10912-B 75th Avenue
Edmonton, Alberta
T6G 0G9

27 Aug. 1999

University of Alberta

Faculty of Graduate Studies and Research

The undersigned certify that they have read, and recommend to the Faculty of Graduate Studies and Research for acceptance, a thesis entitled *Climatology of sounding parameters identifying the potential for convective storm development over central Alberta* submitted by Neil Michael Taylor in partial fulfillment of the requirements for the degree of Master of Science.

G. W. Reuter

G. W. Reuter

Edmund Lozowski

E. P. Lozowski

S. S. Shen

Approved: 17 August 1999

For my wife, for her love and understanding,
and my parents, who always made me believe I could succeed.

Abstract

A 31-year climatology (1966 to 1996) of convective sounding parameters is compiled for central Alberta using 4743 00Z soundings released from Stony Plain (53.5° N, 114.1° W). We analyse the intra-seasonal and inter-annual variability of Convective Available Potential Energy (CAPE), precipitable water (PW), wind shear (S), storm relative helicity (SRH), and other parameters. Parameter values differentiating between soundings associated with large hail (≥ 30mm) and small hail (< 30mm) are presented. Also, soundings associated with severe and non-severe weather days are compared. CAPE climatology results are compared with lightning and hail report climatological data.

During the summer, mean daily CAPE and PW exhibited little day-to-day variability compared to mean daily S and SRH. Surface temperature, tropospheric moisture, and CAPE all peaked in July. Optimal thermal conditions for storm development did not occur "in phase" with optimal shear conditions so that the period 1 July to 15 August was most conducive to severe convection. There was an increase in mean annual CAPE from 1966 to 1996.

More than 50% of days with hail ≥ 30mm had CAPE ≥ 500 Jkg^{-1} and PW ≥ 16mm. CAPE, PW and the energy helicity index were significantly higher for severe days compared to non-severe days. Days with numerous hail reports and larger hail size were associated with larger CAPE and stronger wind shear.

Acknowledgements

I would like to express my gratitude to the following people for their contributions to the completion of this thesis:

- Dr. Gerhard Reuter for his invaluable guidance and time spent editing revisions.
- Mr. Brian Crenna for sharing his knowledge of the world of computer programming and for his patience while doing so.
- Mr. Julian Brimelow for his useful suggestions while reading early drafts of this thesis.
- Mr. Terry Thompson and Mrs. Laura Smith for their assistance in gathering of data and resource materials.

Financial support for this research was provided by NSERC.

Table of Contents

		Page
1	Introduction	
	1.1 Background theory	1
	1.2 Alberta thunderstorm climatologies	2
	1.3 Sounding climatologies	5
	1.4 Thesis objectives	7
2	Data Base and Methods of Analysis	
	2.1 Data base for upper air sounding analysis	10
	2.2 Parameter calculation and significance for deep convection	10
	2.2.1 Convective available potential energy (CAPE)	11
	2.2.2 Precipitable water	14
	2.2.3 Bulk Richardson number	15
	2.2.4 Surface to 500mb vertical wind shear	17
	2.2.5 Storm relative helicity	19
	2.2.6 Energy helicity index	20
	2.3 Program output and analysis	21
	2.4 Sensitivity of sounding parameters to the input data	23
	2.4.1 Errors in radiosonde measurements	23
	2.4.2 Errors in sounding parameter calculations	23
	2.5 Summary	25
3	Thirty-one Year Summertime Climatology of Thermodynamic Sounding Parameters	
	3.1 Intra-seasonal variability of thermodynamic sounding parameters	26
	3.1.1 Maximum surface temperature	26
	3.1.2 Temperature lapse rate	27
	3.1.3 Moisture parameters	29
	3.1.4 Convective available potential energy	32
	3.2 Inter-annual variability of thermodynamic sounding parameters	34
	3.3 The effect of ENSO on CAPE	35
	3.4 Summary	36
4	Summertime Climatology of Wind Shear and Helicity	
	4.1 Surface to 500mb vertical wind shear	38
	4.2 Surface to 3km storm relative helicity	40
	4.3 Bulk Richardson number	42
	4.4 Summary	44

5 Hailstorms During 1990 to 1996

5.1 Large hail days and small hail days 46
5.2 Monthly distributions of SH and LH days 47
5.3 Mean parameter values and histogram distributions 48
5.4 Detection of LH days from 00Z sounding data 50
5.4.1 Evaluation of detection of LH days 50
5.4.2 Methodology 52
5.4.3 Results 52
5.5 Sounding parameter thresholds for small vs. large hail soundings 54
5.6 Summary 56

6 Severe Weather Soundings

6.1 10 Severe weather days from 1990 to 1996 57
6.2 The hailstorm of 16 June 1995 58
6.3 Comparison of severe (SVR) and non-severe (NSVR) soundings 59
6.4 Summary 61

7 Mean CAPE and Severe Weather Climatologies

7.1 Comparison with lightning observations in Alberta 62
7.2 Comparison with hail fall reports 63
7.3 Summary 65

8 Summary and Conclusions 67

References 71

Figures 80

Tables 120

List of Tables

Table		Page
5.6	Evaluation statistics for detection of Large Hail (LH) days using CAPE and Precipitable Water (PW) thresholds.	120
5.7	Evaluation statistics for detection of Large Hail (LH) days using CAPE, Precipitable Water (PW), and wind shear (S) thresholds.	121

List of Figures

Figure		Page
2.1	Tephigram for 00Z 17 June 1995 showing surface temperature (T), dewpoint (T_d), ambient temperature curve (T_a), parcel temperature curve (T_p), level of free convection (LFC) and equilibrium level (EL). The positive area under the pseudoadiabatic curve represents CAPE. The wind profile is given at right in kt.	80
2.2	Hodograph for 00 Z 17 June 1995 showing the storm motion vector ($\vec{c}$). The magnitude of the storm relative helicity in the lowest 3km is twice the shaded area. Wind speeds are in ms^{-1}.	81
2.3	Contours of CAPE for the sensitivity test for 00Z 17 June 1995. Temperature and dewpoint have been varied by 1°C about the control values (T=23.4°C and T_d=15.4°C) in 0.5°C intervals. Approximately equal changes in CAPE occur for variations of 1°C and 2°C in temperature and dewpoint respectively, i.e., CAPE is increased by ~200 Jkg^{-1} and ~400 Jkg^{-1} for 1°C changes in temperature and dewpoint respectively.	82
2.4	Same as for 2.3 except contours of precipitable water. The dashed line is the axis of asymmetry described in the text. For T and T_d higher than the control values, PW is only sensitive to changes in T_d. For T and T_d less than the control values PW is nearly equally dependent on changes in T and T_d.	83
3.1	31-year average sounding parameter value as a function of the day of the summer season (1 May to 30 September). Lapse rate refers to the ΔT_{500} data. The smooth curve is a sixth-order polynomial fitted to the data. The stippled line indicates the peak of the smooth curve.	84
3.2	Monthly histogram distributions of precipitable water for 1 May to 30 September 1966 to 1996.	85
3.3	Monthly histogram distributions of CAPE for 1 May to 30 September 1966 to 1996.	86
3.4	Plot of daily CAPE (Jkg^{-1}) for 1966 to 1996.	87
3.5	Surface plot of T_{max} (°C) for 1966 to 1991.	88
3.6	Surface plot of T_d (°C) for 1966 to 1996.	88
3.7	Plot of daily precipitable water higher than 15 mm for the years 1966 to 1996.	89

3.8	Non-weighted ($\langle CAPE \rangle_{NW}$) and weighted ($\langle CAPE \rangle_{W}$) mean annual CAPE for the years 1966 to 1996. The dashed and solid lines represent the linear regression applied to the $\langle CAPE \rangle_{NW}$ and $\langle CAPE \rangle_{W}$ data respectively.	90
3.9	Non-weighted mean annual CAPE ($\langle CAPE \rangle_{NW}$) for El Niño (grey), La Niña (black), and neutral (white) ENSO years respectively.	90
3.10	Histogram distributions for CAPE by ENSO year from 1966 to 1996 (1 May to 30 September). The average CAPE value for each distribution is shown in the upper right corner.	91
4.1	31-year average sounding parameter value as a function of the day of the summer season (1 May to 30 September). The smooth curve is a sixth-order polynomial fitted to the data.	92
4.2	Monthly histogram distributions of SFC to 500mb mean wind shear.	93
4.3	Monthly histogram distributions of SFC to 3km storm relative helicity.	94
4.4	31-year average bulk Richardson number and CAPE for soundings with CAPE $\geq$ 500 Jkg^{-1}. The stippled line indicates the peak of the smooth curve.	95
4.5	Histogram of bulk Richardson number according to storm type based on 119 mean daily R values with CAPE $\geq$ 500 Jkg^{-1}.	95
4.6	Monthly histogram distributions of bulk Richardson number.	96
5.1	Average of daily CAPE for each month from 1990 to 1996.	97
5.2	Percent occurrence of Small Hail (SH) and Large Hail (LH) days by month from 1990 to 1996.	97
5.3	Histograms of surface temperature and dewpoint, precipitable water, and CAPE for 45 small hail (left column) and 54 large hail (right column) days from 1990 to 1996.	98
5.4	Histograms of mean wind shear, storm relative helicity, bulk Richardson number, and energy helicity index for 45 small hail (left column) and 54 large hail (right column) days from 1990 to 1996.	99
5.5	POD, FAR, and CSI (in percent) for different CAPE threshold values.	100
5.6	Histogram showing the percent of 99 Small Hail (SH) and Large Hail (LH) severe days detected using each CAPE threshold.	100

5.7	Histogram showing the distribution of precipitable water for Small Hail (SH) and Large Hail (LH) days for each CAPE threshold.	101
5.8	Same as Fig. 5.7 but for mean wind shear.	101
5.9	Scatter plot of CAPE and surface temperature for Small Hail (SH) and Large Hail (LH) days from 1990 to 1996 (Top). Below are plots of the same data set separated into SH and LH days for CAPE ≥ 500 Jkg^{-1}.	102
5.10	Same as 5.9 but for CAPE and surface dewpoint.	103
5.11	Same as 5.9 but for CAPE and precipitable water.	104
5.12	Same as 5.9 but for CAPE and mean wind shear.	105
5.13	Same as 5.9 but for CAPE and storm relative helicity. The SRH axis is changed in the lower two figures to increase resolution.	106
5.14	Same as 5.9 but for CAPE and bulk Richardson number derived storm type as indicated on the plots for supercell (10-50), multicell (50-350) and air mass (>350) thunderstorms. The bulk Richardson number axis is changed in the lower two figures to increase resolution.	107
5.15	Same as 5.9 but for CAPE and energy helicity index.	108
5.16	Histograms of surface temperature and dewpoint, precipitable water, and CAPE for Small Hail (SH) and Large Hail (LH) days with CAPE ≥ 500 Jkg^{-1} during 1990 to 1996.	109
5.17	Histograms of mean wind shear, storm relative helicity, bulk Richardson number derived storm type and energy helicity index for Small Hail (SH) and Large Hail (LH) days with CAPE ≥ 500 Jkg^{-1} during 1990 to 1996.	110
6.1	Histograms of temperature, dewpoint, precipitable water, and CAPE for severe (SVR) and non-severe (NSVR) days from 1990 to 1996.	111
6.2	Histograms of wind shear, storm relative helicity, bulk Richardson number and energy helicity index for severe (SVR) and non- severe (NSVR) days from 1990 to 1996.	112
6.3	Histogram of bulk Richardson number-derived storm type for severe (SVR) and non-severe (NSVR) days from 1990 to 1996.	113

7.1 (a) Distribution of the number of cloud to ground (CG) lightning strikes from 1984 to 1995 in Alberta. (b) Number of days with CAPE ≥ 500 Jkg^{-1} for Stony Plain soundings during the same period and, (c) Number of days exceeding CAPE thresholds (500 Jkg^{-1}, 750 Jkg^{-1}, and 1000 Jkg^{-1}) and number of CG strikes as percent occurrence. 114

7.2 Daily CAPE from Stony Plain soundings from 1 June to 31 August for the years 1966 to 1985 (Top). Number of hail reports from Alberta Hail Project data for the same period (Bottom). 115

7.3 Scatter plot of CAPE and the number of hail reports (NR) for severe hail days (1 June to 31 August) during the Alberta Hail Project from 1966 to 1985 (Top). Scatter plot of maximum hail size category and the total number of hail reports for the same period (Bottom). 116

7.4 Histograms of maximum hail size category (Left) and CAPE (Right) for June (Top), July (Middle), and August (Bottom) using Alberta Hail Project data and Stony Plain soundings from 1966 to 1985. 117

7.5 Scatter plot of CAPE and mean wind shear for each hail size category for severe hail days (1 June to 31 August) with CAPE ≥ 500 Jkg^{-1} for the years 1966 to 1985. 118

7.6 Histogram distributions of CAPE (Left column) and mean wind shear (Right column) for each severe maximum hail size category as indicated on the CAPE histograms. The data is from the Alberta Hail Project from 1 June to 31 August for the years 1966 to 1985. 119

1. Introduction

Convective storms occur frequently in central Alberta during the summer months (Renick and Maxwell, 1977). Wojtiw (1975) reported that central Alberta is affected by hail on an average of 61 days in the summer and between 10 and 20 tornadoes are reported annually. Severe thunderstorms can produce large hail and tornadoes which damage personal and public property, leading to millions of dollars in insurance claims (Bullas and Wallace, 1988).

1.1 Background theory

The following conditions have generally been found to be associated with the occurrence of severe convection in Alberta (Smith and Yau 1993a):

1. A large amount of latent energy (i.e., moisture).
2. Strong convective instability (i.e., Convective Available Potential Energy or CAPE).
3. Large vertical shear of the horizontal wind.
4. A triggering mechanism capable of releasing the latent energy.

Forecasting of severe convection in Alberta generally involves identifying conditions 1, 2, and 3 through synoptic data analysis and the use of numerical weather prediction model output. If the potential threat of severe weather exists, condition 4 is determined through empirical methods (e.g., Miller, 1972) and experience.

Large values of latent energy and convective instability often result from the capping of warm, moist, boundary layer air with a deep layer of cool dry air exhibiting a steep environmental lapse rate (Smith and Yau, 1993a). This stratification allows air lifted from the surface to be highly buoyant relative to the ambient air. Tropospheric moisture is quantified by precipitable water (PW), defined as the mass of water vapour in a vertical column of air having unit cross-sectional area. The energy available for vertical motion is determined by CAPE, which represents the "positive area" on a tephigram, bounded by the pseudoadiabatic curve and the

ambient temperature profile. Formal definitions and equations for PW and CAPE are presented in Chapter 2.

Vertical shear of the horizontal winds act to intensify and prolong convective storm circulations. This is accomplished by tilting the updraft, thus preventing precipitation that forms in the updraft from falling through it, and by inducing perturbation pressure forces that favour the right flank of the storm as a preferred region for new growth (Newton, 1963; Fankhauser, 1971; Rotunno and Klemp, 1982). Chisholm and Renick (1972) developed composite hodographs for Alberta thunderstorms showing single-, multi-, and supercell storms to be characterized by light winds with little shear; moderate unidirectional shear; and strong shear concentrated at low levels in the troposphere, respectively. Such observations and modelling studies (e.g., Weisman and Klemp, 1982, 1984) suggest that vertical wind shear largely determines the form that convective storms may take. Weisman and Klemp (1986) describe how interactions between storm updrafts and wind shear can result in the long-lived, quasi-steady, storm structure associated with supercell storms.

In a general sense, the goal of this research is to determine the climatological variability of the first three necessary conditions for the occurrence of severe convection in central Alberta (i.e., PW, CAPE, and wind shear). A brief review of past studies will allow us to focus our research objectives considerably.

1.2 Alberta thunderstorm climatologies

Early Canadian thunderstorm climatologies concentrated on Alberta hailstorms. Most of the data for these studies were collected during the Alberta Hail Studies Project (ALHAS) from 1957 to 1973 and the Alberta Hail Project (AHP) from 1974 to 1985. Radiosonde ascents, radar observations, hail size measurements, and hail surveys were conducted during these periods. Douglas and Hitschfeld (1958) used radar observations from 83 thunderstorms to relate the probability of hail fall to maximum echo tops. Longley and Thompson (1965) used hail observations and upper air data from 1959 to 1963 to construct composite 850mb and 500mb charts

representative of major, minor, and no hail events. The mean maps for major hail days suggest the presence of a surface closed low over southern Alberta and an upper level trough upstream of the event.

Using six years of radiosonde and radar data, Chisholm and Renick (1972) proposed idealized models of radar structure according to storm type. This resulted in airflow models and representative hodographs for single-, multi-, and supercell storms. Ranges in CAPE and wind shear for each storm type were also determined. Chisholm (1973) used a one-dimensional loaded moist adiabatic numerical model to compute various sounding-derived parameters for 29 Alberta hailstorms. CAPE, maximum storm height, maximum updraft velocity and maximum cloud liquid water content were related to the maximum observed hail size at the surface.

The ALHAS data were summarized by Wojtiw (1975). He compiled a hailfall climatology for central Alberta that showed an average of 61.3 hail days occured each summer season. Of these, 33% of summer hail days occurred in July. Using sounding data and a modified version of Chisholm's model, Renick and Maxwell (1977) produced a nomogram intended as a forecasting aid in predicting maximum hail size. The nomogram was compiled from 210 hail days from the years 1969 to 1973 and relates CAPE and in-cloud temperature with maximum observed hail size at the surface.

Strong (1986) and Smith and Yau (1993b) found that severe hailstorms often form as a result of interactions between the mountain-plain mesoscale circulation and synoptic-scale flow. Smith and Yau used case studies of 11 hail days to formulate a conceptual model for deep convection over central Alberta. The model was then substantiated using climatological hailfall data from the Alberta Hail Project. They found that hail days made up 54% of all summer days with 9% of these associated with > 150 hail reports. An upstream 500mb trough was associated with 97% of the days with >150 reports. This association of an upper trough with severe hail events supports the results of Longley and Thompson (1965) and Strong (1986).

The ALHAS and AHP hail data sets show significant yearly and daily variability in the number of hail reports. More hail occurred during the period 1967 to

1972 than 1973 to 1985 with the most hail reports occurring in the last half of July (Smith et al., 1998). Furthermore, hail days were not isolated events but were episodic in nature. Defining a hail episode as more than one day with at least one hail report, Smith et al. (1998) found that Alberta is subject to ~18 hail episodes each summer. Of these, ~7 had at least one report of hail diameter ≥ 33mm (severe episode) and ~11 had no reports of hail ≥ 33mm (non-severe episode). The duration of the severe episodes was at least twice as long as the non-severe episodes. The longer duration of the severe episodes was attributed to the synoptic flow determining the potential for deep convection as an upper trough associated with major hail events takes at least 2-3 days to pass over Alberta.

Paruk and Blackwell (1994) studied population distribution effects on thunderstorm counts for a spatial climatology of Alberta storm events. For the years 1982 to 1991, severe thunderstorm events were compared to population density data from the 1991 census. The uncorrected severe weather report contour map showed a high correlation with population distribution and major transportation corridors (e.g., highways). By normalizing the number of reported events to annual occurrences per unit area and factoring in population density, corrected severe weather contour maps were constructed. The corrected maps showed the maxima in the number of severe weather reports occurred away from major population centers while the maps maintained a high storm density coincident with prevailing storm tracks.

Lightning strike frequency has been linked to soundings with positive CAPE (Rasmussen and Blanchard, 1998). Kozak (1998) compiled a climatology of spatial and temporal distributions of cloud-to-ground lightning strikes in Alberta for the years 1984 to 1995. July had the highest frequency of lightning strikes of the summer months. The diurnal cycle showed a peak in lightning frequency at 1900 MDT. Most lightning was found to occur in western Alberta with combined effects of topography, vegetation evapotranspiration, slope of elevation, and latitude influencing the average spatial distribution of lightning strikes.

1.3 Sounding climatologies

Early sounding climatology studies involved the use of proximity soundings, which are soundings with thermodynamic and wind profiles representative of the environment in which a thunderstorm develops. These proximity soundings were analyzed for environments conducive to tornado formation. Fawbush and Miller (1952) identified 75 soundings that produced tornadoes in the continental United States from 1948 to 1952. They constructed mean soundings using averaged pressure level data to develop composite thermodynamic profiles associated with tornadic storms. This work was expanded upon in 1954 when Fawbush and Miller extended the data set to include 286 soundings from 1948 to 1954. In this latter study, Fawbush and Miller proposed 3 different types of air masses associated with tornadoes. Sounding parameters describing thermodynamic instability (stability and dewpoint indices) were used explicitly in this study and median values of temperature and dewpoint were used to construct updated composite tephigrams. A similar study (Beebe, 1958) used 173 proximity soundings 6 to 12 hours prior to tornado formation to construct contour plots of Showalter Index and depth of the moist layer. The Showalter Index is defined as the difference between parcel temperature and environmental temperature at 500mb when a parcel is lifted from 850mb. The data showed that the greatest instability and deepest moist layers (~5000ft) were found south and south-southwest, respectively, of where the tornadoes subsequently developed.

Darkow and Fowler (1971) examined wind profiles associated with tornadoes. They used "pairs" of soundings from neighbouring radiosonde sites for 45 tornadoes to show that the tornadic environments had stronger wind shear from 1km to 3km above ground level and stronger veering of the winds between 1km and 5km. Environmental winds associated with tornado development were also studied by Maddox (1976) using 159 proximity soundings. From soundings taken in the air mass in front of the thunderstorm, he calculated mean winds and the Total Totals (TT) Index (a measure of thermodynamic instability). The monthly variability in TT and mean wind speed was presented showing a peak in TT (~55) during May and the highest mean wind speeds (~60 kt) in February.

With the advent of faster computers, climatology studies began using vertically integrated sounding parameters (e.g., CAPE) rather than stability indices. Bluestein and Parks (1983) compared 13 supercell storms with low precipitation to 9 storms with higher precipitation. They used a wider variety of sounding parameters to compare the moisture, instability, and vertical wind shear characteristics between the two storm classes. These included CAPE, mean wind shear, and precipitable water. Rasmussen and Wilhelmson (1983) used 25 soundings associated with thunderstorms in a climatological study. Classifying the storms into tornadic, non-tornadic (with mesocyclone), and non-mesocyclone types, they investigated CAPE and mean wind shear values differentiating between each storm type. It was found that tornadic storms occurred in a high CAPE and strong wind shear regime. Classification of 40 severe (tornado and/or hail $\geq$ 20mm) and 44 non-severe squall lines using radar observations and a range of sounding parameters was documented by Bluestein and Jain (1985) and Bluestein et al. (1987). They found that the primary differences between severe and non-severe squall lines were due to differences in CAPE.

Curvature of the wind shear vector in the lowest few km above ground level (AGL) has been quantified using storm-relative helicity (see section 2.2.5 for definition). Davies-Jones et al. (1990) used storm relative helicity values from 28 soundings to differentiate between tornadoes of varying intensity. A data set of 242 soundings associated with tornadoes of intensity F2 (Fujita, 1971) and higher was compiled by Johns et al. (1990). This data set was used to investigate the effects of positive shear for warm (15 May to 31 August) and cold (1 November to 31 March) season tornadoes in the United States between 1980 and 1990. He confirmed, for both seasons, that strong wind shear and high CAPE was required for tornadic development. The same data set was used to investigate the role of storm relative helicity in tornado development for varying depths of the troposphere (Davies and Johns, 1993) and combined CAPE and storm relative helicity parameters (Johns et al., 1993). This latter study also investigated combinations of CAPE and other wind-derived sounding parameters including mean shear and bulk Richardson number shear (see section 2.2.3) related to tornado development. These 1993 studies found that tornadic storms often occurred with strong wind shear and weak CAPE, and vice versa. Also, the strongest wind shear for violent tornadoes was found at low levels

and the highest SRH was determined using the thickest depth of the troposphere (lowest 4km).

Recent sounding climatologies use a set of 6793 soundings compiled by Rasmussen and Blanchard (1998). The data set includes all available 00Z soundings from 1992 with non-zero CAPE for the continental United States. Markowski et al. (1998a) used this data set to emphasize the significance of wind shear in the lowest km of tornadic (>F1) supercell environments. This work was extended to include additional parameters (e.g., CAPE, storm relative helicity, bulk Richardson number) and combined CAPE and shear parameters to distinguish between tornadic and non-tornadic supercells (Rasmussen and Blanchard, 1998). The climatology of Rasmussen and Blanchard serves to provide a baseline climatology to later assess inter-annual variability in these parameters and to suggest climatological values for operational meteorologists.

1.4 Thesis objectives

This thesis focuses on summertime conditions conducive to deep convection in central Alberta. The main objectives of this thesis are:

- To document the intra-seasonal and inter-annual variability of selected convective sounding parameters, such as CAPE, precipitable water, wind shear and storm relative helicity. Also, to identify the period with soundings most conducive to severe storm development.
- To identify mean parameter values differentiating between severe and non-severe weather days, and to suggest threshold parameter values for potentially severe weather.
- To examine the relationship between CAPE and convective weather phenomena using lightning and hailfall climatological data.

To accomplish our first objective, selected thermodynamic and wind-derived sounding parameters are calculated for each 00Z sounding (1 May to 30 September) from Stony Plain for the years 1966 to 1996. The temporal evolution of the daily

climatological values and monthly distributions are determined. The inter-annual variability of selected thermodynamic parameters is examined by comparing daily parameter values and mean annual CAPE for each year. From the intra-seasonal variability results, the period during the summer with thermodynamic and wind profiles most likely to result in thunderstorm development is identified.

There are two main motivations for examining the sounding parameters without considering the actual events. First, there is little documentation of the variability of convective sounding parameters for Alberta. Sounding parameters are used in forecasting without climatological verification. It is desirable to assess the climatological occurrence of physically important parameters before they are proposed for use in operational meteorology (Rasmussen and Blanchard, 1998). The climatological results provide a context in which the operational meteorologist can determine whether parameter values are climatologically "large" or "small" for a given sounding. The second motivation is to provide the forecaster with reference parameter values. That is, for what parameter values (in central Alberta) should the forecaster become concerned about the threat for severe convection?

To fulfill our second objective, we examine mean parameter values and distributions for a number of days on which severe weather occurred in central Alberta. Sounding parameter values are identified that are associated with large hail (hailstone diameter $\geq$ 30mm). The skill of detecting these large hail events using threshold parameter values from 00Z soundings is evaluated. We compile a list of soundings representative of severe weather events that occurred within a specified domain (see section 5.1) encompassing Stony Plain for the summers of 1990 to 1996. The mean parameter values for severe weather days are compared with non-severe weather days. To address the third objective, we compare our climatology of CAPE with results from Alberta lightning (Kozak, 1998) and hailfall (Smith et al., 1998) climatologies.

The outline for the subsequent chapters is as follows: in Chapter 2 we describe the sounding database and parameter calculations used. The significance of the sounding parameters for severe convection is also discussed. Analysis techniques used in the climatological study are introduced and a brief discussion of

uncertainties associated with radiosonde measurements and sounding parameter calculations is presented. In Chapter 3 we present the 31-year climatology results for the thermodynamic sounding parameters. The climatology of wind profiles is dealt with in Chapter 4. In Chapter 5 we describe characteristics of soundings associated with severe hail days by comparing mean parameter values and distributions for large and small hail. The possibility of detecting large hail events from 00Z sounding data is examined and threshold parameter values for large hail events are suggested. In Chapter 6 we discuss a severe weather case day and compile a set of representative severe weather soundings. Parameter values for the severe soundings are compared with those of non-severe soundings. In Chapter 7 our climatology of CAPE is compared against lightning detection and hailfall data. We conclude in Chapter 8 with a summary of our results and conclusions.

2. Data Base and Methods of Analysis

Selected sounding parameters are reviewed to quantify thermodynamic and wind-related properties associated with deep convection. Also, analysis techniques for the climatological study are presented here. Finally, we briefly discuss uncertainties in radiosonde measurements and how these affect our analysis.

2.1 Data base for upper air sounding analysis

The database consists of daily 00Z soundings released from Stony Plain (53.55° N, 114.10° W). The period of analysis spans 1 May to 30 September for the years 1966 to 1996. The soundings were obtained from the National Climate Data Center (NCDC) CD ROM Radiosonde Data of North America. Soundings before 1966 were not considered, as they were not readily available from the NCDC data. The data set contains 4743 soundings, 46 of which had to be discarded due to insufficient data. To calculate the sounding parameters, a computer program was written using C++. The peak time of day for severe weather activity in central Alberta is ~1730 MDT (Vickers, 1997). It is reasonable to assume that the 00Z (1800 MDT) sounding is representative of most severe weather environments. While a few individual storms may be better represented by modification of the 12Z sounding through use of updated surface observations, the large number of soundings involved in the climatology makes this a laborious task not attempted here.

2.2 Parameter calculations and significance for deep convection

The soundings used in our analysis consist of both mandatory and significant pressure level data. The sounding parameters primarily used in our data analysis consist of the following:

- Convective Available Potential Energy (CAPE)
- Precipitable water (PW)

- Bulk Richardson number (R)
- SFC to 500mb mean wind shear (S)
- SFC to 3km storm relative helicity (SRH)
- Energy Helicity Index (EHI)

These parameters are defined below and the equations used to calculate them are presented. Some variables and calculations used are illustrated graphically using a tephigram and hodograph from 00Z 17 June 1995 in Figures 2.1 and 2.2 respectively. Sounding data at mandatory and significant levels have been linearly interpolated to 1mb intervals (e.g., Prosser and Foster, 1966). This allows for greater accuracy in parcel temperature calculations and wind component values at specific heights above ground level (AGL). Parameter values associated with thunderstorm development are also discussed. While the sounding parameters are used to quantify the potential for thunderstorm development and likely storm type, they do not in themselves suggest whether or not convection will actually be triggered.

2.2.1 Convective available potential energy (CAPE)

Parcel theory of cloud convection suggests that CAPE (convective available potential energy; Moncrief and Green, 1972) is a necessary condition for deep convection (Danielsen, 1977). CAPE is the amount of buoyant energy available to an air parcel lifted from the surface and rising vertically through an undisturbed environment (Weisman and Klemp, 1986) and is given by (Djurić, 1994; p. 86):

$$CAPE = R \int_{LFC}^{EL} (T_p - T_e) d \ln p \qquad (2.1)$$

where T_p is the parcel temperature (K), T_e is the ambient temperature (K) and R=287.04 $Jkg^{-1}K^{-1}$ is the specific gas constant for dry air. The integration is performed from the pressure of the Level of Free Convection (LFC) to the pressure of the Equilibrium Level (EL) as indicated in Fig. 2.1. The LFC is the level at which T_p first becomes warmer than T_e and the EL is the level where T_p again becomes cooler

than T_a (Djurić, 1994; p. 82). The integration is illustrated in Fig 2.1 as being performed over the positive area under the pseudoadiabatic curve on a tephigram.

The level at which saturation (with respect to water) occurs in a parcel lifted from the surface is the Lifting Condensation Level (LCL). The temperature at the LCL in °C (t_{LCL}) can be approximated using the formula of Barnes (1968):

$$t_{LCL} \approx t_d - (0.001296 t_d + 0.1963)(t - t_d) \tag{2.2}$$

where t and t_d are the surface temperature and dewpoint (°C). Using the temperature at the LCL and the definition of potential temperature, the pressure at the LCL is given by:

$$p_{LCL} = p_{SFC}\left[\frac{(T_{LCL})}{(T_{SFC})}\right]^{\frac{c_p}{R}} \tag{2.3}$$

where p_{LCL} and p_{SFC} are the LCL and surface pressures expressed in Pa. T_{LCL} and T_{SFC} are the LCL and surface temperatures (K). c_p=1005 $Jkg^{-1}K^{-1}$ is the specific heat capacity of dry air at constant pressure. The LCL is often used to estimate the pressure level (and temperature) at which cumulus clouds will develop.

The parcel temperature is calculated between the surface and 100mb. Below the LCL the parcel temperature is calculated assuming a dry adiabatic process

$$\frac{dT}{dp} = \frac{RT}{pc_p}. \tag{2.4}$$

The parcel temperature T_p at a pressure level n+1 is determined by the parcel temperature at pressure level n (1mb below) using

$$T_{p_{n+1}} = T_{p_n}\left(\frac{p_{n+1}}{p_n}\right)^{\frac{R}{c_p}}. \tag{2.5}$$

Parcel ascent above the LCL is calculated assuming the pseudoadiabatic process

$$\frac{dT}{dp} = \frac{RT}{pc_p}\left(1+\frac{Lw_s}{RT}\right)\left(1+\frac{L^2\varepsilon w_s}{Rc_pT^2}\right)^{-1} \tag{2.6}$$

where, L is the specific latent heat of vapourization (L=2.49x10^6 Jkg^{-1}), w_s is the saturation mixing ratio (a function of T and p) and ε=0.622. The pseudoadiabatic parcel temperature (at pressure level n+1) is calculated by

$$T_{p_{n+1}} = T_{p_n}\left(\frac{p_{n+1}}{p_n}\right)^{\frac{R}{c_p}}\left\{\left(1+\frac{Lw_s}{RT_{p_n}}\right)\left(1+\frac{L^2\varepsilon w_s}{Rc_pT_{p_n}^2}\right)^{-1}\right\}. \tag{2.7}$$

T_a and T_p are evaluated at every mb pressure level. The buoyant energy for each layer is calculated and summed over the depth where T_p>T_a defined by the LFC and EL (Fig. 2.1). That is,

$$CAPE = R\sum_{i=n_{LFC}}^{n_{EL}}\left\{\left(T_{p_{i+1}}-T_{a_{i+1}}\right)\ln\left(\frac{p_{i+1}}{p_i}\right)\right\}. \tag{2.8}$$

Weisman and Klemp (1986) suggest that CAPE values from 1500 Jkg^{-1} to 2500 Jkg^{-1} are indicative of moderately unstable convective days. CAPE in excess of 2500 Jkg^{-1} indicates the potential for severe thunderstorms.

If pressure perturbation effects, water loading, and mixing are neglected, CAPE can be directly related to the maximum adiabatic vertical velocity $(w_{ad})_{max}$ attainable by an ascending parcel (Weisman and Klemp, 1986), i.e.,

$$\frac{1}{2}(w_{ad})_{max}^2 = CAPE. \tag{2.9}$$

Accounting for the hydrodynamic perturbation pressure gradient force, water loading, and entrainment reduces the estimated vertical velocity by ~50% (Weisman and Klemp, 1986) so that (2.9) may be expressed:

$$w_{max} = \frac{1}{2}(w_{cd})_{max} = \frac{1}{2}(2CAPE)^{\frac{1}{2}}. \tag{2.10}$$

This expression is used throughout the thesis to obtain a rough estimate of maximum updraft velocities from CAPE values computed from sounding data.

2.2.2 Precipitable water

Precipitable water is defined as the total mass of water vapour in a column of air with a cross-sectional area of 1m^2 (Djurić, 1994):

$$PW = \int_0^{\infty} q\rho dz = \frac{1}{g}\int_0^{p_s} q dp \tag{2.11}$$

where q is the specific humidity, ρ is the density of humid air, and p_o is the pressure at z=0. The specific humidity at a pressure level l (mandatory or significant level) is determined by $q_l = \varepsilon e_l / p_l$. The vapour pressure e_l is found by $e_l = 6.1\exp[0.073 t_{d_l}]$ (Djurić, 1994). Here, t_{d_l} is the dewpoint at mandatory and significant levels in °C. Most moisture in the troposphere is concentrated in the boundary layer, and dewpoint sounding data are often missing at upper levels, so we approximate PW with the following summation:

$$PW \approx \frac{1}{g}\sum_{j=0}^{l_{500}} \frac{1}{2}(q_j + q_{j+1})(p_{j+1} - p_j) \tag{2.12}$$

where l_{500} is the 500mb level and an average q is calculated from the q at the top and bottom of the layer.

Precipitable water gives an upper limit to the amount of water vapour in the troposphere available for latent heat release. PW is often expressed in units of mm of water depth (1kgm^{-2} of water is 1mm deep). Values of PW $\gtrsim$ 25mm are conducive to thunderstorm development in the southern United States (Djurić, 1994).

2.2.3 Bulk Richardson number

The bulk Richardson number for convective storms is defined by (Weisman and Klemp, 1982, 1984)

$$R = \frac{CAPE}{\frac{1}{2}\left(\overline{U}^2 + \overline{V}^2\right)}. \tag{2.13}$$

Here, $\overline{U}$ and $\overline{V}$ are the components of the difference between the pressure weighted SFC to 6km mean wind and the wind at 500m AGL (Weisman and Klemp, 1986). That is,

$$\overline{U} = \overline{u} - u_{500m}. \tag{2.14}$$

where the mean wind component $\overline{u}$ is calculated by

$$\overline{u} = \left[\sum_{g=0}^{n_{6k}} u\left(p_{g+1} - p_g\right)\right]\left[\sum_{g=0}^{n_{6k}}\left(p_{g+1} - p_g\right)\right]^{-1}. \tag{2.15}$$

Here, n_{6k} is the pressure level closest to 6km AGL. The wind component for each layer is multiplied by the change in pressure (1mb) and summed over the lowest 6km. This quantity is then divided by the total difference in pressure from the surface to 6km. The interpolated wind components with height closest to 500m are used for u_{500m} and v_{500m}.

The numerator in the bulk Richardson number (see 2.13) is a measure of potential updraft strength while the denominator may be interpreted as a measure of the inflow kinetic energy made available to the storm by the vertical wind shear (Weisman and Klemp, 1982). Converting CAPE to vertical kinetic energy using (2.9), the numerator may be expressed as $1/2(w_{ad})^2_{max}$ so that (2.13) becomes

$$R = \frac{\frac{1}{2}(w_{ad})^2_{max}}{\frac{1}{2}(\overline{U}^2 + \overline{V}^2)}. \qquad (2.16)$$

This is an expression of the ratio of the vertical to horizontal kinetic energy available to the storm. Convective storm type is strongly dependent on the ratio of these energies and therefore to the value of R (Weisman and Klemp, 1986). Increased environmental wind shear acts to tilt thunderstorm updrafts. Tilting of the updraft reduces the negative buoyancy effects caused by precipitation particles falling through the updraft as they are carried down-wind. This results in an extended updraft duration leading to a more organized, longer-lived storm. The bulk Richardson number has been used to classify storm type (e.g., Weisman and Klemp, 1982, 1984). The approximate ranges of R and associated storm type are given in Table 2.1.

Table 2.1: Bulk Richardson Number and associated storm type (adapted from Weisman and Klemp, 1986).

R	Storm Type
~10-50	Supercell
~50-350	Multicell
>350	Air-Mass

Problems with R corresponding to the actual severity of thunderstorms arise in either high CAPE and weak wind shear environments or vice versa. In these cases R may be in the supercell range when there is an insufficient amount of CAPE to complement the wind shear, or strong shear may inhibit convection from beginning altogether. In this thesis we adopt the approach of Weisman and Klemp (1986) of using R for cases where CAPE exceeds a minimum storm potential threshold. The

CAPE threshold used in our analysis is taken to be 500 Jkg^{-1} corresponding to a maximum updraft velocity (from 2.10) of w_{max}~16ms^{-1}.

2.2.4 Surface to 500mb vertical wind shear

The magnitude of the mean wind shear (S) from the surface to 500mb is defined as follows:

$$S = \frac{\int_0^{Z_{500}} \left[\left(\frac{\partial u}{\partial z} \right)^2 + \left(\frac{\partial v}{\partial z} \right)^2 \right]^{\frac{1}{2}} dz}{\int_0^{Z_{500}} dz} \tag{2.17}$$

Here, Z_{500} is the height AGL at 500mb and u and v represent the zonal and meridional wind components, respectively. The height AGL is interpolated at each 1mb level from the interpolated temperature values using the integrated form of the hydrostatic equation to determine the height at a pressure level n+1 from the height of pressure level n, 1mb below. That is,

$$z_{n+1} - z_n = \frac{RT_n}{g} \ln\left(\frac{p_n}{p_{n+1}} \right) \tag{2.18}$$

where T_n is the temperature (K) at pressure level p_n. The mean shear is approximated by

$$S = \left[\sum_{k=0}^{n_{500}} \left[\left(\frac{\partial u}{\partial z} \right)^2 + \left(\frac{\partial v}{\partial z} \right)^2 \right]_k^{\frac{1}{2}} (z_{k+1} - z_k) \right] \left[\sum_{k=0}^{n_{500}} (z_{k+1} - z_k) \right]^{-1} \tag{2.19}$$

Numerically, the changes in u and v are determined separately for each 1mb layer by dividing the difference in each component by the difference in heights at the

top and bottom of the layer. The magnitude of this vector is computed and multiplied by the difference in height between the top and bottom of the layer. These values are summed for all layers from the surface to 500mb and divided by the total height AGL at 500mb (Z_{500}). S is expressed in units of $ms^{-1}m^{-1}$ or s^{-1}.

Convection is greatly influenced by environmental wind shear. Cumulus cloud modelling studies indicate that severe thunderstorms form in strong wind shear environments with large CAPE (Weisman and Klemp, 1982, 1984). While strong shear may at first inhibit convection, it later enhances the separation of updrafts and downdrafts resulting in a quasi-steady, long-lived, intense thunderstorm often identified as a supercell (Browning, 1964; Lemon and Doswell, 1979).

In a strongly sheared environment with sufficient CAPE, tilting of streamwise vorticity into the vertical results in rotation on the flank of the updraft and a perturbation pressure deficit which is strongest several kilometers AGL (Rotunno, 1981; Davies-Jones, 1984). The resulting shear-induced pressure gradient promotes the quasi-steady supercell updraft and characteristic deviation from the mean wind (Rotunno and Klemp, 1982). The perturbation pressure deficit results from strong wind shear through the mid-levels of the storm ~4-6km AGL (Weisman and Klemp, 1986). The 500mb level is taken as the upper level for computing mean wind shear in order to use a consistent calculation for all the soundings. A pressure of 500mb corresponds to a height of 5574m in the ICAO standard atmosphere.

The wind shear between two heights is proportional to the horizontal gradient of the thickness of the layer. This results in the thermal wind shear equation (Holton, 1992)

$$\frac{\partial \vec{V}_g}{\partial z} = \frac{g}{fT}\hat{k} \times \vec{\nabla} T \qquad (2.20)$$

where $\vec{V}_g$ is the geostrophic wind vector and f is the coriolis parameter. This relation has importance for interpreting the climatological wind shear results in Chapter 4.

2.2.5 Storm relative helicity

Helicity is a measure of the potential for the formation of rotating upward air currents (Desautels and Verret, 1996). Storm relative helicity is defined as (Moller et al., 1994)

$$SRH \equiv -\int_{SFC}^{3km} \hat{k} \cdot (\vec{v} - \vec{c}) \times \left(\frac{\partial \vec{v}}{\partial z} \right) dz \qquad (2.21)$$

where $\hat{k}$ is the unit vector in the vertical, $\vec{v}$ is the horizontal wind vector and $\vec{c}$ is the storm motion vector (section 2.2.4).

The storm motion vector ($\vec{c}$) can be estimated from the sounding data by taking 75% of the magnitude of the surface to 6km pressure weighted mean wind and adding 30° to the direction (Maddox, 1976). This storm vector assumes that the resulting thunderstorm is a right-moving storm (Rotunno and Klemp, 1982), with its propagation direction deviating to the right of the mean wind. The magnitude of SRH is twice the area enclosed by the storm motion vector and the hodograph between the surface and 3km as illustrated in Fig. 2.2 (Davies-Jones et al., 1990).

For numerical calculation of SRH we use the approximation of Davies-Jones et al. (1990):

$$SRH = \sum_{m=0}^{m_{3k}-1} \left[(u_{m+1} - c_x)(v_m - c_y) - (u_m - c_x)(v_{m+1} - c_y) \right]. \qquad (2.22)$$

Here, u and v are the components of the environmental wind, and c_x and c_y are the zonal and meridional components of the storm motion vector. SRH is summed over each 1mb layer with m=0 representing the surface and m_{3k} representing the level corresponding to 3km AGL. SRH is expressed in units of m^2s^{-2}.

Storm relative helicity (SRH) has been found to be useful for forecasting mesocyclones (Lilly, 1986; Davies-Jones et al., 1990). As the most severe weather is

generally associated with supercells which always have mesocyclones, SRH is an indicator of potential severe storm severity.

The use of SRH in addition to S has some advantages in determining wind environments conducive to supercell development. While S is a useful ground-relative shear parameter it does not factor in storm motion (Davies, 1993). In addition, the integral form of SRH does not de-emphasize low-level shear magnitudes as the averaging of S may do (Davies, 1993). Values of SRH for weak, strong, and violent tornadoes (Davies-Jones et al., 1990) are summarized in Table 2.2. A complication in calculation of SRH is its dependence on the storm motion vector (as this is generally calculated from sounding data and not through observed storm motion). Temporal and spatial changes in helicity can cause additional uncertainty (Markowski et al., 1998b).

Table 2.2: SRH values for varying degrees of tornado intensity (Davies-Jones et al., 1990).

Tornado Intensity	Suggested SRH (m^2s^{-2})
Weak	150-299
Strong	300-449
Violent	> 450

2.2.6 Energy helicity index

An assessment of combined CAPE and SRH is possible through use of the EHI (Energy Helicity Index; Hart and Korotky, 1991). The EHI is useful to differentiate between high SRH environments with insufficient instability to promote deep convection and those with sufficient CAPE and hodograph curvature for supercell formation. The EHI (a dimensionless quantity) is calculated by the following (Davies, 1993):

$$EHI = \frac{CAPE \cdot SRH}{160000\, m^4 s^{-4}}. \qquad (2.23)$$

Values of EHI >1 are generally associated with tornadoes, while values >2.5 can be associated with violent tornadoes (Brooks et al., 1994). This parameter is used in Chapters 5 and 6 for severe weather sounding comparisons.

2.3 Program output and analysis

The sounding parameters are computed for each sounding and written to a separate file for each day. These data strings are then imported into a spreadsheet matrix containing 8 columns with 4697 rows. A sample line of the program output data is presented in Table 2.3. The data matrix is used to investigate climatological variability in the sounding parameters.

Table 2.3: Sample line of program output.

Sounding	T(°C)	T_d(°C)	PW(mm)	CAPE(Jkg^{-1})	S(s^{-1})	R	SRH(m^2s^{-2})
66071700	24	17	28.5	2758	0.00416	849	29.5

Intra-seasonal variability of the sounding parameters will be presented in Chapters 3 and 4. To examine daily variability, the output data are arranged in a spreadsheet so that the average parameter value for each day over the 31-year period is calculated. That is, $\bar{x}$, the mean daily value of sounding parameter x, is given by

$$\bar{x} = \frac{x_1 + x_2 + \ldots + x_{NP}}{NP} \tag{2.24}$$

where NP is the total number of parameter values for each particular day from the 31-year period (i.e., NP=31 unless a day is missing a sounding). The mean daily parameter values are plotted for each day of the summer season (1 May to 30 September). A smooth curve, $\langle x \rangle$, is fitted through the mean daily $\bar{x}$ data points using a sixth-order polynomial.

The monthly distributions of the parameter values are also examined in Chapters 3 and 4. Histogram analysis is applied to the data by month so that each monthly histogram includes all the days for that month from the 31-year period. For these histograms, bin ranges are selected to best capture the distributions. The data in each bin range are expressed as a percent occurrence. This is the percent of all the data used for the histogram that appears in each bin range. Percent occurrence is used to allow for comparison of sounding parameter data obtained from varying numbers of soundings. A mean monthly value is calculated for each parameter. As

an example, we consider the mean monthly CAPE, denoted by $CAPE_{MM}$. It is computed using

$$CAPE_{MM} = \frac{\left(\overline{CAPE}_1 + \overline{CAPE}_2 + ..\overline{CAPE}_{ND}\right)}{ND} \tag{2.25}$$

where ND is the number of days in the month and $\overline{CAPE}$ denotes the mean daily CAPE values.

In section 3.2, mean seasonal CAPE is calculated using a non-weighted approach and indicated by $\langle CAPE \rangle_{NW}$. This is an attempt to quantify the mean CAPE over the summer season including the sounding for each day. The non-weighted annual CAPE is calculated by taking the average of the mean monthly CAPE for each month from the total 31-years. That is,

$$\langle CAPE \rangle_{NW} = \frac{1}{5}\left(CAPE_{MM_{May}} + CAPE_{MM_{Jun}} + CAPE_{MM_{Jul}} + CAPE_{MM_{Aug}} + CAPE_{MM_{Sep}}\right). \tag{2.26}$$

July has more days with higher CAPE than any other month (Chapter 3) and could conceivably contribute more weight to the mean seasonal CAPE than the other months. To address this we also use a weighted calculation of mean seasonal CAPE denoted by $\langle CAPE \rangle_{W}$. The specific weighting scheme used is

$$\langle CAPE \rangle_{W} = \frac{1}{5}\left(\frac{0.1}{2.5}CAPE_{MM_{May}} + \frac{0.5}{2.5}CAPE_{MM_{Jun}} + \frac{1}{2.5}CAPE_{MM_{Jul}} + \frac{0.8}{2.5}CAPE_{MM_{Aug}} + \frac{0.1}{2.5}CAPE_{MM_{Sep}}\right) \tag{2.27}$$

thus the weight given to May and September are 1/10 that of July.

2.4 Sensitivity of sounding parameters to the input data

2.4.1 Errors in radiosonde measurements

Measurements of temperature, humidity, pressure and wind recorded by balloon radiosondes are always subject to errors. Estimations of root-mean square (rms) errors in radiosonde data have been reported by Sienkiewicz et al. (1981), Sackiw and Strong (1983), and Reuter and Aktary (1993). Some of the results of Sienkiewicz et al. (1981) are summarized in Table 2.4 below.

Table 2.4: Estimated rms errors in radiosonde measurements (adapted from Strong, 1986).

Measured Variable	rms Error
Temperature (°C)	0.5
Pressure (mb)	~1.0
Humidity (%)	10
Altitude (gpm)	10-50 (for pressures 500mb to 50mb)
Wind Speed (ms^{-1})	~1-8 (for pressures 700mb to 300mb)
Wind Direction (degrees)	1-18 (for pressures 700mb to 300mb)

2.4.2 Errors in sounding parameter calculations

The parcel temperature used in calculations of CAPE (section 2.2.1) is highly dependent on surface temperature (T) and moisture (T_d) values. Mueller et al. (1993) found that surface temperature and moisture can vary within an air mass by 3°C and 2.5°C in T and T_d, respectively, over a summer day along the Colorado front range. These variations affect CAPE and therefore, also the buoyancy-derived maximum updraft velocity.

Crook (1996) found that, for a non-convective case day, by varying the surface temperature (T) to 1°C lower and higher than the control value, the maximum vertical velocity was varied from ~3 ms^{-1} to ~26 ms^{-1}. In variations of the surface dewpoint (T_d) of 2.5°C above and below the control, w_{max} varied from ~21 ms^{-1} to ~30 ms^{-1}. On a day when convection occurred, the changes in w_{max} were ~3 ms^{-1} to ~21 ms^{-1} for the same variation in temperature and ~8 ms^{-1} to ~ 25 ms^{-1} for the same changes in surface moisture. Using (2.10), changes in CAPE are in the

range of 900-1000 Jkg^{-1} for total changes in surface T and T_d of 2°C and ~5°C respectively (a dewpoint variation of 2.5°C corresponds to a water vapour saturation mixing ratio variation of approximately 1 gkg^{-1}; Mueller et al., 1993). These case studies indicate that spatial and temporal uncertainty in surface temperatures and dewpoints can result in uncertainty in the intensity of convection (i.e., CAPE).

Precipitable water is highly dependent on boundary layer moisture, as this is where most of the tropospheric moisture is concentrated. While errors in moisture measurements may affect the calculated PW, any biases in the measurement will be applied to all soundings. The nature of the wind-derived sounding parameters is such that small errors in wind measurements are likely smoothed out for calculation of S and R. Storm relative helicity is a cumulative variable as the wind components are summed over the lowest 3km. This type of calculation may have increased uncertainty through cumulative errors but again we expect the same bias to be applied to all the wind data in the sounding.

We have conducted a sensitivity experiment for CAPE and precipitable water (PW) using the sounding of 16 June 1995 (Fig. 2.1). Using an interactive rawinsonde observation program (RAOB; Environmental Research Services, 1997), we have varied the surface temperature and dewpoint in 0.5°C increments to a total range of 1°C above and below the surface values reported in the sounding. With each change in temperature, RAOB mixes the ambient temperature curve dry adiabatically until the new curve intercepts the original curve. The new ambient temperature curve is then used to calculate CAPE. For changes in dewpoint, RAOB decreases (increases) the slope of the dewpoint curve between mandatory or significant levels for increases (decreases) in surface dewpoint and the new moisture profile is used for PW calculations. The results are presented in Figs. 2.3 and 2.4 as contour plots for CAPE and PW respectively. For CAPE we find that an increase in T of 1°C results in an increase in CAPE of ~200 Jkg^{-1} while the same increase in T_d results in a ~400 Jkg^{-1} increase in CAPE. CAPE varies in this experiment by ~1000 Jkg^{-1} (~1600 Jkg^{-1} to ~2600 Jkg^{-1}) with nearly equal changes in CAPE resulting from changes in T and T_d of 2°C and 1°C respectively.

The results for precipitable water are more dependent on the actual values of T and T_d. There is an "axis of asymmetry" in the contour plot between the maximum T and T_d values (see Fig.2.4). Above this axis, PW remains virtually unchanged for increases in T at constant T_d. Conversely, a 1°C increase in T_d at constant T increases PW by ~0.5mm. The exception is that PW does not decrease much below 28.0mm. Below the "axis of asymmetry" (i.e., lower left) there seems to be a one-to-one relationship for increases in T and T_d for 28.0mm < PW < 28.4mm. The space between the contours of 28.4mm and 28.5mm is likely a product of the moisture stratification of this particular sounding. For T and T_d higher than the control values, PW is only sensitive to changes in T_d. For T and T_d less than the control values, PW seems to be nearly equally dependent on changes in T and T_d.

While the data used in this thesis are susceptible to uncertainties in radiosonde measurements and the subsequent sounding parameter calculations, the nature of the research is such that small uncertainties in these values are likely not significant. Climatology results are based on averages and distributions from 31 years of sounding data for each day of the summer season. Uncertainties in the sounding data and calculations tend to be smoothed out through averaging of such a large data set.

2.5 Summary

The main data set for this thesis consists of daily 00Z soundings from Stony Plain, Alberta from 1 May to 30 September over the years 1966 to 1996. We have presented equations for computing CAPE, PW, R, S, SRH, and EHI. The significance of these parameters for severe convection was explained. The uncertainty of sounding parameters due to errors in radiosonde measurements has also been discussed.

3. Thirty-one Year Summertime Climatology of Thermodynamic Sounding Parameters

High values of CAPE are a necessary condition for deep convection (Danielsen, 1977). We examine the climatology of selected thermodynamic sounding parameters characteristic of the potential for deep convection. The analysis uses sounding data spanning 1 May to 30 September over the 31-year period 1966 to 1996. The intra-seasonal variability and implications for summertime convective weather are discussed. Also, the inter-annual variability of CAPE is examined relative to the El Niño Southern Oscillation (ENSO) cycle.

3.1 Intra-seasonal variability of thermodynamic sounding parameters

3.1.1 Maximum surface temperature

Figure 3.1 shows the mean daily value (average of the 31-year daily values) of selected parameters for the 153 summer days. The top graph shows the daily mean of the maximum surface temperature $\overline{T}_{max}$ at Stony Plain. The smooth curve $\langle T_{max} \rangle$ represents the "climatological" values of $\overline{T}_{max}$ using the method discussed in section 2.3. The stippled line intersecting the smooth curve indicates its peak value. Due to data not readily available, the T_{max} data result from the years 1966-1991 only. The use of T_{max} instead of the surface temperature at the time of the sounding associates increased thermodynamic instability with the highest observed surface temperatures.

The increase in $\langle T_{max} \rangle$ from 1 May is steepest in the first two weeks of May and reaches a peak value of ~24°C on 29 July. The increase in $\langle T_{max} \rangle$ varies from ~0.3°C day^{-1} for 1-15 May to ~0.07°C day^{-1} until ~12 July. The decrease in $\langle T_{max} \rangle$ after the peak is more rapid at ~0.1°C day^{-1} from 9 August to the end of the season. The statistics for $\overline{T}_{max}$ and $\langle T_{max} \rangle$ are listed in Table 3.1. The values of $\langle T_{max} \rangle$ increase to a maximum in July of ~22°C while September experiences the lowest $\langle T_{max} \rangle$ of

~14°C. The range of max/min values and standard deviation of $\overline{T}_{max}$ are smallest for June and July suggesting that daily variability of $\overline{T}_{max}$ is less during mid-summer than for spring and fall.

Table 3.1: Daily and seasonal statistics for T_{max} (all values in °C).

	Variability in $\overline{T}_{max}$				Variability in $\langle T_{max} \rangle$	
Month	**Max**	**Min**	**Mean**	**σ**	**Max**	**Min**
May	19.2	13.9	16.8	1.6	18.6	13.6
June	21.7	18.5	20.0	0.8	21.0	18.6
July	23.6	19.8	21.8	0.8	22.4	21.0
August	23.4	18.1	21.0	1.4	22.2	18.6
September	19.5	13.4	15.8	1.5	18.6	13.5

3.1.2 Temperature lapse rate

To quantify the "lapse rate" between the surface and 500mb, we compute $\overline{\Delta T}_{500} = \overline{T}_{max} - \overline{T}_{500}$, where $\overline{T}_{500}$ is the mean daily temperature at 500mb. This is the difference between the mean daily values of maximum temperature at the surface and the temperature at 500mb. As the troposphere is heated primarily from below through radiation and surface heating (Djurić, 1994; p. 1), diurnal and seasonal changes in T_{max} and T_{500} are not necessarily in phase. The $\overline{\Delta T}_{500}$ and $\langle \Delta T_{500} \rangle$ data are presented in Fig. 3.1.

Changes in ΔT_{500} do not follow the same cycle as T_{max} (Table 3.2). $\langle \Delta T_{500} \rangle$ values decrease for virtually the entire summer from a maximum of 38°C on 16 May to a minimum of ~33°C on 28 September. As with $\langle T_{max} \rangle$, the period of highest rate of decrease is the month of September with an approximate decrease of 1.9°C day^{-1}. The mean values of $\overline{\Delta T}_{500}$ remain relatively constant for the first three months (37°C to 38°C) before decreasing more significantly in July and August (36°C and 33°C respectively). The $\overline{\Delta T}_{500}$ data shows less daily variability than for $\overline{T}_{max}$ with the range in $\overline{\Delta T}_{500}$ values hovering around 3°C-4°C and σ<1°C indicating that no

particular month tends to be more variable in $\overline{\Delta T}_{500}$. Similarly, the range in $\langle \Delta T_{500} \rangle$ is only ~5°C for the five month period.

Table 3.2: Daily and seasonal statistics for ΔT_{500} (all values in °C).

	Variability in $\overline{\Delta T}_{500}$				Variability in $\langle \Delta T_{500} \rangle$	
Month	**Max**	**Min**	**Mean**	**σ**	**Max**	**Min**
May	39.3	35.2	37.9	0.8	38.0	37.5
June	39.1	35.6	37.4	0.8	37.8	37.2
July	38.3	34.9	37.2	0.7	37.2	36.8
August	37.8	33.7	35.9	0.8	36.8	34.7
September	35.6	31.7	33.4	0.9	34.7	32.8

Values of ΔT_{500} may be put in context by comparing our climatological results with ideal values indicative of thermodynamic instability from a tephigram. Using a surface pressure of 915mb (summertime surface pressures from 00Z soundings are generally around this value) and temperature values of 20°C and 30°C approximating the range of typical temperature maxima in the summer, we can determine values of ΔT_{500} representative of dry adiabatic and pseudoadiabatic processes. The dry adiabatic process lapse rate is ~0.01°Cm^{-1} while the pseudoadiabatic process corresponds to an approximate (non-linear) lapse rate of 0.007°Cm^{-1} (Djurić, 1994; p. 78). Lapse rates less than pseudoadiabatic and greater than dry adiabatic correspond to absolutely stable and unstable atmospheres, respectively. The results for the idealized values of ΔT_{500} are given in Table 3.3.

Table 3.3: Ideal values for dry adiabatic and pseudoadiabatic processes.

Air Parcel Lifting Process	ΔT_{500} for surface temperatures of 20°C and 30°C	
	20°C	30°C
Dry Adiabatic	46°C	48°C
Pseudoadiabatic	24°C	19°C

The mean values of $\overline{\Delta T}_{500}$ for the sounding data (Table 3.2) vary between ~33°C and ~38°C. A temperature profile having a lapse rate between dry adiabatic and pseudoadiabatic is indicative of a conditionally unstable troposphere (Rogers and Yau, 1996; p. 32). Thus, when compared to the ideal values for dry adiabatic

(~47°C) and pseudoadiabatic processes (~22°C), the mean values of $\overline{\Delta T}_{500}$ are consistent with a conditionally unstable troposphere throughout the entire summer season.

From the $\langle T_{max} \rangle$ data, the highest surface temperatures are observed on 29 July implying that maximum surface heating is experienced at this time. The $\langle \Delta T_{500} \rangle$ data show a maximum occurring on 16 May so that the optimum values for maximum thermal instability of these two parameters occur out of phase. However, the difference in $\langle \Delta T_{500} \rangle$ over the summer season is only ~5°C compared to a change in $\langle T_{max} \rangle$ of ~9°C. Thus, thermal instability seems to be influenced more by surface heating than cooling aloft. From these results, maximum thermal instability should coincide with the maximum surface heating at the end of July.

3.1.3 Moisture parameters

Water vapour condensing in a rising parcel of air releases latent energy serving to heat the air, thus increasing its buoyancy relative to the surrounding air. Tropospheric moisture both at the surface and in a column extending to 500mb AGL is quantified here by the surface dewpoint (T_d) and precipitable water (PW). The use of PW complements the surface moisture measurement as T_d disregards the thickness of the humid layer that is common in the lower troposphere (Djurić, 1994). A thick humid layer above the surface supplies more latent energy to thunderstorm updrafts than surface moisture alone, resulting in more vigorous convection and increased precipitation. The seasonal cycles of both T_d and PW are illustrated in Fig. 3.1 and the statistics for these curves appear in Tables 3.4 and 3.5. The smooth curves have similar attributes consistent with most tropospheric moisture being concentrated at low levels.

The moisture parameter curves have attributes similar to those of maximum surface temperature. The $\langle T_d \rangle$ data shows a steady increase in moisture of ~0.2°C day^{-1} from 1 May until 23 June. The curve has its peak of 10°C on 29 July and begins a near linear decrease on 21 August of ~0.2°C day^{-1}. Mean $\overline{T}_d$ increases from

a minimum of 0.2°C in May to a maximum of 9.7°C in July. The smallest range in $\overline{T}_d$ and σ follows the same trend as for $\overline{T}_{max}$, i.e., variability in dewpoint decreases with increasing values in July. A mean $\overline{T}_d$ of 9.7°C and σ of 0.7°C indicates that July is characterized by the highest and least variable dewpoints. The variation in $\langle T_d \rangle$ is 12.5°C over the summer compared to the highest variability in $\overline{T}_d$ of 8°C.

Table 3.4: Daily and seasonal statistics for T_d (all values in °C).

	Variability in $\overline{T}_d$				Variability in $\langle T_d \rangle$	
Month	**Max**	**Min**	**Mean**	**σ**	**Max**	**Min**
May	3.9	-4.1	0.2	2.1	3.3	-2.5
June	8.6	2.5	6.2	1.6	8.5	3.3
July	11.4	8.5	9.7	0.7	10.0	8.5
August	11.7	7.3	9.3	1.3	10.0	7.3
September	6.9	1.5	4.3	1.6	7.3	2.2

The Precipitable Water (PW) seasonal cycle has the same qualitative characteristics as for dewpoint. There is a linear increase in $\langle PW \rangle$ from 1 May to 28 June of ~0.1mm day^{-1}. Following the peak of 19mm on 28 July, $\langle PW \rangle$ decreases linearly from 22 Aug at ~0.1 mm day^{-1}. As with the dewpoint data, July has the highest mean $\overline{PW}$ (18.4mm), the lowest range in variability (2.5mm), and the lowest standard deviation (σ=0.7).

Table 3.5: Daily and seasonal statistics for PW (all values in mm).

	Variability in $\overline{PW}$				Variability in $\langle PW \rangle$	
Month	**Max**	**Min**	**Mean**	**σ**	**Max**	**Min**
May	13.9	8.8	11.3	1.4	13.3	9.1
June	18.0	13.1	15.4	1.2	17.3	13.3
July	19.7	17.2	18.4	0.7	19.0	17.3
August	20.2	15.3	17.9	1.4	18.9	15.8
September	15.7	11.7	13.6	1.2	15.8	11.6

Precipitable water amounts of 25mm are generally sufficient to support showers and thunderstorms in the southern and central United States (Djurić, 1994). Results from Chapters 5 and 6 in this thesis suggest that PW values of ~16mm can

be sufficient to result in severe thunderstorms over central Alberta. While PW gives an indication of how much water vapour is present in the troposphere, localized rainfall accumulations can be in excess of the value of PW determined from the sounding due to moisture convergence.

A histogram of PW is constructed for each month with bin ranges appropriately chosen to capture the monthly distributions. The vertical axis indicates the percent of the monthly total number of soundings falling into each PW bin range. The seasonal trends in PW are reflected by changes in the monthly histogram distributions of CAPE (Fig. 3.2). Shifting of the peak range from a minimum in May (8-10mm) to a maximum in July and August (16-18mm) supports the result of increasing PW before July, with a decrease thereafter. The proportion of the soundings with PW in the peak range fluctuates by month but remains near 20% throughout. Beginning with a distribution positively skewed with the tail towards larger PW values in May, the distribution peak shifts to higher ranges as summer progresses finally having a somewhat negatively skewed distribution with the tail towards lower values in September. The distribution spectrum broadens in July. The shift of the peak and broadening of the spectrum support the results of the seasonal analysis where the maximum moisture content in the 500mb deep column above the surface occurs in July.

Analysis of T_d and PW seasonal variability show July to be the month having the highest tropospheric moisture content. The seasonal moisture cycle is similar for both parameters with the highest rate of moisture decrease in September (a pattern also observed for T_{max}). The peaks of $\langle T_d \rangle$ and $\langle PW \rangle$ occur within one day of each other suggesting a close relationship between surface moisture and moisture in the column. The moisture parameters exhibit less day-to-day variability as moisture increases in June and July. Over the summer, seasonal variability exceeds the daily variability. The monthly distribution of PW is consistent with the seasonal data as the peak of the distribution shifts to higher bin ranges in July. The highest moisture is found during 28 to 29 July, consistent with the thermal parameters.

3.1.4 Convective available potential energy (CAPE)

CAPE quantifies the amount of potential energy available to thunderstorm updrafts (Chapter 2). It determines the maximum updraft velocity (section 2.2.1), thus giving an estimate of thunderstorm intensity. The values of $\overline{CAPE}$ calculated from the 00Z Stony Plain soundings are plotted in Fig. 3.1 with statistics listed in Table 3.6.

$\overline{CAPE}$ increases gradually during the month of May at ~3 Jkg^{-1} day^{-1}. From the beginning of June the increase is more rapid at 8 Jkg^{-1} day^{-1} until ~15 July when the curve levels off leading up to the peak of 480 Jkg^{-1} on 24 July. During August, $\overline{CAPE}$ decreases at ~9 Jkg^{-1} day^{-1} consistent with the rapid decrease in $\langle T_{max} \rangle$ and the moisture parameters. The $\langle CAPE \rangle$ curve is symmetric about its maximum from 14 June to 29 August with these dates having $\langle CAPE \rangle$ of ~200 Jkg^{-1}. Table 3.6 shows that maximum $\overline{CAPE}$ and $\langle CAPE \rangle$ occur in July. In contrast to T_{max} and the moisture parameters, the lowest range in daily max/min $\overline{CAPE}$ values and σ does not occur in June or July but in May and September. These months do, however, have relatively low mean values of 68 Jkg^{-1} and 64 Jkg^{-1} respectively. The highest range in $\overline{CAPE}$ is 426 Jkg^{-1} in June while the seasonal range from the $\langle CAPE \rangle$ data is 460 Jkg^{-1}.

A comment about the decrease in $\overline{CAPE}$ during the period 23 to 25 July (days 84 to 86) is needed. Similar decreases appear in the $\overline{PW}$ and $\overline{T}_d$ data on 24 July implying that the lack of moisture reduces the CAPE. The numerical data shows a large number of "dry" days occurring in the period 23 to 25 July in the 31-years have offset $\overline{CAPE}$ from its expected value at this time of year.

Table 3.6: Daily and seasonal statistics for CAPE (all values in Jkg^{-1}).

	Variability in $\overline{CAPE}$				Variability in $\langle CAPE \rangle$	
Month	Max	Min	Mean	σ	Max	Min
May	210	23	68	41	100	20
June	503	77	216	103	360	100
July	632	234	441	93	480	360
August	563	148	341	132	460	180
September	140	7	64	36	180	20

Calculation of CAPE utilizes the surface temperature and dewpoint so that by constructing histograms for CAPE, surface temperature (T) and dewpoint (T_d) are implicitly represented. Here, a doubling scale is used to capture the distribution. The monthly histogram distributions of CAPE (Fig. 3.3) support the result of maximum CAPE occurring in July as determined from the seasonal curve. There is a high number of low CAPE soundings evidenced by the highest percent occurrence of CAPE being in the 0-100 Jkg^{-1} range for all months. This peak ranges in percent occurrences from a maximum of 83% in May and September to a minimum of 36% in July consistent with an increased frequency of higher CAPE events. A secondary peak in the 400-800 Jkg^{-1} range occurs in July. With the exception of July, all months have distributions that are positively skewed with the tail towards higher values. The spectrum of the distribution broadens in the middle three months extending up to the 1600-3200 Jkg^{-1} range.

The maximum $\langle CAPE \rangle$ occurs within 4-5 days of the maximum of all other thermodynamic parameters (Table 3.7). This 4-5 day span appears to be a lead-time by which CAPE reaches its seasonal maximum ahead of its constituents. This effect is attributed to an increased rate of cooling of the troposphere aloft with respect to the surface. Surface temperature and moisture cause large CAPE values throughout 24-29 July but the cooling aloft (apparent in the large values of ΔT_{500} during this period) results in maximum $\langle CAPE \rangle$ occurring before the peak in $\langle T_{max} \rangle$, $\langle T_d \rangle$, and $\langle PW \rangle$.

Table 3.7: Peaks of the thermodynamic smooth curves.

Parameter	Date of Maximum	Value of Maximum
CAPE	24 July	480 Jkg^{-1}
PW	28 July	19mm
T_{max}	29 July	23°C
T_d	29 July	10°C
ΔT_{500}	16 May	38°C

Both the seasonal and monthly distributions of CAPE indicate that July experiences the highest mean CAPE and the highest occurrence of large CAPE values. This result is consistent with severe weather statistics where July has the highest occurrence of large hail events (Wojtiw, 1975; Vickers, 1997). The correlation between high CAPE in July and the high frequency of large hail events supports the result that large CAPE is needed for strong updrafts and large hailstones.

3.2 Inter-annual variability of thermodynamic parameters

The daily CAPE values from the 31-year period show marked inter-annual variability (Fig. 3.4). No single day has consistently high CAPE every year. Many CAPE events are episodic in nature in the sense that they last several days. The highest CAPE events tend to have the longest duration. The majority of significant CAPE events occur in the months of June to August.

Surface plots have been constructed for T_{max} and T_d (Figs. 3.5 - 3.6). A composite PW plot is shown in Fig. 3.7. The range in the data makes surface plots more appropriate for T_{max} and T_d than individual curves as for CAPE. The range of each contour shade is indicated at the top of the figure. The qualitative characteristics are the same for each parameter, low values occur in May and September and the highest concentration of high parameter values occurs in July consistent with the seasonal curves.

If surface temperatures (e.g., at Stony Plain) are increasing due to global warming it is conceivable that some effects should be observed in inter-annual changes in CAPE. To investigate this possibility, it is necessary to find a

representative mean annual CAPE value. Two methods have been used here as described in section 2.3. A non-weighted value with equal weight applied to each month, and a weighted value giving the most weight to CAPE values from July. The non-weighted and weighted annual mean CAPE data are shown in Fig. 3.8. Weighting the annual CAPE values has the effect of lowering them relative to the non-weighted values, while the trends in the data remain virtually unchanged. Thus, for inter-annual comparisons it makes little difference as to whether the weighted or non-weighted data are used. The years 1969 and 1988 have the lowest CAPE values for the 31 years and the values seem to be slightly higher for the period after 1988. The highest mean annual CAPE occurs in 1994, a year that experienced an above-average number of hail events but fewer than average tornadoes (Vickers, 1997).

By applying linear regression analysis to the mean annual CAPE values a linear trend line may be generated (see Fig. 3.8). The slope of this line is 1.7 Jkg^{-1} y^{-1} and 1.4 Jkg^{-1} y^{-1} for $\langle CAPE \rangle_{NW}$ and $\langle CAPE \rangle_{W}$ values respectively. While it may be suggested that global warming is responsible for the increasing trend of CAPE, there are too many other factors involved in determining CAPE (e.g., moisture and temperature profile aloft) beyond surface temperature to attribute this effect to global warming alone. Many of the determining factors may vary diurnally due to local forcing from synoptic or mesoscale systems.

3.3 The effect of ENSO on CAPE

In recent years, much emphasis has been placed on the Southern Pacific oscillations of El Niño and La Niña, collectively known as ENSO (the El Niño Southern Oscillation). The nature of the ENSO cycle is discussed by Glantz et. al. (1991). Agee and Zurn-Birkhimer (1998), Bove (1998), and Browning (1998) investigated the relationship between ENSO, tornadic activity, and severe weather in the United States. In this study we are interested in the relationship between the ENSO cycle and CAPE for the 31-years of Stony Plain soundings.

The non-weighted mean annual CAPE ($\langle CAPE \rangle_{NW}$) values are plotted in Fig. 3.9 for warm and cold ENSO cycles. The list of years for warm (El Niño) and cold (La Niña) cycles was obtained from the Center for Ocean - Atmosphere Prediction website: http://www.coaps.fsu.edu/~legler/jma_index.html. There is no definitive pattern found in the data relating the ENSO cycle to changes in $\langle CAPE \rangle_{NW}$. Unavailability of sounding data before 1966 hinders any patterns from becoming evident for a longer period than the 31 years in question. The average mean annual CAPE values for warm and cold cycles are given in Table 3.8.

Table 3.8: Mean CAPE for ENSO cycle (CAPE in units of Jkg^{-1}).

Years Included	Weighted CAPE	Non-weighted CAPE
All years	167	228
El Niño	142	192
La Niña	177	239
Neutral ENSO cycle	176	238

La Niña and neutral cycle years tend to have slightly higher mean CAPE than El Niño years.

Histogram distributions of the CAPE values for each of the ENSO cycle categories are presented in Fig. 3.10. La Niña soundings have a slightly higher frequency of days in the 200-400 Jkg^{-1} range and El Niño soundings have more days in the 0-100 Jkg^{-1} range (> 60% as opposed to slightly less than 60% for the other categories). The comparison of CAPE and ENSO events suggests that La Niña years have more days with higher CAPE than do other years.

3.4 Summary

We have determined the climatology for maximum surface temperature (T_{max}), SFC-500mb temperature difference (ΔT_{500}), surface dewpoint (T_d), SFC to 500mb precipitable water (PW), and CAPE in central Alberta. The seasonal

variability of these parameters has similar characteristics. Both surface temperature and tropospheric moisture increase from May to July and decrease more rapidly in September. With the exception of ΔT_{500}, all the parameters have their seasonal and monthly mean peak occurring in July. The peak in CAPE occurs 4-5 days before those of the other parameters suggesting that cooling aloft causes the seasonal maximum in thermodynamic instability to occur prior to the warmest surface temperatures and highest tropospheric moisture.

For all the parameters (except CAPE) daily variability is exceeded by seasonal variability (i.e., the range in values of $\bar{x}$ are greater than those of $\langle x \rangle$). There is no marked difference between total intra-seasonal and daily variability for the CAPE data. Monthly histogram distributions of PW and CAPE show a shift in the peak bin range towards higher values and a broadening of the spectrum in July. The thermal and moisture parameter results indicate that July and the first part of August constitute the "warmest" and "wettest" period of the summer with the highest CAPE values. The thermodynamic results suggest that there is a six-week period during which the thermodynamic profile from 00Z soundings is most conducive to development of deep convection (i.e., 1 July to 15 August). Severe weather summaries from Environment Canada report that the highest frequency of hail-related convective activity in Alberta occurs in July (Vickers, 1997).

Mean annual CAPE increases slightly over the 31-year period at a rate of 1-2 $Jkg^{-1}y^{-1}$. Comparing the ENSO cycle with $\langle CAPE \rangle_{NW}$ indicates that La Niña years have a slightly higher frequency of days with higher CAPE compared to El Niño years.

4. Summertime Climatology of Wind Shear and Helicity

The intensity and duration of thunderstorm convection are determined through interactions between the updraft and the environmental winds (Chisholm and Renick, 1972; Weisman and Klemp, 1982, 1984, 1986; Davies-Jones et al., 1990). The surface to 500mb wind shear (S), surface to 3 km storm relative helicity (SRH), and bulk Richardson number (R) are discussed here as they contribute to the potential for long-lived convection, mesocyclone formation, and determination of storm morphology. Using the 31-year sounding data set from Stony Plain, the intra-seasonal behaviour of these wind-derived sounding parameters is presented with emphasis on the implications for summertime convection in Alberta.

4.1 SFC to 500mb vertical wind shear

Strong wind shear, when combined with vigorous updrafts, results in dynamic conditions conducive to long-lived thunderstorms capable of producing large hail and tornadoes (Weisman and Klemp, 1986; Johns and Doswell, 1992). Figure 4.1 shows the mean daily shear $\overline{S}$ and the smoothed shear $\langle S \rangle$ as a function of the day between 1 May and 30 September. The statistics are presented in Table 4.1. The $\langle S \rangle$ curve is nearly horizontal through May and has a slight decline in value through May and June reaching a minimum of 4.50 $x10^{-3}s^{-1}$ from 8 to 22 July. The mean $\overline{S}$ data shows an increase from ~4.60 $x10^{-3}s^{-1}$ to 4.72 $x10^{-3}s^{-1}$ and 5.15 $x10^{-3}s^{-1}$ in August and September, respectively. The variation in $\langle S \rangle$ is only 0.70 $x10^{-3}s^{-1}$ over the entire summer, while variability in $\overline{S}$ has a range in excess of 1.0 $x10^{-3}s^{-1}$ for each of the five months. The standard deviations are highest from July to September indicating that $\overline{S}$ becomes more variable in late summer.

The wind shear calculation used here considers wind changes in the lowest 500mb of the troposphere (~5574m or 4808m AGL at Stony Plain). The 500mb wind is generally less variable in direction and stronger in magnitude than at lower levels (Holton, 1992; p. 73). Averaging the winds accounts for the lack of variability in $\langle S \rangle$ during the summer. As fall approaches and the polar jet stream migrates

southwards, the baroclinicity (i.e., horizontal temperature gradient) strengthens. From the geostrophic thermal wind shear equation (section 2.2.4), it follows that strong temperature gradients yield larger vertical wind shear. This is consistent with the larger $\overline{S}$ values in September compared to July.

Table 4.1: Daily and seasonal statistics for S (all values $\times 10^{-3}$ s^{-1}).

	Variability in $\overline{S}$				Variability in $\langle S \rangle$	
Month	**Max**	**Min**	**Mean**	**σ**	**Max**	**Min**
May	5.25	4.16	4.67	0.26	4.65	4.65
June	5.39	4.20	4.64	0.26	4.65	4.59
July	5.88	3.69	4.49	0.40	4.56	4.50
August	5.54	3.82	4.72	0.38	4.90	4.56
September	6.39	4.61	5.15	0.41	5.20	4.90

The monthly histogram distributions (Fig. 4.2) show little variability in S. The peak of the wind shear distribution shifts from 3-4 $x10^{-3}s^{-1}$ to 4-5 $x10^{-3}s^{-1}$ in June and September while the percent occurrence of the peak values for each month undergoes little change remaining between 20% and 25%. The monthly distributions are all positively skewed with the distribution for June and September being slightly less skewed due to the higher peak range. The range of the distribution remains nearly constant for each month (1-11 $x10^{-3}s^{-1}$), though May and June have a broader distribution of 1-13 $x10^{-3}s^{-1}$.

Chisholm and Renick (1972) compiled representative hodographs for single-cell (i.e., air mass), multicell, and supercell storms in Alberta. From these hodographs, the values of S have been estimated by calculating the surface to 6km mean wind shear (Table 4.2).

Table 4.2: Estimated values of S by storm type.

Storm Type	SFC to 6km wind shear
air mass	2.1 $x10^{-3}s^{-1}$
multicell	4.7 $x10^{-3}s^{-1}$
supercell	7.9 $x10^{-3}s^{-1}$

By averaging the mean shear values in Table 4.1, a yearly average wind shear is calculated to be 4.7 $x10^{-3}s^{-1}$. This corresponds well to the wind shear for multicell

storms (Table 4.2) which can produce severe hail and tornadoes. It seems that throughout most of the summer in Alberta, wind shear sufficient to sustain deep convection is often present. However, from the seasonal CAPE data (section 3.1.4) there is only a short time in the season when corresponding maximum updraft velocities are sufficient to support sustained vigorous convection. The low CAPE and relatively strong shear environmental conditions during May and September are indicative of the low frequency of severe thunderstorm activity in Alberta during these months (e.g., Vickers, 1997).

4.2 SFC to 3km storm relative helicity

SFC to 3km storm-relative helicity (SRH) provides an indication of the potential for the development of rotating updrafts (Desautels and Verret, 1996). SRH has been used to assess the potential for supercell storm development (e.g., Davies-Jones et. al., 1990). The variable nature of the $\overline{SRH}$ data (Fig. 4.1) in comparison to that for wind shear is due in part to SRH depending on the veering of the wind in the lowest 3km AGL, and not on the more persistent upper tropospheric wind.

Table 4.3: Daily and seasonal statistics for SRH (all values m^2s^{-2}).

	Variability in $\overline{SRH}$				Variability in $\langle SRH \rangle$	
Month	**Max**	**Min**	**Mean**	**σ**	**Max**	**Min**
May	81	8	39	19	60	33
June	63	0	37	13	39	35
July	60	11	35	14	38	35
August	79	6	43	17	50	36
September	114	31	64	18	70	50

The highest values of $\langle SRH \rangle$ occur at the beginning and end of the summer (Table 4.3). High positive SRH values represent strong clockwise hodograph curvature (i.e., veering of winds). All the $\overline{SRH}$ values are positive implying that, on average, the winds veer with height during the summer in the central Alberta region. Veering of winds in the lowest 3km is dynamically consistent with geostrophic low-level warm air advection. This enhances conditional moist instability and the

likelihood of deep convection. Mean $\overline{SRH}$ values change only marginally from May to July. An increase from 43 m^2s^{-2} to 64 m^2s^{-2} occurs during August and September. The range in max/min of $\overline{SRH}$ is smallest in July (49 m^2s^{-2}) and largest in May (73 m^2s^{-2}) and September (83 m^2s^{-2}). The standard deviation results also show that July has the least variability of all the months; σ changes by only 5 m^2s^{-2} over the entire summer. The total range in $\langle SRH \rangle$ is 37 m^2s^{-2}.

As with wind shear, there is little monthly variability in the SRH histogram distributions (Fig. 4.3). The monthly distributions of SRH show some soundings have negative SRH values. The peak range is the same for all months (40-80 m^2s^{-2}) except in September, when it shifts to 80-160 m^2s^{-2}. The distributions for May to July are nearly bimodal with secondary peaks occurring in the 0-20 m^2s^{-2} range. The peak percent occurrence increases from 17% in June to a maximum of 23% in August. All the distributions are negatively skewed with the tail towards lower values.

Values of SRH in excess of 100 m^2s^{-2} are generally indicative of supercell storm environments (Moller et. al., 1994). SRH values in the range 300-450 m^2s^{-2} are consistent with the occurrence of strong tornadoes (Davies-Jones et. al., 1990). While the values of $\overline{SRH}$ in Alberta are all lower than 100 m^2s^{-2}, daily values can be much higher (see Chapter 5). The highest $\overline{SRH}$ values occur in Alberta during May and September when mean CAPE values are lowest. Moreover, when there is significant CAPE in July and August, $\overline{SRH}$ values are low (~ 35 m^2s^{-2}). This implies that during the summer in Alberta these two parameters are out of phase in forming conditions conducive to supercell storm development. As a result, few supercell storms are expected to occur over Alberta during the summer convective season. From 1987-1996 there was an average of 9 tornadoes reported each year in Alberta (Vickers 1997), less than might be expected if helicity values in Alberta were higher.

4.3 Bulk Richardson number

The ranges in bulk Richardson number (R) indicative of air mass, multicell or supercell storm development have been found in case study (Chisholm and Renick, 1972) and modeling investigations (e.g., Weisman and Klemp, 1982, 1984). The bulk Richardson number was calculated for each 00Z Stony Plain sounding, whenever CAPE exceeded 500 Jkg^{-1}. This threshold in CAPE corresponds closely to the suggested range in CAPE for multicell storms (i.e., 200 Jkg^{-1} to 450 Jkg^{-1}) of Chisholm and Renick (1972). The $\overline{R}$ and $\overline{CAPE}$ data are presented in Fig. 4.4 and Tables 4.4 and 4.5. $\langle R \rangle$ and $\langle CAPE \rangle$ data for May and September were not analyzed due to the scarcity of days (119) in the 31-year period having CAPE ≥ 500 Jkg^{-1}.

Table 4.4: Daily and seasonal statistics for R.

	Variability in $\overline{R}$				Variability in $\langle R \rangle$	
Month	Max	Min	Mean	σ	Max	Min
May	187	12	82	67	-	-
June	502	17	104	109	140	60
July	791	26	142	146	145	140
August	633	25	136	123	145	80
September	504	6	73	107	-	-

Table 4.5: Daily and seasonal statistics for CAPE from soundings with CAPE ≥500 Jkg^{-1}.

	Variability in $\overline{CAPE}$				Variability in $\langle CAPE \rangle$	
Month	Max	Min	Mean	σ	Max	Min
May	2308	542	958	596	-	-
June	1900	612	1056	310	1150	900
July	1916	754	1146	257	1175	1150
August	1621	676	1134	251	1175	1000
September	1885	450	910	393	-	-

Eliminating the low CAPE bias (<500 Jkg^{-1}) from the sounding data set results in the $\langle CAPE \rangle$ data having higher values and less of a sinusoidal appearance than in Fig. 3.1. Some $\overline{CAPE}$ values result from only one day of the 31-year sounding data set (e.g., $\overline{CAPE}$ of 1921 Jkg^{-1} on 4 May). Considering only the portion of the smooth curve after 31 May, the peak of $\langle CAPE \rangle$ is on 5 August at a value of 1198 Jkg^{-1} compared with the maximum of 480 Jkg^{-1} on 24 July (section 3.1.4). The seasonal change of $\overline{R}$ and $\overline{CAPE}$ is similar (Fig. 4.4) consistent with the

dependence of R on CAPE (section 3.2.3). The difference in the values is attributed to wind shear dependence. There are no discontinuities in either curve between June and August in view of the increased frequency of significant $\overline{CAPE}$ events during this period.

A representative ⟨R⟩ maximum is derived from the $\overline{R}$ data after May. In this case the ⟨R⟩ curve has its peak of 145 on 25 July. The mean $\overline{R}$ values (Table 4.4) show a maximum in July similar to the trends of the thermodynamic parameter curves. No month has its mean bulk Richardson number in the supercell range (10-50). The greatest range and variability in $\overline{R}$ occur in July, as does the highest standard deviation. These results are consistent with the characteristics of both the thermodynamic and wind-derived parameters, illustrating the hybrid nature of the bulk Richardson number as it relates these effects. Variability of $\overline{R}$ (up to 765) is greater than for ⟨R⟩ (240), similar to the results for wind shear and SRH.

A histogram is included in Fig. 4.5 depicting the percent occurrence of all soundings from the $\overline{R}$ data consistent with each storm type. Of the 119 days having $\overline{CAPE} \geq 500$ Jkg^{-1}, 81 (68%) have $\overline{R}$ consistent with the multicell storm development range ($50<R\leq350$). Only 28 (24%) of those days have $\overline{R}$ in the supercell range ($10\leq R\leq50$). The 5 percent occurrence of air mass thunderstorms ($R>350$) is attributed to the fact that $\overline{R}$ is calculated for soundings with CAPE ≥ 500 Jkg^{-1} only, and wind shear is relatively strong throughout the season. The remaining 3% of the 119 days have strong wind shear compared to CAPE and $R < 10$ consistent with no thunderstorm development. It should be emphasized again that the R derived from a sounding does not, on its own, imply that a thunderstorm will develop. This histogram conforms with observations in that few supercells are identified in Alberta and most hail damage resulting from severe weather is associated with multicell storms (Chisholm and Renick, 1972).

When compared with the monthly histograms for wind shear and SRH, the bulk Richardson number histograms show the greatest monthly variability (see Fig. 4.6). May has a somewhat broken distribution with ~20% of the soundings having

R<8 and the remainder with R>16. This is the only month to have bulk Richardson numbers in the 0-2 range consistent with the seasonal CAPE data for May (Fig. 4.4). The peak of the histogram distribution occurs in the 32-64 range for the first three months (~25-35%, highest in June). The distribution for the first three months is nearly symmetrical. In August the distribution becomes bimodal about the 16-32 and 64-128 ranges. In September the distribution is positively skewed with the peak maximum of >25% in the 8-16 range. The range in R is greatest in August (0-2048) and least in September (4-512).

As discussed in section 2.2.3, there are some problems in the ability of the bulk Richardson number to represent actual storm severity (Weisman and Klemp, 1986). A low CAPE and strong wind shear environment may result in R being in the supercell range, even though the CAPE (and, therefore, the updraft velocity) may be insufficient to support the severity of weather (e.g., large hail, tornadoes) often associated with supercell storms. The percent occurrence of supercell type R's from Fig.4.5 is probably an overestimate and does not correspond to the low frequency of supercell storms in Alberta during the summer (Chisholm and Renick, 1972). This climatological study does not take into account triggering mechanisms that are often needed to initiate thunderstorm development (see Smith and Yau, 1993; McGinley, 1986). Clearly, such triggers are not always present when the environmental conditions are conducive to supercell development as evidenced by the rarity of these storms in Alberta.

4.3 Summary

The day-to-day variability of surface to 500mb vertical wind shear and surface to 3km storm relative helicity differs from that of the thermodynamic sounding parameters, which are driven by the seasonal cycle of incoming short wave radiation. Variability in the wind parameters is caused by pressure gradients associated with evolving weather systems. Fronts, outflow boundaries, and the mountain-plain circulation (Strong, 1986; Smith and Yau, 1993b) contribute to local winds.

Both wind shear and SRH show little seasonal change in contrast to their daily variability. Seasonal and monthly wind shear data suggests that, annually, the environmental wind shear is sufficiently strong to support long-lived convection (provided there is sufficient CAPE and an appropriate triggering mechanism). SRH data indicates that the lowest 3km environmental winds in Alberta tend to veer with height during the summer indicative of warm air advection and increased thermodynamic instability. Both wind shear and SRH have their highest values in September as the jet stream shifts southwards with the approaching fall season. There appears to be only a six-week period from 1 July to 15 August when climatological values of CAPE, wind shear, and SRH are favourable for supercell thunderstorm development. The climatological variability of the bulk Richardson number is determined primarily through seasonal changes in CAPE. R data indicate that the summer months in Alberta are more conducive to multicell storm development than supercell storms consistent with observational evidence (Chisholm and Renick, 1972).

5. Hailstorms During 1990 to 1996

The focus of this chapter is on identifying sounding parameter values that are associated with severe convective storms. Specifically, we categorize thunderstorms into two severity classes depending on the maximum observed hail size diameter using hailfall data from the Alberta Hail Project from 1990 to 1996. Sounding parameter threshold values indicative of the possibility of hail larger than 30mm in diameter are proposed.

5.1 Large hail days and small hail days

In central Alberta, severe convection is usually associated with hailfall. The maximum observed hail size tends to be a reliable indicator of the severity of the storm. The structural damage to agricultural crops, livestock, vehicles and buildings depends primarily on the kinetic energy of the falling hailstones (Strong, 1974). The kinetic energy is proportional to the fourth power of the equivalent diameter of the falling hailstone. The fourth power proportionality arises from the fact that mass $\propto$ diameter^3 and fall speed $\propto$ diameter$^{1/2}$.

The following two storm categories are examined:

Large Hail (LH) day: A convective storm day with recorded hail diameters larger than 30mm or within the golf ball size category (32-52mm; Renick and Maxwell, 1977).

Small Hail (SH) day: A day with recorded hailstone diameters within the 20-30mm range. Alternatively, a day on which a convective storm produced a tornado.

We consider only convective storms that passed through the geographical region bounded by 56.7° N (Fort McMurray), 52.2° N (Red Deer), 111.4° W (St. Paul), and 116.5° W (Edson). The confinement of storms within this region was motivated by

the need to have a sounding representative of the air mass in which the storm developed. The soundings launched from Stony Plain (53.5° N, 114.1° W) provide good proximity soundings for storms within the selected "storm" region. The issue of selecting good proximity soundings has been investigated by Darkow (1969), Golden et. al. (1986), and Brooks et al. (1994). Based on severe weather reports in the Severe Weather Summary for Central and Northern Alberta (Vickers, 1997) we identified 54 LH days and 45 SH days. These 99 severe days were compiled from seven consecutive years spanning from 1990 to 1996.

5.2 Monthly distributions of SH and LH days

The monthly number of SH and LH days is listed in Table 5.1 and compared with mean monthly CAPE (Fig. 5.1). This mean value of CAPE was calculated by taking the average of all the soundings for each month for the years 1990 to 1996. The number of SH and LH days are expressed as a percent occurrence of the total number of soundings for the SH and LH categories (Fig. 5.2). July had the highest frequency of hail days. Wojtiw (1975) and Kochtubajda and Gibson (1992) also found that July experiences more hailfall activity than any other month.

There are few hail days in May and September for both SH and LH distributions. The SH data show more hail days in May than September, while the LH data show the opposite result with more hail days in September than May. For the period of June to August, there is the same percent occurrence of SH days (~30% of all SH days) for each month. There is a marked increase in LH frequency in July over SH days as 50% of all LH days occur in this month. June has a slightly higher frequency of LH days than August, ~24% to ~15% respectively.

Table 5.1: Number of Small Hail and Large Hail days.

Month	SH days	LH days
May	5	1
June	12	13
July	13	27
August	13	8
September	2	5

5.3 Mean parameter values and histogram distributions

Histograms of the thermodynamic parameters (Fig. 5.3) contrast the parameter distributions for SH and LH days. The surface temperature histograms show a shift in the peak bin range to higher values for the LH data resulting in a negatively skewed distribution. There is also a wider range in temperatures for the LH days with the highest temperatures exceeding 28°C. The surface dewpoint distributions are similar for both SH and LH days, although the LH data is more negatively skewed. Precipitable Water (PW) shows a contrast between SH and LH days. The SH distribution is negatively skewed while the LH distribution is more symmetric with a lower peak bin range. For both SH and LH days, more than 70% of the soundings have PW in excess of 16mm. The greatest contrast between the two categories of severe days appears in the CAPE data. The SH days have more than 40% of the soundings falling into the 0-100 Jkg^{-1} range with a secondary maximum of 22% of the soundings in the 400-800 Jkg^{-1} range. The LH CAPE data has a bimodal distribution with peaks in the lowest (0-100 Jkg^{-1}) and highest (1600-3200 Jkg^{-1}) ranges. For LH days, 22% of the soundings fall in the 1600-3200 Jkg^{-1} range compared to only 4% in the same range for SH days. In summary, the thermodynamic parameter distributions show a tendency for LH days to have slightly higher surface temperatures and dewpoints, similar PW values, and a higher frequency of high CAPE soundings compared to SH days.

We now consider the distributions for the wind-derived sounding parameters (Fig. 5.4). The wind shear distributions are similar for SH and LH days, as both are symmetric in appearance, with a peak range of 5-6 $x10^{-3}s^{-1}$ including 24% of all the soundings. The greatest difference between the two distributions is that the SH range of wind shears is higher, with one sounding (2% of the total) having $S > 0.01$ $x10^{-3}s^{-1}$. The SRH distribution for LH days is negatively skewed compared to the more symmetric SH distribution. The SRH histogram shows that LH day soundings tend to have higher SRH. The bulk Richardson number distribution for SH days has a peak range of 32-64 and peak value of ~38%. 62% of the SH soundings fall in the 8-64 range (approximating the supercell range of R). The rest of the distribution is spread out over ranges from 4-1024 with most of the ranges containing only ~5% of the SH soundings. The LH distribution is positively skewed with a peak range of 16-

32 and 55% of the LH soundings in the 8-64 range. In order to examine the combined values of CAPE and SRH, we have calculated the Energy Helicity Index (EHI). The EHI distribution for SH days has a nearly symmetrical distribution centered at the 0-0.2 range. The LH data has a positively skewed distribution centered on the -0.2-0.0 range and extending up to the 3.4-3.6 range. In terms of wind-derived sounding parameter distributions, LH days tend to be associated with a higher frequency of larger SRH and EHI values and R peaking at lower values in the supercell range.

The average of each sounding parameter value for all the SH and LH days is presented in Table 5.2. The surface temperature (T) and dewpoints (T_d) are ~3°C and ~1°C higher respectively for LH soundings. A change in surface temperature of 1°C can result in a 200 Jkg^{-1} change in CAPE while a 1°C change in T_d can change CAPE by ~ 400 Jkg^{-1}. These changes in CAPE correspond to changes in maximum updraft velocity of ~10 ms^{-1} and ~14 ms^{-1}, respectively (see Chapter 2). The mean PW values are nearly the same for SH and LH days and mean CAPE is more than twice that of the LH days. Wind shear is slightly higher for LH days and SRH is low for both categories. The mean bulk Richardson numbers for SH and LH days are both in the multicell range. There is an increase by a factor of three in EHI values from 0.06 to 0.20. Values of EHI > 1 are generally associated with strong tornadoes (Brooks et al., 1994). With the exception of S and SRH, all the sounding parameters have higher mean values for LH days compared to SH days. The parameters showing the most significant higher mean values for LH days are T_d and CAPE. This highlights the importance of low-level moisture and large CAPE in producing large hail.

Table 5.2: Mean sounding parameter values for small hail and large hail days.

Sounding	SH	LH
T	17.4 °C	20.1 °C
T_d	9.9 °C	11.1 °C
PW	19.6 mm	19.8 mm
CAPE	418 Jkg^{-1}	861 Jkg^{-1}
S	5.52 x10^{-3} s^{-1}	5.32 x10^{-3} s^{-1}
SRH	48.2 m^2s^{-2}	21.5 m^2s^{-2}
R	116	217
EHI	0.06 Jkg^{-1}	0.20 Jkg^{-1}

5.4 Detection of LH days from 00Z sounding data

This section examines the relationship between sounding parameter values and the occurrence of LH events. We estimate the likely degree of certainty for which the threshold values are indicative of LH events by evaluating the number of LH days detected from the 99-day data set. Our discussion is confined to the determination of sounding parameter thresholds associated with the occurrence of potentially damaging large hail having diameters larger than 30 mm (or golfball). A detailed discussion on the forecasting and nowcasting of severe hail is beyond the scope of the present work and the reader is referred to Renick and Maxwell (1977), Moore and Pino (1990), Edwards and Thompson (1998), and Brimelow (1999).

While the parameter values determined in the previous section give some indication of those associated with LH events, they are intended as guideline values only. In this section we take a more systematic approach and simplify matters by considering only selected sounding parameters. The parameters we will discuss are CAPE, PW, and wind shear (S). The use of CAPE and PW allow us to distinguish, to some degree, thermodynamic instability from moisture in the column as the moist adiabatic curve results from surface moisture only (see Chapter 2). We have selected the three conditions that determine severe thunderstorm development, namely, buoyant energy, moisture availability, and vertical wind shear.

5.4.1 Evaluation of detection of LH days

Standard methods of forecast verification are used to assess the skill of the sounding parameter threshold values to detect LH events (e.g., Burgess and Ray, 1986). Definitions of the HIT, MISS, and FAIL variables are as follows:

HIT Sounding parameter value is above the threshold value for a LH event and a LH event is reported.

MISS Sounding parameter value is below the threshold value for a LH event and a LH event is reported.

FAIL Sounding parameter value is above threshold value for LH event and a SH event is reported.

The above variables are combined to evaluate the skill of the forecast. The following definitions are employed:

Probability of Detection (POD): A measure of the ability of the forecast to correctly identify a LH event.

False Alarm Ratio (FAR): A measure of the tendency of the forecast to falsely predict a LH event.

Critical Success Index (CSI): A combined index evaluating the overall reliability of a forecast.

High values of POD and CSI are desirable while a high FAR is undesirable for characterization of forecast skill. The above indices are calculated as follows:

$$POD = \frac{HIT}{(HIT + MISS)} \times 100\%$$

$$FAR = \frac{FAIL}{(HIT + FAIL)} \times 100\%$$

$$CSI = \frac{HIT}{(HIT + MISS + FAIL)} \times 100\%$$

These indices are calculated for the threshold studies and are used to evaluate the skill of different combinations of sounding parameters in nowcasting LH events.

5.4.2 Methodology

The methods used to determine the sounding parameter threshold values are as follows. We consider the entire data set of 99 severe weather events and examine the values of CAPE first. We take an initial CAPE threshold of 500 Jkg^{-1} to be consistent with our previous work (e.g., regarding bulk Richardson number). All the soundings with CAPE below 500 Jkg^{-1} are discarded. The number of HITS, MISSES, and FAILS are determined and the evaluation indices calculated. This process is repeated, increasing the CAPE threshold in increments of 250 Jkg^{-1} to a maximum of 1500 Jkg^{-1}. The other parameters are included in a cumulative manner so that after the CAPE evaluation a similar process includes CAPE and Shear. For the use of more than one parameter, the threshold of all parameters must be met to constitute a HIT or FAIL. Conversely, only one parameter must be below its threshold to constitute a MISS. The resulting table of statistics is included here for CAPE only (Table 5.3), while the corresponding tables for CAPE and PW, and CAPE, PW, and S are included in Tables 5.6 and 5.7.

5.4.3. Results

Table 5.3 indicates that increasing the threshold value of CAPE decreases the number of both SH and LH days that are included in the evaluation of the forecast. The number of HITS and FAILS decreases with increasing CAPE while the number of MISSES increases. This is reflected in the evaluation index values where the POD, CSI, and FAR decrease with increasing CAPE.

Table 5.3: Threshold Statistics for CAPE only (CAPE in Jkg^{-1}).

CAPE	# SH Days	# LH Days	Total Days	HIT	MISS	FAIL	POD	FAR	CSI
≥500	16	29	45	29	25	16	54	36	41
≥750	7	24	31	24	30	7	44	23	39
≥1000	6	18	24	18	36	6	33	25	30
≥1250	3	15	18	15	39	3	28	17	26
≥1500	2	12	14	12	41	2	23	14	22

The best evaluation results are for CAPE ≥ 500 Jkg^{-1}. For this threshold, 54% of the LH days were detected and 36% of the soundings gave false alarms of LH occurring.

The best CSI value achieved is 41%. While starting with CAPE of lower values increases the POD of LH events, the increased FAR deems the forecast not much better than a guess. The changes in the evaluation indices for increasing CAPE are illustrated in Fig. 5.5. In general, increasing the threshold CAPE from 500 Jkg^{-1} decreases the desirable attributes of the forecast.

The number of SH and LH days included with each increasing threshold varies in accordance with the assumption that larger CAPE is required to produce larger hail. For CAPE values < 500 Jkg^{-1} the percentage of the total days contributed to by SH days exceeds that of LH days (30% compared to 24%). For CAPE values above 500 Jkg^{-1} however, the contribution to the total number of days is dominated by LH days (Fig. 5.6). That is, fewer SH days are associated with larger CAPE than LH days. At a CAPE threshold of 1500 Jkg^{-1} the percentage of the total 99 days is six times higher for LH days than SH days.

The mean values of PW and S for the SH and LH days can be calculated for the soundings included with each CAPE threshold (Fig. 5.7-5.8). The resulting variation in both parameters is small for increasing CAPE. The mean PW and S for SH days is greater than for LH days for CAPE < 500 Jkg^{-1}. While there are slightly higher mean values of SH and LH PW for thresholds above 500 Jkg^{-1}, there is no further increase when CAPE increases. This suggests that for larger CAPE, higher PW is not necessarily a requirement for larger hail to develop. The wind shear graph (Fig. 5.8) shows a similar result with little variation in values of S for SH and LH days with increasing CAPE. For CAPE values higher than 500 Jkg^{-1} the LH days tend to have higher shears for each increasing CAPE threshold.

Following the CAPE threshold study, a similar study was conducted including the PW and S parameters (Tables 5.6 and 5.7). The PW thresholds were increased in increments of 2mm from 16mm to 26mm. For wind shear, the threshold was increased from 0.003 s^{-1} to 0.006 s^{-1} in increments of 0.001 s^{-1}.

For all values of the sounding parameters in all combinations, the variability of the evaluation indices is determined primarily by the changes in CAPE. The best results were achieved through the combined use of CAPE and PW. For these

parameters the POD was not improved over the use of CAPE alone but the FAR was decreased by 2% and the CSI increased by 3%, thus improving the skill of the forecast. Including S did not improve the POD or CSI, although the FAR decreased by 1%. Combining only CAPE and S did not improve the skill of the forecast, nor did using only PW and S or each parameter individually. This suggests again that CAPE is the primary determining factor for LH days in central Alberta. The evaluations for the different sounding parameter combinations are summarized below in Table 5.4.

Table 5.4: Verification statistics (%) for detection of LH events from sounding data.

Parameters	POD	FAR	CSI
CAPE	54	36	41
CAPE and PW	54	33	43
CAPE, PW, and S	49	32	40

The combination of CAPE and PW gives a POD of 54%. That is, 54% of the LH days had CAPE $\geq$ 500 Jkg^{-1} and PW $\geq$ 16mm. One must keep in mind that the results in Table 5.4 apply to LH (i.e., $\geq$30 mm) occurrence and that for the case of a false alarm (FAR), severe hail ($\geq$ 20mm) did still occur on that day. While this study has not rigorously scrutinized the representativeness of the soundings, it provides a simple criterion to alert the forecaster to the possibility of LH events. If the sounding indicates that CAPE and PW are in excess of 500 Jkg^{-1} and 16mm respectively, the forecaster should be aware of the possibility of large hail.

5.5 Sounding parameter thresholds for small vs. large hail soundings

Scatter plots of CAPE vs. each sounding parameter for the thermodynamic (Figs. 5.9-5.11) and wind-derived (Figs. 5.12-5.15) sounding parameters are constructed to contrast parameter differences between SH and LH days. For each parameter there is a plot containing both SH and LH data (as indicated in the figures) for all CAPE values and individual plots for SH and LH data for CAPE $\geq$ 500 Jkg^{-1} only. The scatter plot results are summarized for the severe days having CAPE $\geq$ 500 Jkg^{-1} in histogram distributions (Figs. 5.16-5.17). From the total number of soundings consisting of 45 SH days and 54 LH days, the numbers are reduced to 16 SH days and 29 LH days for soundings having CAPE $\geq$ 500 Jkg^{-1} only. By

considering separately the parameter data for higher CAPE values we hope to eliminate data not representative of the severe events.

From the scatter plots and histograms, we suggest a threshold value for each sounding parameter for which no less than 50% of the LH soundings and no more than 50% of the SH soundings are included. The results are summarized in Table 5.5. The parameters showing the greatest skill in detecting LH days are T_d and CAPE followed by T and EHI. The parameter having the greatest difference in the percentages above the threshold for each hail category is the EHI (28%).

Table 5.5: Sounding parameter values associated with > 50% of LH events having CAPE ≥ 500 Jkg^{-1}.

Parameter	Threshold	% SH Above	% LH Above
T	22°C	38	59
T_d	14°C	38	62
PW	22 mm	50	55
CAPE	1000 Jkg^{-1}	38	62
S	4.5x10^{-3} s^{-1}	44	55
SRH	30 m^{2}s^{-2}	25	52
R	18	50	55
EHI	0.2	31	59

There are a few interesting results that are not apparent from Table 5.5:

- For all severe days with CAPE $\geq$ 500 Jkg^{-1} the surface dewpoint is higher than 8°C and only one SH day has a dewpoint higher than 15°C.
- There are no LH days with PW < 16mm and 17% of the LH days have PW > 25mm compared to 0% of the SH days.
- 41% of the LH soundings (with CAPE $\geq$ 500 Jkg^{-1}) have CAPE > 1500 Jkg^{-1} compared to only 12% of the SH soundings.
- Most values of R for the severe days are below 100 consistent with the high frequency of low CAPE soundings throughout the summer season. The storm type histogram distributions (Fig. 5.17) show a preference for soundings associated with severe events to be in the supercell and multicell storm type categories, with slightly more of each storm type associated with LH days. 12% of the SH soundings have R corresponding to no storm development, while no

LH days fall into this category. For air mass thunderstorms, the percent occurrences are 12% and 7% for SH and LH days, respectively.

- The EHI data shows that 41% of LH day EHI values are higher than 0.5 while only 6% of SH days are above this value.

While parameter values from a sounding may be the same as or higher than the values listed in Table 5.6, this does not mean that a LH event will occur. These mean values do, however, suggest values that may be associated with LH events. That is, should sounding analysis result in parameters having these values, one should consider the possibility of large damaging hail occurring.

5.6 Summary

The issue of sounding representativeness has been addressed through selection of severe weather events reported within a spatial boundary defining the central region of Alberta. The result is a set of 99 severe weather days from 1990 to 1996 that are classified according to hail size (SH < 30mm ≤ LH). There were 45 Small Hail (SH) days and 54 Large Hail (LH) days. The months of the summer with the most active hail activity are June, July, and August, with July having a maximum of 27 LH days for the seven-year period.

Histogram distributions and mean parameter values have been compiled for all the SH and LH days showing that, with the exception of S and SRH, all the parameters have higher mean values for LH days. The parameters having the most pronounced increase between the severity categories are T_d and CAPE. A systematic parameter threshold study results in suggested thresholds indicative of LH events of CAPE of 500 Jkg^{-1} and PW of 16mm. From the 99 severe days, 54% of the 54 LH days had CAPE and PW exceeding these thresholds. The corresponding FAR and CSI for this parameter combination were 36% and 41% respectively. The addition of other sounding parameters does not improve detection of LH days. This suggests that variability in shear plays less of a role in severe thunderstorm development in Alberta than CAPE. That is, thermodynamic instability appears to be the primary determinant in production of large hail in Alberta.

6. Severe Weather Soundings

6.1 10 severe weather days from 1990 to 1996

Maddox (1976), Leftwich (1984), and Moore and Pino (1990) investigated how representative sounding data is used to characterize the actual pre-storm environment. In most cases, soundings had to be launched within 100km and 3 hours of the storm to capture the storm environment. For this study we use spatial and temporal constraints of 120 km from Stony Plain and 3 hours after 00Z (1800 MDT), respectively. In addition, we require that the severe weather report be made from a location "down wind" of the radiosonde site. Also, soundings indicating rain at the time of the launch were discarded, as these soundings are not representative of a pre-storm environment. These stringent criteria lead to a set of 10 severe storm soundings, a subset of the 99 soundings (Chapter 5), considered representative of severe events that occurred on those days.

Table 6.1 contains the ten severe storm events. The date, weather event, location, and time of the report are given. Hail and tornado events are denoted by H and T respectively. All tornadoes were classified as F0 tornadoes using the Fujita Scale (Fujita, 1971). The maximum wind speed for F0 tornadoes is 116 kmh^{-1}. Hail size is indicated in parentheses using the ranges in hail size used by Renick and Maxwell (1977).

Table 6.1: List of sounding represented severe days from 1990-1996.

Date	Event	Location	Time (MDT)
26 Aug 1990	T	26km SE of Camrose	1945
1 Aug 1991	T	Edmonton	1900
19 Jul 1993	H (21-32mm)	NW of Edmonton	1930
29 Jul 1993	H (33-52mm)	Camrose	2050
8 Jul 1994	H (33-52mm)	Near Tomahawk / S of Breton to Pigeon Lake	1820
21 Aug 1994	H (21-32mm)	N of Newbrook	1915
16 Jun 1995	H (33-52mm) + T	Westlock (H) / Legal(H) Legal (T)	1930 1945
10 Jul 1995	H (21-32mm)	SE of Wetaskiwin	1815
1 Jul 1996	H (21-32mm)	Drayton Valley Edmonton	1830 2000
2 Aug 1996	H (33-52mm)	Leduc HWY 637 N Villeneuve	1800 1825

6.2 The hailstorm of 16 June 1995

Here we focus on the analysis of sounding parameters for a storm that occurred on 16 June 1995. The 00Z 17 June sounding is an example of a representative severe day sounding with the tephigram, hodograph, and sounding parameters corresponding well with those expected for severe storm development. The storm developed approximately 50km north of Stony Plain and resulted in hail as large as golfballs (33-52mm) and an F0 tornado.

The tephigram for 00Z 17 June 1995 (Fig. 2.1) shows a deep layer of conditionally unstable air. The positive area on the tephigram ranged from the Lifting Condensation Level (LCL) at 824mb to the equilibrium level at 234mb. The hodograph (Fig. 2.2) indicates veering of the winds of more than 90° in the lowest 3km with unidirectional shear aloft. The shape of the hodograph is similar to the model hodograph for a right-moving, rotating, supercell storm (Weisman and Klemp, 1986). Table 6.2 contains the thermodynamic and wind-derived sounding parameters for this sounding. The CAPE and PW values on 16 June exceeded the threshold values of 500 Jkg^{-1} and 16mm derived for large hail in Chapter 5. Using (2.10), the maximum storm updraft velocity is estimated at 32 ms^{-1}. The maximum hail size corresponding to such an updraft speed is within the golfball size category, according to the nomogram of Renick and Maxwell (1977).

Table 6.2: Sounding parameters for 16 June 1995.

Sounding Parameter	Value
surface T	23.4°C
surface T_d	15.4°C
precipitable water	27mm
CAPE	2054 Jkg^{-1}
mean wind shear	6.12 x10^{-3} s^{-1}
storm relative helicity	265m^2s^{-2}
bulk Richardson number	21.5
energy helicity index	3.4

The strong veering of the winds is evident in the high value of storm relative helicity. The wind shear is consistent with the suggested range for multicell storms in Alberta (Chisholm and Renick, 1972), and the storm relative helicity is in the range

for weak tornadoes (Davies-Jones et al., 1990). The bulk Richardson number is in the supercell range and the energy helicity index is in the tornadic range (Brooks et al., 1994). As with the thermodynamic parameters, the wind-derived sounding parameters exceeded the threshold values suggested in Chapter 5 for large hail.

6.3 Comparison of severe (SVR) and non-severe (NSVR) soundings

Throughout this Chapter we will refer to severe and non-severe days (i.e., soundings) as SVR and NSVR respectively. All of the severe days from Table 6.1 occurred in either June, July, or August consistent with these months having the highest mean CAPE and frequency of higher CAPE (i.e., > 500 Jkg^{-1}) soundings. Histograms for surface temperature (T), dewpoint (T_d), PW and CAPE for SVR and NSVR days are compared in Fig. 6.1.

The surface temperature distribution for SVR soundings shows one sounding with a temperature lower than 15°C. The "peak" in the distribution occurs in the 20-24°C ranges compared to the 18-20°C range for NSVR soundings. Eighty percent of the SVR soundings have T > 20°C. The moisture parameters show that all the SVR soundings have T_d > 8°C and PW > 16mm. The peak in the T_d distribution occurs in the 14-16°C range for the SVR compared to the 4-6°C range for the NSVR soundings. For PW, the peak range shifts from 14-16 mm to 22-24 mm for the NSVR and SVR soundings, respectively. Sixty percent of the SVR soundings have T_d > 14°C and PW > 20mm. The two distributions for CAPE are markedly different as 55% of the NSVR soundings have CAPE in the 0-100 Jkg^{-1} range while all the SVR soundings have CAPE > 400 Jkg^{-1}. The NSVR sounding distribution is highly positively skewed while the SVR sounding distribution is not skewed with 70% of the SVR soundings having CAPE > 800 Jkg^{-1}. Severe storm soundings in central Alberta have higher T, T_d, PW and CAPE than non-severe soundings.

The wind-derived parameter histogram distributions (Fig. 6.2) are similar for SVR and NSVR days with the peak range in wind shear (S) shifting from 0.004-0.005 s^{-1} to 0.005-0.006 s^{-1} for the SVR days. The peak percentage increases from a maximum of 22% (NSVR days) to a maximum of 30% for SVR days. 60% of the SVR

soundings have S > 0.005 s^{-1} compared to 46% for the NSVR days. There is little contrast in the SRH (storm relative helicity) distributions for SVR and NSVR days, although for SVR days there are fewer soundings in the -20-0 m^2s^{-2} and 0-20 m^2s^{-2} ranges. A secondary peak of 20% in the SVR SRH distributions appears in the 20-40 m^2s^{-2} range and both distributions show 40% of the soundings have SRH > 40 m^2s^{-2}. The bulk Richardson number distributions are similar for both SVR and NSVR days. For SVR soundings, the distribution becomes bimodal with peaks of 30% in the 16-32 and 64-128 ranges. Comparing the energy helicity index (EHI) distributions, 30% of the SVR soundings have EHI > 0.5 compared to ~2% of the NSVR soundings. More than 50% of the NSVR soundings have EHI between 0 and 0.5.

The corresponding R derived storm type histogram distributions for SVR and NSVR days are shown in Fig. 6.3. 40% to 50% of both the SVR and NSVR soundings corresponding to supercell and multicell storm types based on the ranges of R from section 2.2.3. This underscores the concept of strong shear often being present throughout the summer as the NSVR day soundings in the supercell range probably have low CAPE and moderate shear environments. For the supercell SVR days, high CAPE and high wind shear are more likely to result in the supercell range R values.

SVR and NSVR histogram distributions for the wind-derived sounding parameters differ less than those for the thermodynamic parameters. The distributions for S and SRH are similar with severe days tending to have a slightly higher percentage of soundings with higher wind shear. The bulk Richardson number distributions suggest that variability in CAPE is the primary determinant of R derived storm type, as similar wind shear magnitudes occur on both non-severe and severe days. The greatest difference in the wind-derived parameter distributions arises from the EHI with severe days having a higher frequency of EHI > 0.5 than non-severe days.

The mean parameter values for the severe days and the remaining non-severe days from the 7-year period are listed in Table 6.3. These values are calculated by taking the average of the parameter values for each sounding in the severe and non-severe data sets. For example, in calculating the average T for the

severe days, $T_{avg} = (T_1 + T_2 + ... + T_{10})/10$ where T denotes the surface temperature from each SVR sounding. The difference column indicates by how much the parameter values are higher for the severe days. There are significant differences for all the parameters except T, S, and SRH. The greatest differences for the severe days are seen in the thermodynamic sounding parameters. Mean CAPE is six times greater for the severe days. The PW and CAPE values for all of the severe days are above the threshold values of 16mm and 500 Jkg^{-1} suggested in Chapter 5 for differentiating between small hail and large hail events.

Table 6.3: Mean sounding parameter values for SVR and NSVR soundings 1990-1996.

Parameter	Severe Days	Non-Severe Days	Difference
T	20.8°C	17.5°C	~3°C
T_d	13.5°C	6.4°C	~7°C
PW	21.5 mm	15.6 mm	~6 mm
CAPE	1500 Jkg^{-1}	258 Jkg^{-1}	1242 Jkg^{-1}
S	5.39 x$10^{-3}s^{-1}$	5.31 x$10^{-3}s^{-1}$	0. 08 x$10^{-3}s^{-1}$
SRH	58.3 m^2s^{-2}	43.8 m^2s^{-2}	~14 m^2s^{-2}
R	141	44	97
EHI	0.63 Jkg^{-1}	0.06 Jkg^{-1}	0.57 Jkg^{-1}

6.4 Summary

A set of 10 representative severe weather soundings has been compiled using spatial, temporal, and thermodynamic (e.g., rain at time of sounding) constraints. All of these events occurred during June, July, or August between 1990 and 1996, with half of the events occurring in July. Thermodynamic and wind-derived sounding parameter distributions and mean values for the severe and non-severe days have been compared and contrasted. The thermodynamic sounding parameters (T, T_d, PW and CAPE) show a tendency to have higher values on severe weather days. The CAPE and PW values for all the severe days exceeded the criteria of Chapter 5 for CAPE ≥ 500 Jkg^{-1} and PW ≥ 16mm. Although differences in the wind-derived sounding parameters is less evident, higher S and EHI values tend be associated with severe days compared to non-severe days.

7. Mean CAPE and Severe Weather Climatologies

In this chapter we compare the climatology of CAPE values with climatologies of lightning strikes and surface hailfall reports. The relationship between CAPE, wind shear, and maximum hail size is also examined.

7.1 Comparison with lightning observations in Alberta

Kozak (1998) compiled the cumulative incidence of cloud-to-ground lightning (CG) strikes in Alberta for the years 1984 to 1995. His data included the period 1 June to 31 August for all 11 years. The lightning frequency is shown in Fig. 7.1a. There is an increase in strikes after 1990 (except 1995). Wagner and Telford (1981) suggest that charge separation in convective clouds results from updraft and downdraft interactions. Since charge separation in clouds causes lightning, some vigorous updraft is required to generate lightning strikes. As in Chapter 5, we will use a threshold CAPE of 500 Jkg^{-1} corresponding to a maximum updraft velocity of ~16 ms^{-1}. The total number of days of the summer from June to August with CAPE $\geq$ 500 Jkg^{-1} from 1984 to 1995 are presented in Fig. 7.1b.

Qualitatively speaking, many of the features of Figs. 7.1a,b are similar. The highest frequency of CG lightning strikes (559 $x10^3$) and days with CAPE $\geq$ 500 Jkg^{-1} (33) occurs in 1994. The trend of increasing CG strikes from 1992 to 1994 is reflected in the increasing number of days with CAPE $\geq$ 500 Jkg^{-1} for the same period. The minimum in 1995 is also similar in both of the figures. In an attempt to correlate the number of days with CAPE greater than some threshold value and the frequency of lightning strikes, we have plotted the number of days with CAPE $\geq$ 750 Jkg^{-1} and $\geq$ 1000 Jkg^{-1} with the lightning data in Fig. 7.1c. In this case all the data are expressed as a percent occurrence of the total number of data points in each data set. That is, the number of days meeting the threshold criteria is divided by the total number of days meeting the criteria for all 12 years. Similarly, the number of CG strikes for each year is divided by the total number of CG strikes for the 12-year period. The resulting graph shows weak correlation between the number of summer

days with CAPE higher than a threshold value and the number of CG strikes in the same year. After 1988 the inter-annual trends in the percent occurrence of summer days and CG strikes are similar. The agreement in the data is not significantly improved by increasing the threshold value of CAPE. The number of lightning strikes appears to depend on more tropospheric parameters than CAPE alone.

7.2 Comparison with hail fall reports

The hail report data set used in this section were collected during the Alberta Hail Project (AHP) for the period of June to August 1966 to 1985 (Smith and Yau, 1993a, b; Smith et al., 1998). The data used here consist of the total number of hail reports (NR) collected for each day of the summer season and the maximum observed hail size using the category system of Renick and Maxwell (1977) summarized in Table 7.1. In this section, hail of grape size or larger is considered to be severe. Values of CAPE and S calculated from the Stony Plain 00Z soundings on hail days are compared to the number of reports and maximum hail size for each day.

Table 7.1: Hail size categories (adapted from Renick and Maxwell, 1977).

Hail Size Category	Hailstone Diameter (mm)
Shot	1-3
Pea	4-12
Grape	13-20
Walnut	21-32
Golfball	33-52
> Golfball	> 52

Renick and Maxwell (1977) presented data that showed maximum hail size for a day in central Alberta depends on the magnitude of CAPE from the Penhold soundings taken a few hours before severe convection. We first examine the CAPE and NR relationship for the 20-year period (Fig. 7.2). The data show significant daily and inter-annual variability in both CAPE and the number of hail reports (Smith et al., 1998). The highest CAPE and NR values occur during the six weeks following 1 July. As noted in Chapter 3, days with high CAPE soundings often occur in periods lasting

more than one day; a similar result is found for the occurrence of severe hail events (Smith et al., 1998). While some large CAPE days correspond to a high NR, there is insufficient agreement in the data to suggest that a large number of hail reports will always result from a sounding with high CAPE.

The number of hail reports recorded on a single day has been used as an indication of the severity of hailstorm outbreaks (e.g., Smith and Yau, 1993a). Fig. 7.3 (top) shows a scatter plot of CAPE vs. NR. The lower CAPE soundings are more likely to be non-representative of the severe hail events. The graph shows the highest concentration of data points for CAPE <2000 Jkg^{-1} and NR <200. There are fewer hail days for the highest NR values as widespread hail events occur less frequently than more localized events (Chisholm and Renick, 1972). While the number of hail reports may be appropriate for an indication of spatial extent of hailfall, we find little agreement between a high NR and large CAPE values. The relationship between hail size and the number of reports is illustrated in Fig. 7.3 (bottom). The number of hail reports increases significantly with maximum hail size. This is likely due to the more organized storms with longer hail swaths producing the larger hail (Smith and Yau, 1993a). Conversely, small air mass thunderstorms with short lifetimes produce shorter hail swaths.

The relationship between CAPE and maximum hail size is examined using the monthly CAPE distribution approach from Chapter 3. In Fig. 7.4, histograms of maximum hail size and CAPE distributions for June, July, and August are included for the 20-year period (1966 to 1985). The CAPE distributions are similar to those found for the 31-year period of 1966 to 1996. The maximum hail size distributions change by month in accordance with the changing frequency of larger CAPE days. Larger hail is associated with higher CAPE. The distribution for July shows the highest percent occurrence for each severe hail size category (except golfball) of the three months. August experiences more golfball and > golfball hail than June. June and August had the highest percent occurrence of non-severe hail days (< grape).

While CAPE is important for determination of hail size; the magnitude of the wind shear also affects storm type and hailstone size (Chisholm and Renick, 1972; Cotton and Anthes, 1989). Figure 7.5 shows a scatter plot of CAPE vs. S, for the

AHP data set, for severe hail days with CAPE ≥ 500 Jkg^{-1} only. The maximum observed hail size on each day is indicated with different symbols for the severe hail size categories. The largest concentration of the severe hail days occurs for wind shears between 0.002 s^{-1} and 0.006 s^{-1}. Fewer grape- and walnut-sized hail days occur at higher CAPE values. The corresponding histogram distributions for CAPE and S for each hail size category are given in Fig. 7.6.

For the CAPE distributions, we see a shift to higher values with increasing hail size category. As the hail size increases from grape to > golfball the percentage of the soundings with CAPE in ranges higher than 400 Jkg^{-1} increases from ~31% to ~54%. For the largest hail, more than 50% of the soundings have CAPE > 400 Jkg^{-1} with most soundings falling in the 800-1600 Jkg^{-1} range. A shift to higher values is also apparent in the wind shear distributions, as the percentage of the soundings with S > 0.006 s^{-1} increases from ~13% for grape sized hail to a maximum of ~35% for > golfball sized hail. The shape of the distribution is altered and becomes less positively skewed with increasing hail size. These findings confirm the importance of CAPE and wind shear in determining maximum hail size at the surface.

The mean values of CAPE and S for all the days associated with each hail size category are listed in Table 7.2. Following the shift in peak bin range to higher values in the histogram distributions for CAPE and S for larger hail days, the mean parameter values also increase with hail size, reaching a maximum for the > golfball hail days.

Table 7.2: Mean CAPE and wind shear by hail size for severe days.

Hail Size	Mean CAPE (Jkg^{-1})	Mean Shear (s^{-1})
Grape	373	0.0043
Walnut	433	0.0045
Golfball	476	0.0048
> Golfball	680	0.0050

7.3 Summary

We compared CAPE values with cloud-to-ground lightning strike observations for the period 1 June to 31 August for the 11 years from 1984 to 1995. There was

some agreement between high CAPE days and lightning occurrence. The data suggest that increased lightning activity does not necessarily result from a higher frequency of high CAPE days alone.

Using data from the Alberta Hail Project from 1966 to 1985, relationships between CAPE and hailfall were examined. There is substantial daily variability in both CAPE and the number of hail reports for the 20-year period. There is little correlation between significant CAPE events and the number of hail reports, it cannot be concluded that hail activity depends only on high CAPE values. A plot of CAPE vs. the number of hail reports (Fig. 7.2) suggests that the highest concentration of hail days occur at CAPE values < 2000 Jkg^{-1} with fewer than 200 reports collected. The relationship between the number of hail reports and hail size is clearly illustrated with the number of hail reports increasing significantly with increasing hail size.

The roles of CAPE and wind shear in determining hail size have been examined with plots of CAPE vs. S (for CAPE $\geq$ 500 Jkg^{-1}) and histograms of CAPE and S for each hail size category. The majority of hail days had wind shears in the range of 0.002 s^{-1} to 0.006 s^{-1}. The histograms show a shift in the peak to higher values of both CAPE and wind shear with increasing hail size. This suggests that large hail tends to develop in a high CAPE and strong wind shear environment.

8. Summary and Conclusions

A 31-year climatology (1966 to 1996) of convective sounding parameters was compiled for central Alberta. The data set contained 4743 00Z soundings released from Stony Plain (53.5° N, 114.1° W). The major parameters analyzed were:

- Convective Available Potential Energy (CAPE), which quantifies the amount of energy released when thermodynamic instability is triggered.

- Precipitable Water (PW), which quantifies the total water vapour in the troposphere.

- Mean wind shear (S), which quantifies the amount of vertical shear in the environmental wind profile.

- Storm Relative Helicity (SRH), which quantifies the curvature of the wind shear vector, in a storm relative sense, for the lowest 3km of the troposphere.

Also examined were the maximum observed surface temperature (T_{max}), surface dewpoint (T_d), temperature lapse rate (ΔT_{500}), bulk Richardson number (R), and Energy Helicity Index (EHI). We examined both intra-seasonal and inter-annual variability of the sounding parameters.

Comparisons were made between soundings associated with convective storms that produced Large Hail (LH) and Small Hail (SH). Here, a maximum threshold diameter of 30mm distinguished between LH and SH days. We also compared soundings associated with severe weather with those associated with non-severe weather. Finally, we compared our CAPE climatology with lightning and hail report climatological data.

The major findings were:

- The mean daily thermodynamic sounding parameters (T_{max}, T_d, PW, and CAPE), averaged over 31 years, follow a seasonal cycle exhibiting little day-to-day variability. Surface temperature, tropospheric moisture, and CAPE all reach peak values in July. The peak in CAPE precedes those of the other parameters by about 5 days, suggesting that cooling aloft is significant in determining maximum CAPE prior to the warmest surface temperatures and highest tropospheric moisture content.

- Mean daily temperature lapse rate data suggest that, on average, the troposphere is moist conditionally unstable during the summer.

- The mean daily wind derived sounding parameters (S, SRH, and R) exhibit a high degree of daily variability. S and SRH have peak values in September. The wind shear data suggest that environmental wind shear is sufficiently strong to support long-lived convection throughout the summer, provided there is sufficient CAPE and an appropriate triggering mechanism. SRH data indicate that the lowest 3km environmental winds tend to veer with height during the summer months.

- CAPE and PW have their seasonal peaks in mid-summer, with maximum values close to 24 July. In contrast, the wind shear is strongest in fall with relatively low values occurring in June, July and August. Optimal thermal conditions for storm development do not occur "in phase" with the optimal shear conditions for long-lasting organized convection. There seems to be a six-week period between 1 July to 15 August where both thermal and wind shear conditions are suitable to support severe convection.

- The seasonal variation of bulk Richardson number is determined primarily by the seasonal variations in CAPE, whereas the seasonal variation in wind shear is relatively less important.

- Conditions conducive to multicell storms are more frequent than those for supercell storms, based on R values. This is in agreement with observed storm type frequency using radar data (Chisholm and Renick, 1972).

- During the 31 years (1966 to 1996) values of mean annual CAPE (averaged from May to September) tended to increase. With regards to the El Niño Southern Oscillation (ENSO) cycle, we find that La Niña years tend to have a slightly higher frequency of high CAPE days compared to El Niño or neutral years.

- A comparison was made between sounding parameters associated with large hail (≥30mm) and small hail (20-29mm), respectively. CAPE was the parameter that best differentiated between large hail and small hail days. More than 50% of the days associated with large hailstones had CAPE ≥ 500 Jkg^{-1} and PW ≥ 16mm. The magnitudes of S and SRH did not differ significantly between days with large hail and days with small hail.

- Severe weather days (i.e., days with hail > 20mm and/or tornado) had significantly higher values of CAPE, PW, T_d and EHI compared to non-severe days. For example, the average CAPE for ten severe cases was 1500 Jkg^{-1} compared to only 258 Jkg^{-1} for the non-severe cases.

- Days with larger CAPE values often occurred in episodes lasting a few days, rather than as isolated, single-day events. Smith et al. (1998) found a similar result for hailfall in central Alberta.

- We compared daily CAPE values with daily numbers of hail fall reports and maximum-recorded hail size. In general, days with larger hail size tended to be associated with larger CAPE and stronger wind shear.

Our results suggest that severe convective storms in central Alberta tend to be associated with CAPE values exceeding 500 Jkg^{-1}. The importance of large CAPE values was also stressed by Chisholm (1972), Chisholm and Renick (1973), Renick and Maxwell (1977), and Smith and Yau, 1993(a, b). Minimum threshold values of

CAPE, PW, and wind shear in Alberta were found to be lower than those proposed for the Great Plains of the United States (e.g., Weisman and Klemp, 1986; Johns et al., 1993; Brooks et al., 1994). The importance of sounding parameters for convective storm development implies that more than a single radiosonde site, and multiple soundings on unstable days, would be beneficial. This improved spatial and temporal resolution in sounding data could facilitate the issuance of more accurate and timely weather watches and warnings.

References

Agee, E., and S. Zum-Birkhimer, 1998: Variations in USA tornado occurrences during El Niño and La Niña. Preprints, *19th Conf. on Severe Local Storms*, Minneapolis, Minnesota, Amer. Meteor. Soc., 287-290.

Barnes, S. L.,, 1968: An empirical shortcut to the calculation of temperature and pressure at the lifted condensation level. *J. Appl. Meteor.*, **7**, 511.

Beebe, R. G., 1958: Tornado proximity soundings. Proc. of the 3rd *Conf. on Severe Local Storms*, Urbana, Illinois, p.6.

Bluestein, H. B., and C. R. Parks, 1983: A synoptic and photographic climatology of low-precipitation severe thunderstorms in the Southern Plains. *Mon. Wea. Rev.*, **111**, 2034-2046.

Bluestein, H. B., and M. H. Jain, 1985: Formation of mesoscale lines of precipitation: severe squall lines in Oklahoma during the spring. *J. Atmos. Sci.*, **42**, 1711-1732.

Bluestein, H. B., G. T. Marx, and M. H. Jain, 1987: Formation of mesoscale lines of precipitation: nonsevere squall lines in Oklahoma during the spring. *Mon. Wea. Rev.*, **115**, 2719-2727.

Bove, M. C., 1998: Impacts of ENSO on United States tornado activity. Preprints, *19th Conf. on Severe Local Storms*, Minneapolis, Minnesota, Amer. Meteor. Soc., 313-316.

Brimelow, J. C., 1999: Numerical modelling of hailstone growth in Alberta storms. M.Sc. Thesis, Department of Earth and Atmospheric Sciences, University of Alberta, 153 pp.

Brooks, H. E., C. A. Doswell III, and J. Cooper, 1994: On the environments of tornadic and non-tornadic mesocyclones. *Wea. Forecasting*, **9**, 606-618.

Browning, K. A., 1964: Airflow and precipitation trajectories within severe local storms which travel to the right of the winds. *J. Atmos. Sci.*, **21**, 634-639.

Browning, P, 1998: ENSO related severe thunderstorm climatology of Northwest Missouri. Preprints, *19th Conf. on Severe Local Storms*, Minneapolis, Minnesota, Amer. Meteor. Soc., 291-292.

Bullas, J. M. and A. F. Wallace, 1988: The Edmonton tornado, July 31, 1987. Preprints, *15th Conf. on Severe Local Storms*, Baltimore, Maryland, Amer. Meteor. Soc., 437-443.

Burgess, D. and P. S. Ray, 1986: Principles of radar. *Mesoscale Meteorology and Forecasting*, P. S. Ray, Ed., Amer. Meteor. Soc., 85-117.

Chisholm, A. J., 1973: Alberta Hailstorms. Part I: Radar case studies and airflow models. *Meteor. Monogr.*, No. 36, Amer. Meteor. Soc., 1-36.

Chisholm, A. J. and J. H. Renick, 1972: The kinematics of multi-cell and supercell Alberta hailstorms. Alberta Hail Studies 1972. Alberta Research Council, Edmonton, Alberta, Hail Studies Report 72-2, 24-31.

Cotton, W. R. and A. A. Anthes, 1989: **Storm and Cloud Dynamics**, Vol. 44, Academic Press Inc., San Diego, 883 pp.

Crook, N. A., 1996: Sensitivity of moist convection forced by boundary layer processes to low-level thermodynamic fields. *Mon. Wea. Rev.*, **124**, 1767-1785.

Danielsen, E. F., 1977: Inherent difficulties in hail probability prediction. *Meteor. Monogr.*, No. 38, 135-143.

Darkow, G. L., 1969: An analysis of over sixty tornado proximity soundings. Preprints, *6th Conf. on Severe Local Storms*, Chicago, Illinois, Amer. Meteor. Soc., 218-221.

Darkow, G. L., and M. G. Fowler, 1971: Tornado proximity wind sounding analysis. Preprints, *7th Conf. on Severe Local Storms*, Kansas City, Missouri, Amer. Meteor. Soc., 148-151.

Davies, J. M., 1993: Hourly helicity, instability, and EHI in forecasting supercell tornadoes. Preprints, *17th Conf. on Severe Local Storms*, St. Louis, Missouri, Amer. Meteor. Soc., 107-111.

Davies, J. M., and R. H. Johns, 1993: Some wind and instability parameters associated with strong and violent tornadoes. 1. Wind shear and helicity. In *The Tornado: Its Structure, Dynamics, Prediction, and Hazards (Geophys. Monogr. 79)*, Church, Doswell, and Davies-Jones, ed., 573 - 582.

Davies-Jones, R. P., 1984: Streamwise vorticity: The origin of updraft rotation in supercell storms. *J. Atmos. Sci.*, **41**, 2991-3006.

Davies-Jones, R. P., 1993: Helicity trends in tornado outbreaks. Preprints, *17th Conf. on Severe Local Storms*, St. Louis, Missouri, Amer. Meteor. Soc., 56-60.

Davies-Jones, R. P., D. Burgess, and M. Foster, 1990: Test of helicity as a tornado forecast parameter. Preprints, *16th Conf. on Severe Local Storms*, Kananaskis Park, Alberta, Amer. Meteor. Soc., 588-592.

Desautels, G. and R. Verret, 1996: Canadian meteorological centre summer severe weather package (storm relative helicity). Preprints, 18th *Conf. on Severe Local Storms*, San Francisco, California, Amer. Meteor. Soc., 689-697.

Djurić, D., 1994: **Weather Analysis**. Prentice-Hall, Inc., Englewood Cliffs, New Jersey.

Doswell, C. A. III, and E. N. Rasmussen, 1994: The effect of neglecting the virtual temperature correction on CAPE calculations. *Wea. Forecasting*, **9**, 625-629.

Douglas, R. H. and W. Hitschfeld, 1958: Studies of Alberta Hailstorms, 1957. McGill University, Storm Weather Group, Sci. Rep. MW-27, 79 pp.

Edwards, R. and R. L. Thompson, 1998: Nationwide comparisons of hail size with WSR-88D vertically integrated liquid water and derived thermodynamic sounding data. *Wea. Forecasting*, **13**, 277-285.

Fankhauser, J. C., 1971: Thunderstorm-environment interactions determined from aircraft and radar observations. *Mon. Wea. Rev.*, **99**, 171-192.

Fawbush, E. J. and R. C. Miller, 1952: A mean sounding representative of the tornadic air-mass environment. *Bull. Amer. Meteor. Soc.*, **33**, 303-307.

Fawbush, E. J. and R. C. Miller, 1954: The types of air masses in which American tornadoes form. *Bull. Amer. Meteor. Soc.*, **35**, 164-165.

Fujita, T. T., 1971: Proposed characterization of tornadoes and hurricanes by area and intensity, *SMRP Research Paper* No. 91, University of Chicago.

Glantz, M. H., R. W. Katz, and N. Nichols, 1991: **Teleconnections Linking Worldwide Climate Anomalies**. Cambridge University Press.

Golden, J. H., R. Serafin, V. Lalley, and J. Facundo, 1986: Atmospheric sounding systems. *Mesoscale Meteorology and Forecasting*, P. S. Ray, Ed., Amer. Meteor. Soc., 50-70.

Hart, J. A. and W. Korotky, 1991: The SHARP workstation v1.50 users guide. National Weather Service, NOAA, U. S. Dept. of Commerce, 30 pp. [Available from NWS Eastern Region Headquarters, 630 Johnson Ave., Bohemia, NY 11716.]

Hitschfeld, W., 1960: The motion and erosion of convective storms in severe vertical wind shear. *J. Meteor.*, **17**, 270-282.

Holton, J. R., 1992: **An Introduction to Dynamic Meteorology**. Academic Press, Seattle, Washington.

Johns, R. H., J. M. Davies, and P. W. Leftwich, 1990: An examination of the relationship of 0-2 km AGL "positive" wind shear to potential buoyant energy in strong and violent tornado situations. Preprints, *16th Conf. on Severe Local Storms*, Kanaskis Park, Alberta, Amer. Meteor. Soc., 593-598.

Johns, R. H., J. M. Davies, and P. W. Leftwich,1993: Some wind and instability parameters associated with strong and violent tornadoes. 2. Variations in the combinations of wind and instability parameters. In *The Tornado: Its Structure, Dynamics, Prediction, and Hazards (Geophys. Monogr. 79)*, Church, Doswell, and Davies-Jones, ed.

Johns, R. H. and C. A. Doswell III, 1992: Severe local storms forecasting. *Wea. Forecasting*, **7**, 588-612.

Kochtubajda, B. and C. Gibson, 1992: A study to evaluate existing hail detection algorithms for the Alberta region. Atmospheric Environment Service, Downsview, Ontario, Canada.

Kozak, S. A., 1998: Lightning strikes in Alberta thunderstorms: Climatology and case studies. M.Sc. Thesis, Department of Earth and Atmospheric Sciences, University of Alberta, 129 pp.

Leftwich, P. W., 1984: Operational experiments in prediction of maximum expected hailstone diameter. Preprints, *10th Conf. on on Weather Forecasting and Analysis*, Amer. Meteor. Soc., Clearwater Beach, 525-528.

Lemon, L. R., and C. A. Doswell III,1979: Severe thunderstorm evolution and mesocyclone structure as related to tornadogenesis. *Mon. Wea. Rev.*, **107**, 1184-1197.

Lilly, D. K., 1986: The structure, energetics, and propagation of rotating convective storms, II, Helicity and storm stabilization. J. Atmos. Sci., **43**, 126-140.

Longley, R. W. and C. E. Thompson, 1965: A study of the causes of hail. *J. Appl. Meteor.*, **4**, 69-82.

Maddox, R. A., 1976: An evaluation of tornado proximity wind and stability data. *Mon. Wea. Rev.*, **104**, 133-142.

Markowski, P. M., J. M. Straka, and E. N. Rasmussen, 1998a: The sensitivity of storm-relative helicity to small hodograph changes and resolution. Preprints, *19th Conf. on Severe Local Storms*, Minneapolis, Minnesota, Amer. Meteor. Soc., 363-366.

Markowski, P. M., J. M. Straka, and E. N. Rasmussen, 1998b: A preliminary investigation of the importance of helicity 'location' in the hodograph. Preprints, *19th Conf. on Severe Local Storms*, Minneapolis, Minnesota, Amer. Meteor. Soc., 230-233.

McGinley, J., 1986: Nowcasting mesoscale phenomena. *Mesoscale Meteorology and Forecasting*, P. S. Ray, Ed., Amer. Meteor. Soc., 657-688.

Miller, R. C., 1972: Notes on analysis and severe storm forecasting procedures of the Air Force Global Weather Central. *Tech. Rep.* 200, Air Force Weather Service (MAC), USAF, Offut, Neb., May, 1972.

Moller, A. R., Doswell, C. A., III, Foster, M. P., and Woodall, G. R.,1994: The operational recognition of supercell thunderstorm environments and storm structures. *Wea. Forecasting*, **9**, 327-347.

Moore, J. T. and J. P. Pino, 1990: An interactive method for estimating maximum hailstone size from forecast soundings. *Wea. Forecasting*, **5**, 508-526.

Moncrieff, M. W. and J. S. A. Green, 1972: The propagation and transfer properties of steady convective overturning in shear. *Quart. J. Roy. Meteor. Soc.*, **98**, 336-352.

Mueller, C. K., J. W. Wilson, and N. A. Crook, 1993: The utility of sounding and mesonet data to nowcast thunderstorm initiation. *Wea. Forecasting*, **8**, 132-146.

Newton, C. W., 1963: Dynamics of severe convective storms. *Meteor. Monogr.*, No. 27, Amer. Meteor. Soc., 33-58.

Paruk, B. J. and S. R. Blackwell, 1994: A severe thunderstorm climatology for Alberta. *National Weather Digest*, 19, 27-33.

Prosser, N. E. and D. S. Foster, 1966: Upper air sounding analysis by use of an electronic computer. *J. Appl. Meteor.*, **5**, 296-300.

Rasmussen, E. N., and R. B. Wilhelmson, 1983: Relationships between storm supercell thunderstorm. *J. Atmos. Sci.*, **49**, 1997-2014.

Rassmussen, E. N. and D. O. Blanchard, 1998: A baseline climatology of sounding derived supercell and tornado forecast parameters. Accepted for publication in *Wea. Forecasting*.

Reuter, G. W. and L. Aktary, 1995: Convective and symmetric instabilites and their effects on precipitation: Seasonal variations in central Alberta during 1990 and 1991. *Mon. Wea. Rev.*, **123**, 153-162.

Renick, J. H. and J. B. Maxwell, 1977: Forecasting hailfall in Alberta. *Meteor. Monogr.*, No 38, Amer. Meteor. Soc., 145-151.

Rogers, R. R. and M. K. Yau, 1996: **A Short Course in Cloud Physics**. Butterworth-Heinemann, Linacre House, Jordan Hill, Oxford, 290 pp.

Rotunno, R., 1981: On the evolution of thunderstorm rotation. *Mon. Wea. Rev.*, **109**, 171-180.

Rotunno, R. and J. B. Klemp, 1982: The influence of the shear-induced pressure gradient on thunderstorm motion. *Mon. Wea. Rev.*, **110**, 136-151.

Sackiw, C. M. and G. S. Strong, 1983: The spatial / temporal resolution study (STRESS) of upper air data. Presented at 17th Ann. Congr. Can. Meteor. and Oc. Soc., Banff, Alta., 03-05 May, 1983, published by Alta., Res. Coun., Edmonton, 13-25.

Sienkiewicz, M. E., L.P. Gilchrist, and R. E. Turner, 1981: AVE-SESAME V: 25mb sounding data. NASA Tech. Memo. TM-82417, May 1981, Marshall Space Flight Center, Ala., 409 pp.

Smith, S. B. and M.K. Yau, 1993a: The causes of severe convective outbreaks in Alberta. Part I: A comparison of a severe outbreak with two non-severe events. *Mon. Wea. Rev.*, **109**, 1099-1125.

Smith, S. B. and M.K. Yau, 1993b: The causes of severe convective outbreaks in Alberta. Part II: Conceptual model and statistical analysis. *Mon. Wea. Rev.*, **109**, 1126-1133.

Smith, S. B., G. W. Reuter, and M. K. Yau, 1998: The episodic occurrence of hail in central Alberta and the Highveld of South Africa. *Atmos. Ocean.*, **36**, 169-178.

Strong, G.S., 1974: The objective measurement of Alberta hailfall. M.Sc. Thesis, Department of Geography, University of Alberta, 182 pp.

Strong, G. S., 1986: Synoptic to mesoscale dynamics of severe thunderstorm environments: A diagnostic study with forecasting implications. Ph.D. Thesis, Department of Geography, University of Alberta, 345 pp.

Vickers, G, 1997: 1996 summer severe weather report for central and northern Alberta. Northern Alberta Environmental Services Centre, Environment Canada.

Wagner, P. B. and J. W. Telford, 1981: Cloud dynamics and an electric charge separation mechanism in convective clouds. *J. Rech. Atmos.*, **15**, 97-120.

Weisman, M. L., and J. B. Klemp, 1982: The dependence of numerically simulated convective storms on vertical wind shear and buoyancy. *Mon. Wea. Rev.*, **110**, 504-520.

Weisman, M. L. and J. B. Klemp, 1984: The structure and classification of numerically simulated convective storms in directionally varying wind shears. *Mon. Wea. Rev.*, **112**, 2479-2498.

Weisman, M. L. and J. B. Klemp, 1986: Characteristics of isolated storms. *Mesoscale Meteorology and Forecasting*, P. S. Ray, Ed., Amer. Meteor. Soc., 331-357.

Wojtiw, L., 1975: Climatic summaries of hailfall in central Alberta (1957-1073). Alberta Research Council, Edmonton, Alberta, Atmos. Sci. Rep. 75-1, 102 pp.

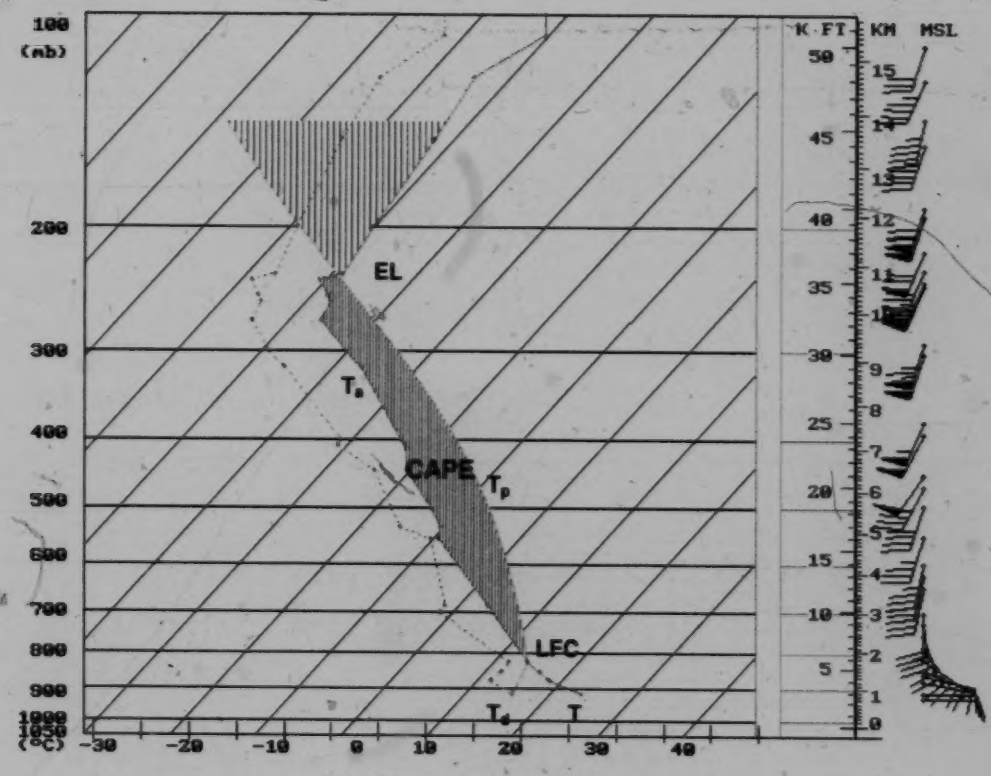

Figure 2.1: Tephigram for 00Z 17 June 1995 showing surface temperature (T), dewpoint (T_d), ambient temperature curve (T_a), parcel temperature curve (T_p), level of free convection (LFC) and equilibrium level (EL). The positive area under the pseudoadiabatic curve represents CAPE. The wind profile is given at right in kt.

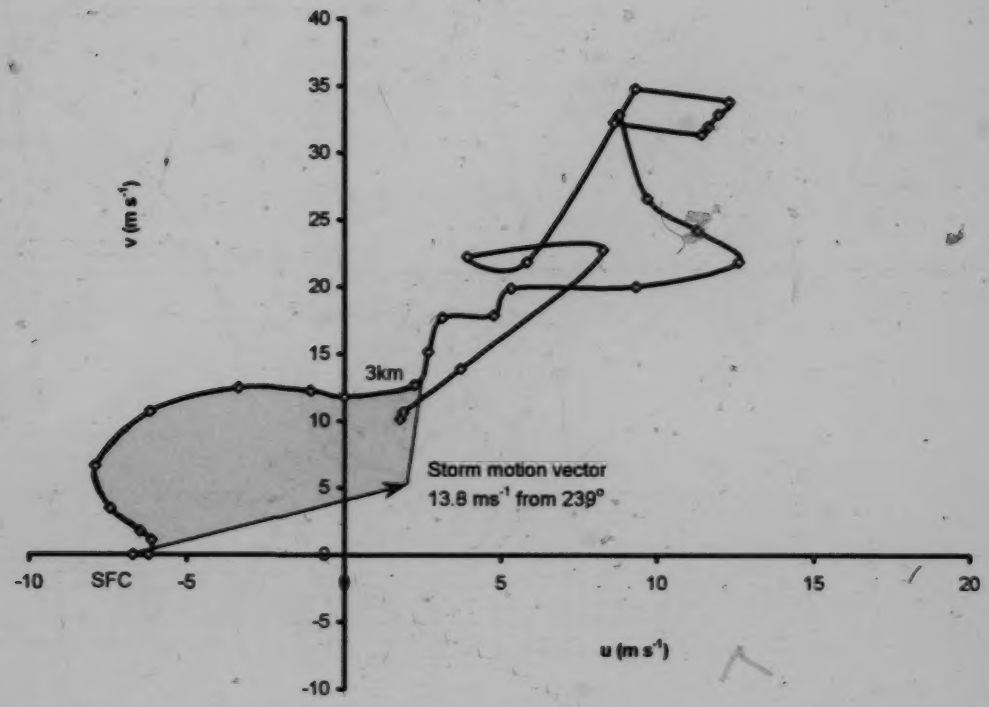

Figure 2.2: Hodograph for 00 Z 17 June 1995 showing the storm motion vector ($\vec{c}$). The magnitude of the storm relative helicity in the lowest 3km is twice the shaded area. Wind speeds are in ms^{-1}.

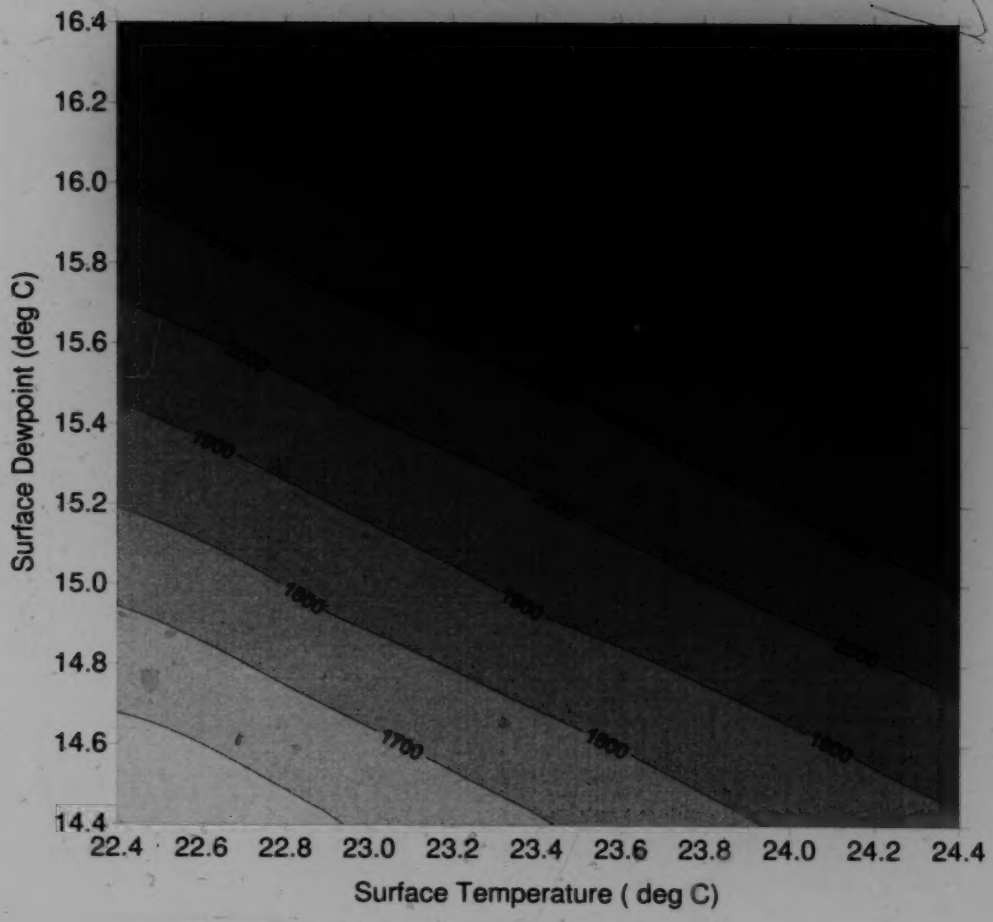

Figure 2.3: Contours of CAPE for the sensitivity test for 00Z 17 June 1995. Temperature and dewpoint have been varied by 1°C about the control values (T=23.4°C and T_d=15.4°C) in 0.5°C intervals. Approximately equal changes in CAPE occur for variations of 1°C and 2°C in temperature and dewpoint respectively, i.e., CAPE is increased by ~200 Jkg^{-1} and ~400 Jkg^{-1} for 1°C changes in temperature and dewpoint respectively.

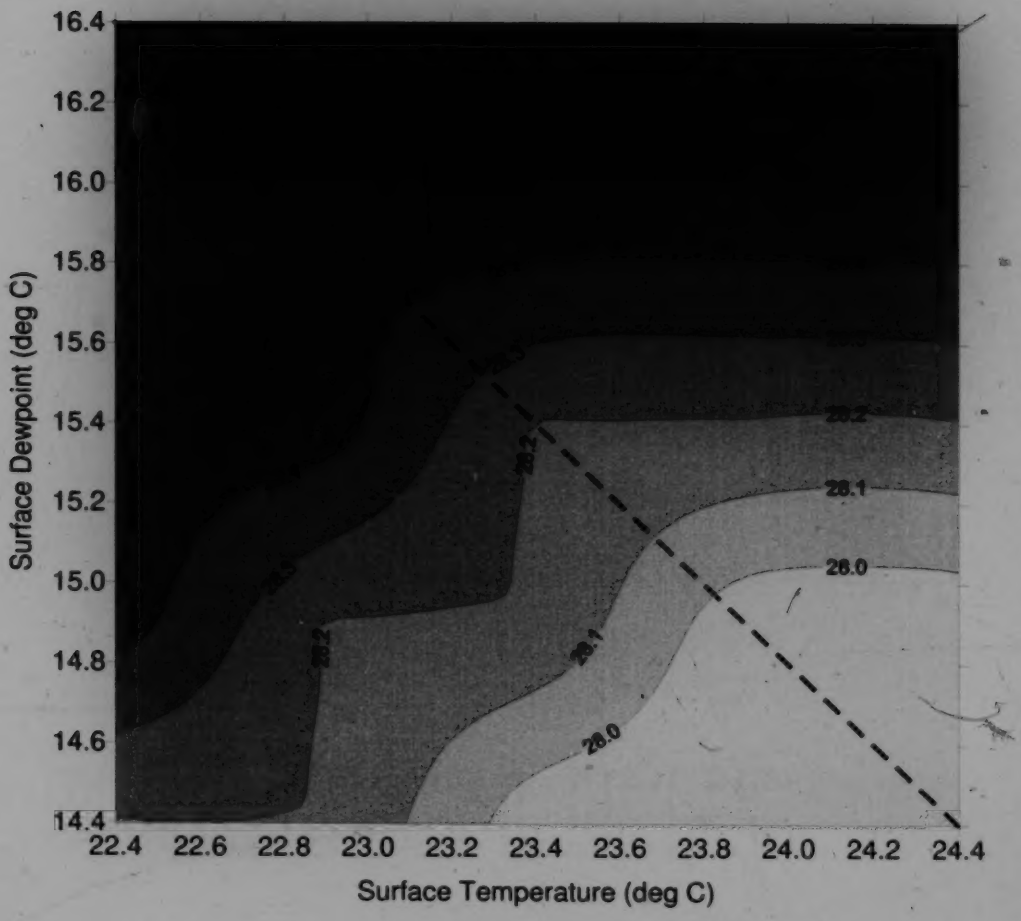

Figure 2.4: Same as for 2.3 except contours of precipitable water. The dashed line is the axis of asymmetry described in the text. For T and T_d higher than the control values, PW is only sensitive to changes in T_d. For T and T_d less than the control values PW is nearly equally dependent on changes in T and T_d.

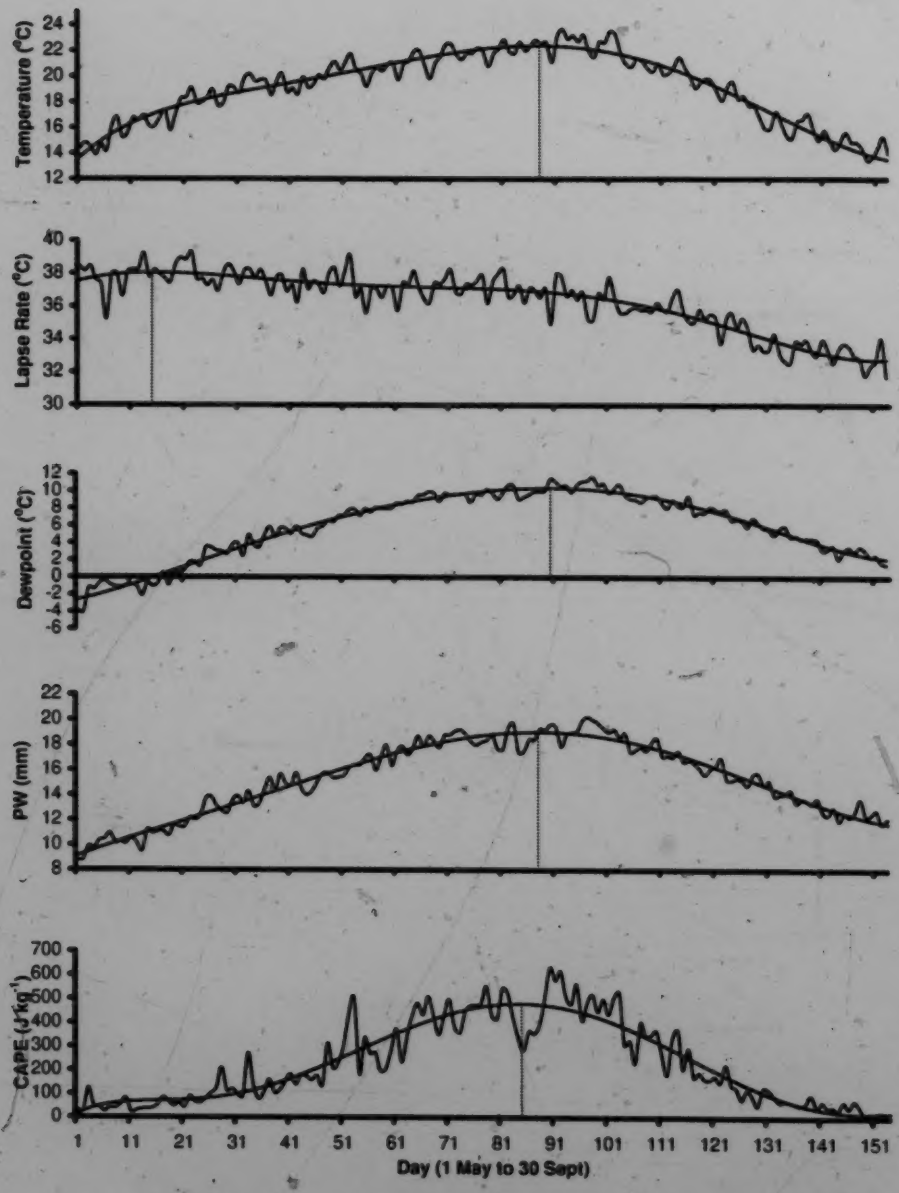

Figure 3.1: 31-year average sounding parameter value as a function of the day of the summer season (1 May to 30 September). Lapse rate refers to the ΔT_{500} data. The smooth curve is a sixth-order polynomial fitted to the data. The stippled line indicates the peak of the smooth curve.

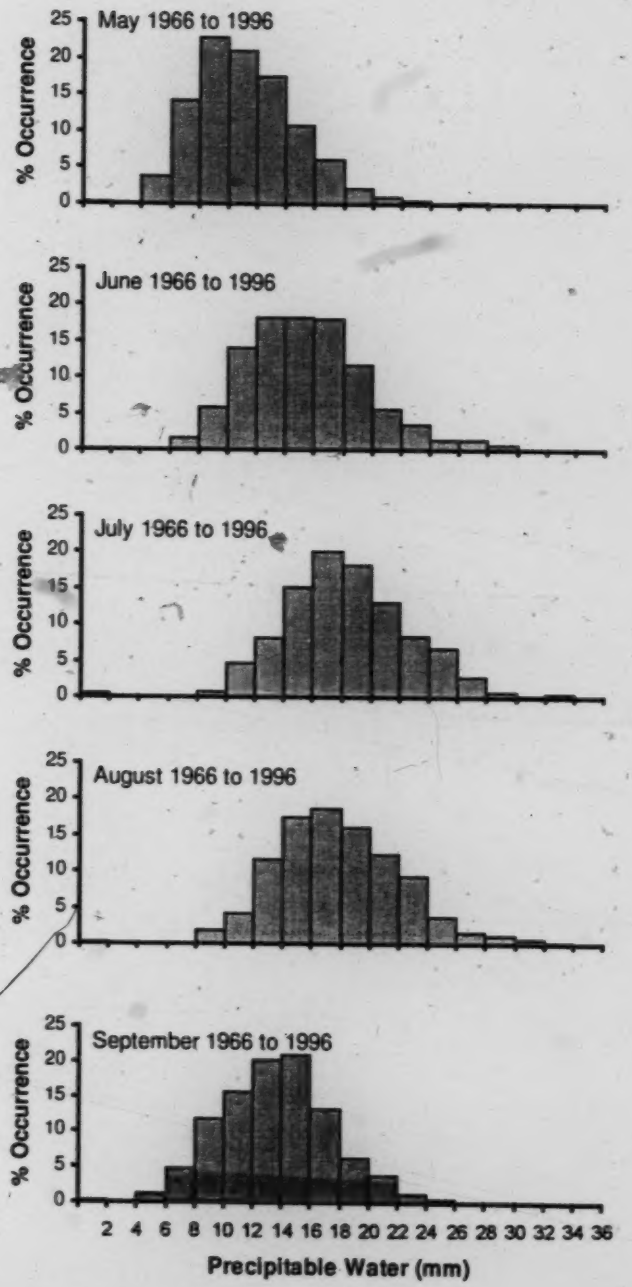

Figure 3.2: Monthly histogram distributions of precipitable water for 1 May to 30 September 1966 to 1996.

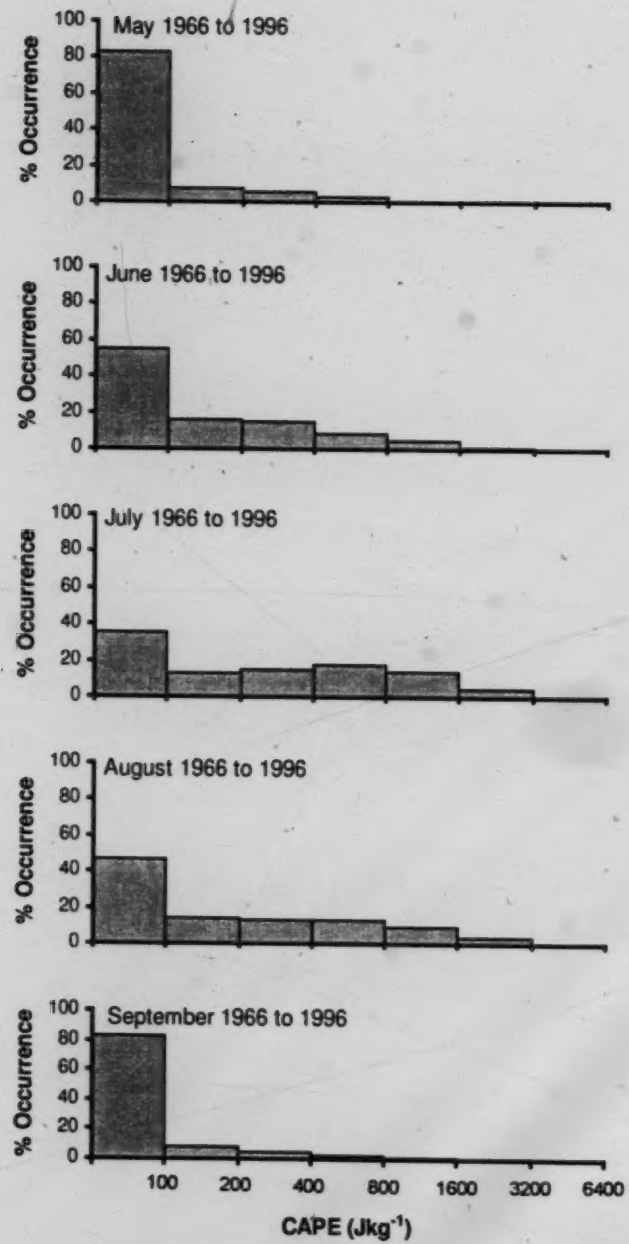

Figure 3.3: Monthly histogram distributions of CAPE for 1 May to 30 September 1966 to 1996.

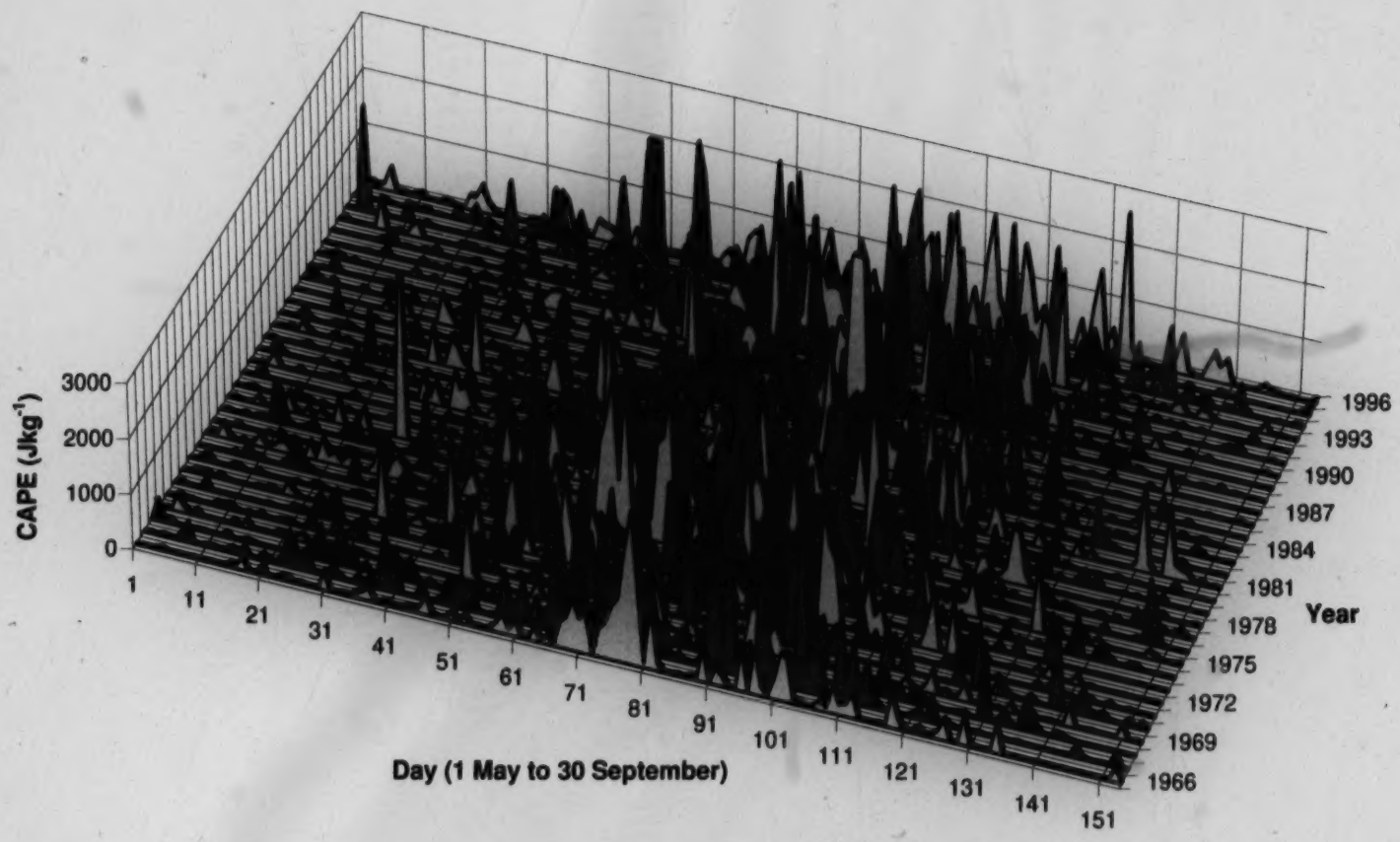

Figure 3.4: Plot of daily CAPE (Jkg^{-1}) for 1966 to 1996.

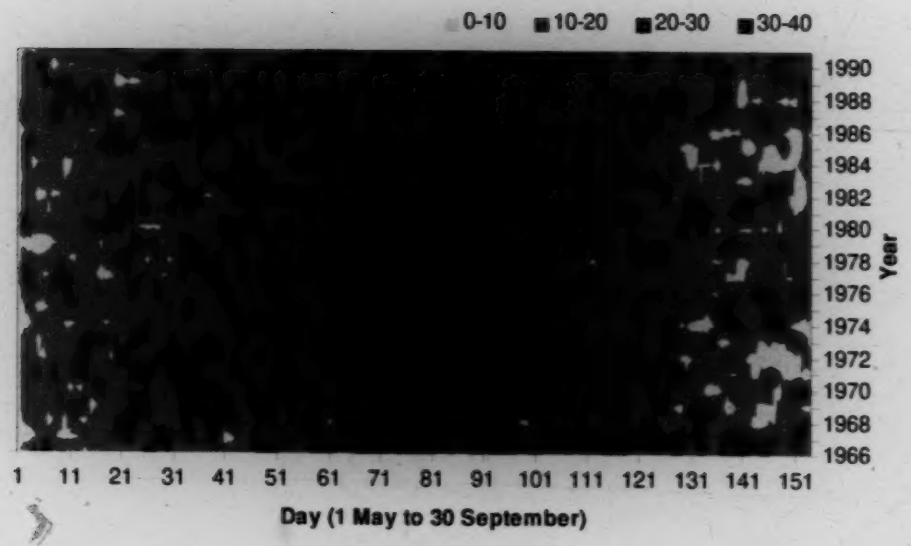

Figure 3.5: Surface plot of T_{max} (°C) for 1966 to 1991.

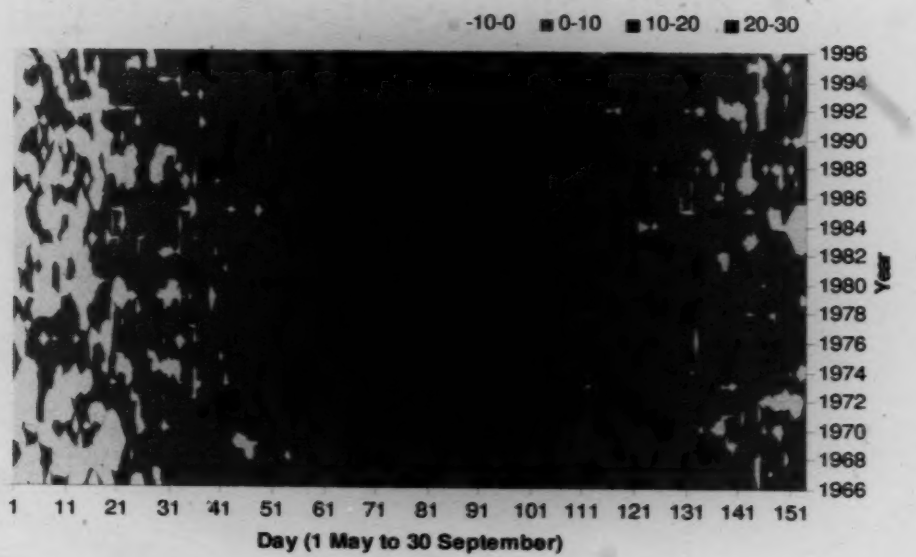

Figure 3.6: Surface plot of T_d (°C) for 1966 to 1996.

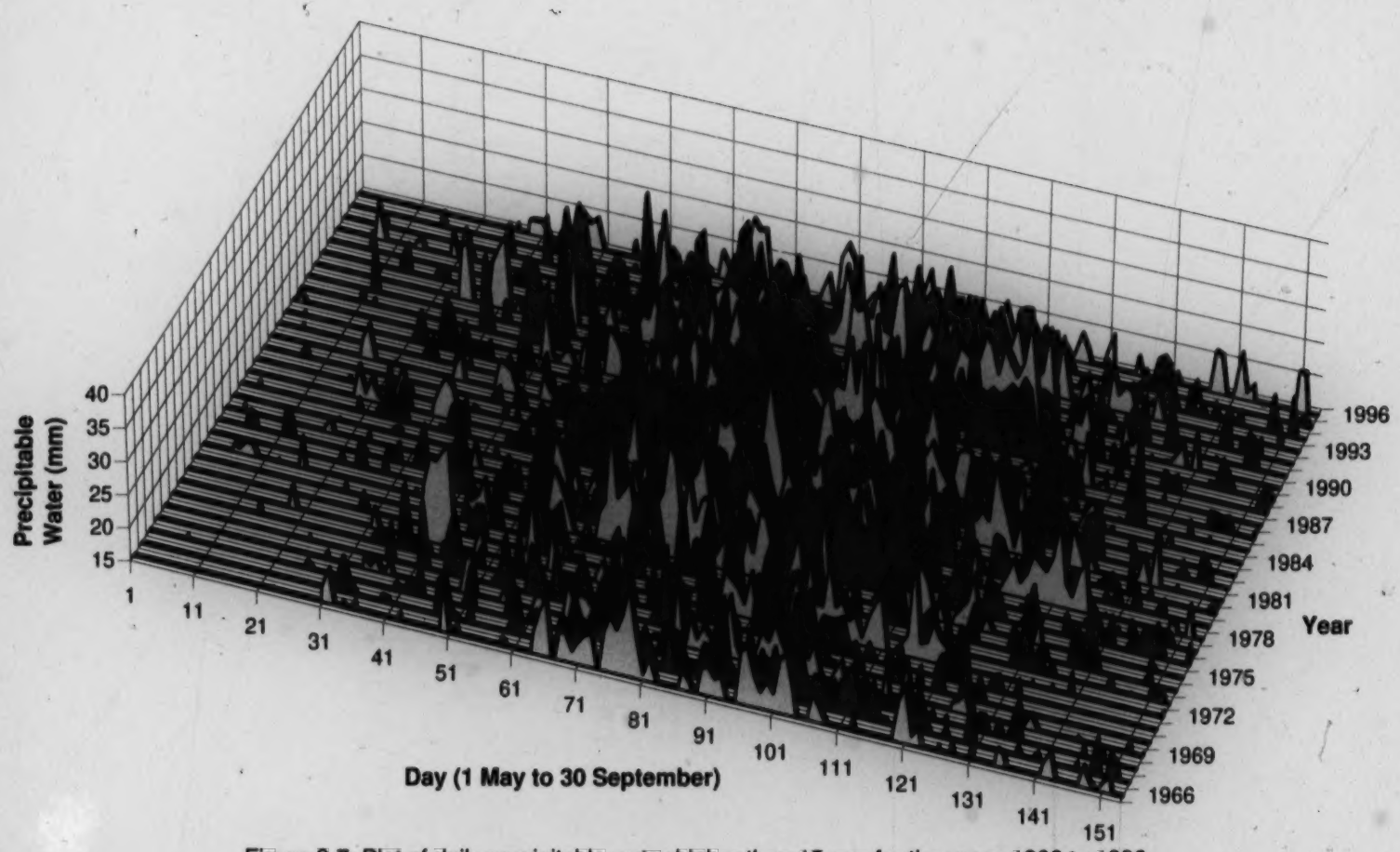

Figure 3.7: Plot of daily precipitable water higher than 15 mm for the years 1966 to 1996.

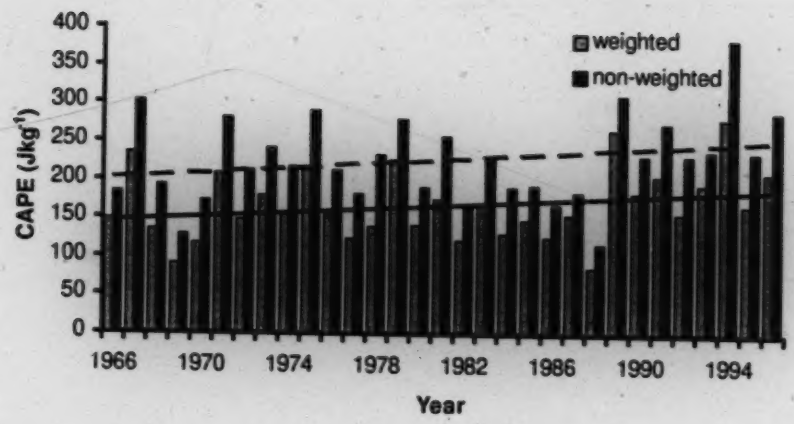

Figure 3.8: Non-weighted ($\langle CAPE \rangle_{NW}$) and weighted ($\langle CAPE \rangle_{W}$) mean annual CAPE for the years 1966 to 1996. The dashed and solid lines represent the linear regression applied to the $\langle CAPE \rangle_{NW}$ and $\langle CAPE \rangle_{W}$ data respectively.

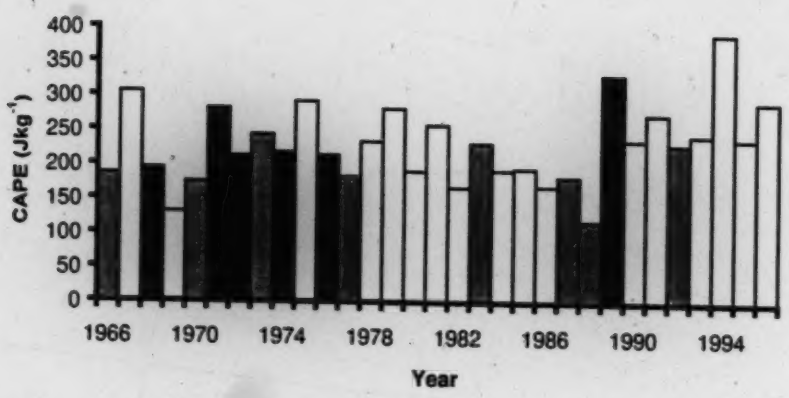

Figure 3.9: Non-weighted mean annual CAPE ($\langle CAPE \rangle_{NW}$) for El Niño (grey), La Niña (black), and neutral (white) ENSO years respectively.

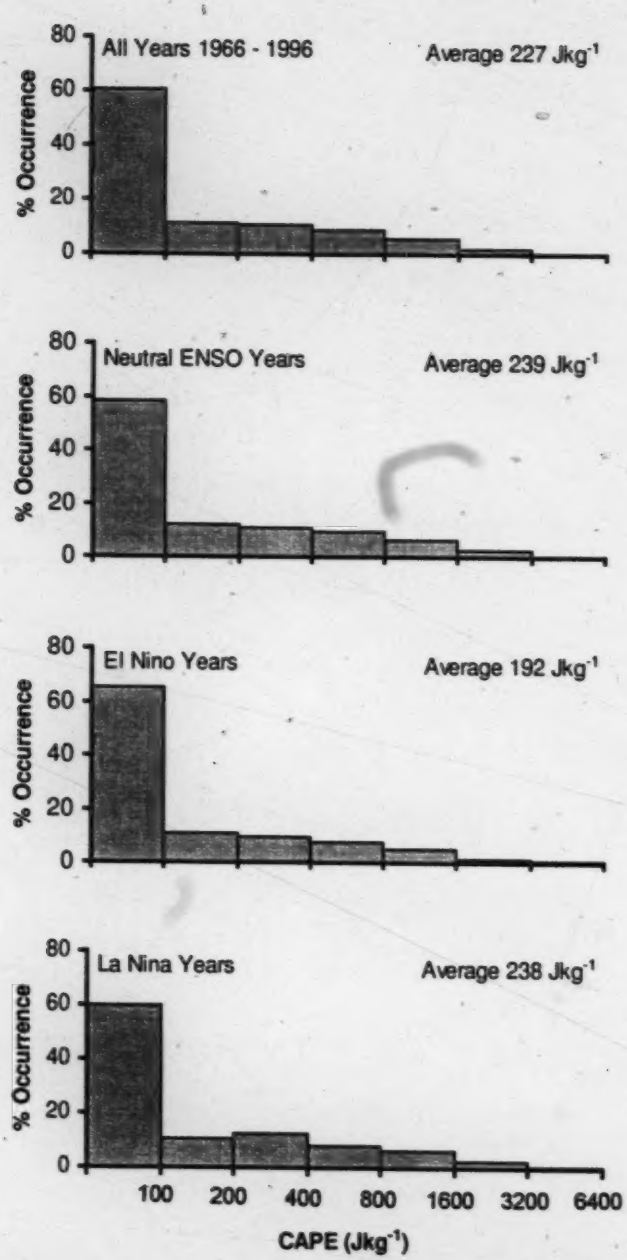

Figure 3.10: Histogram distributions for CAPE by ENSO year from 1966 to 1996 (1 May to 30 September). The average CAPE value for each distribution is shown in the upper right corner.

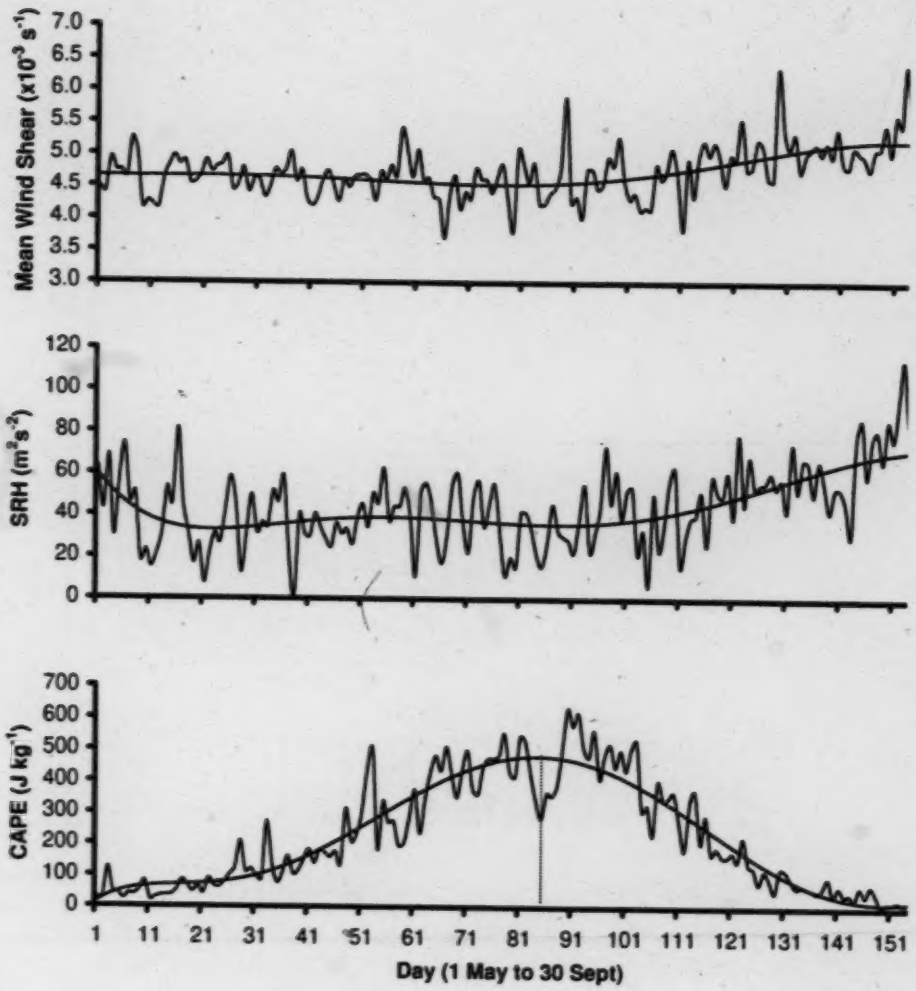

Figure 4.1: 31-year average sounding parameter value as a function of the day of the summer season (1 May to 30 September). The smooth curve is a sixth-order polynomial fitted to the data.

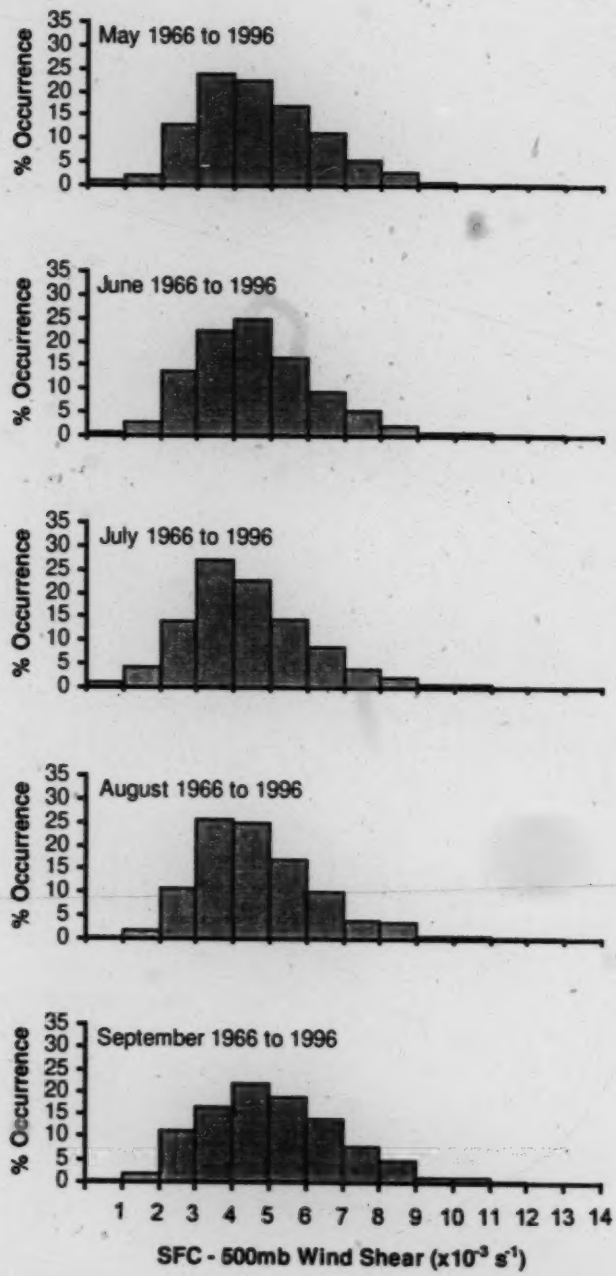

Figure 4.2: Monthly histogram distributions of SFC to 500mb mean wind shear.

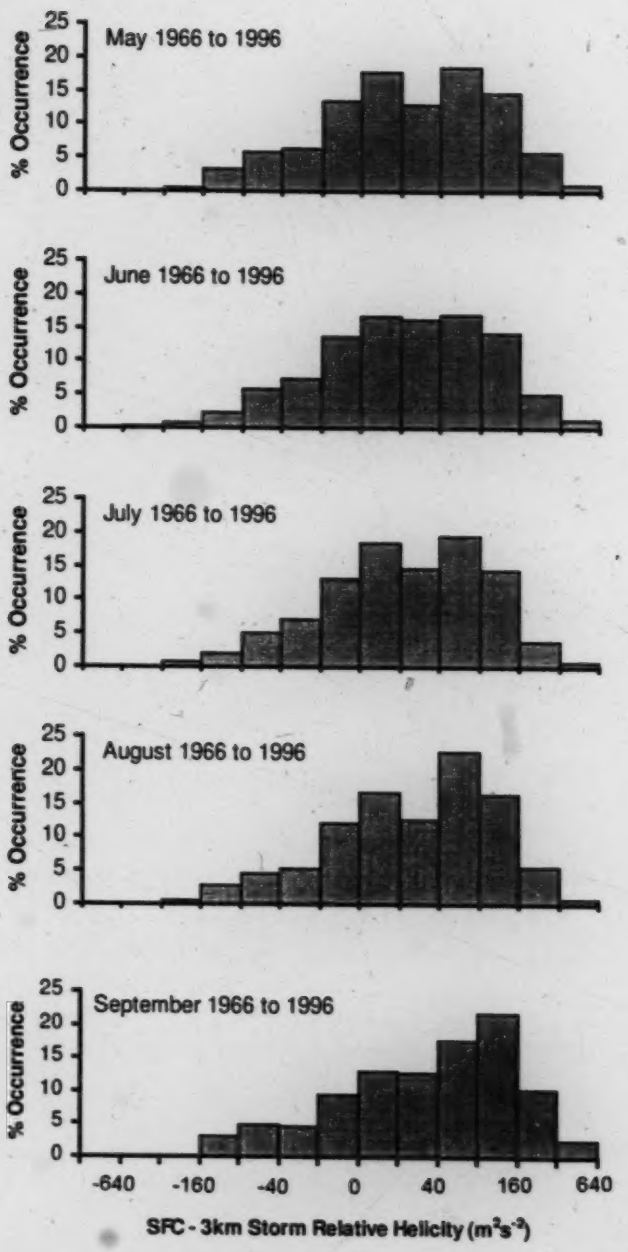

Figure 4.3: Monthly histogram distributions of SFC to 3km storm relative helicity.

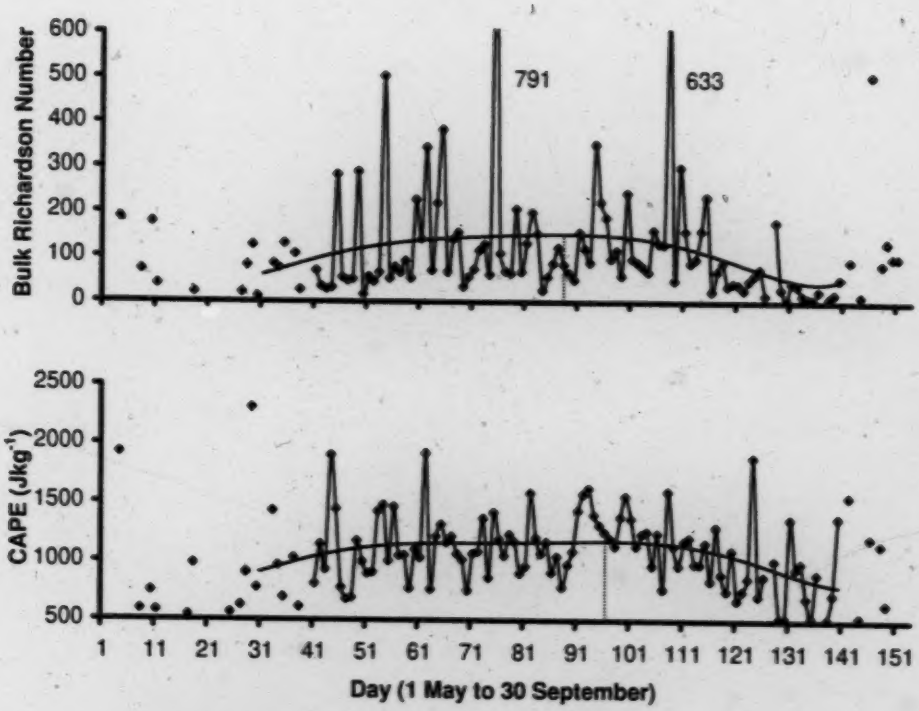

Figure 4.4: 31-year average bulk Richardson number and CAPE for soundings with CAPE≥ 500 Jkg^{-1}. The stippled line indicates the peak of the smooth curve.

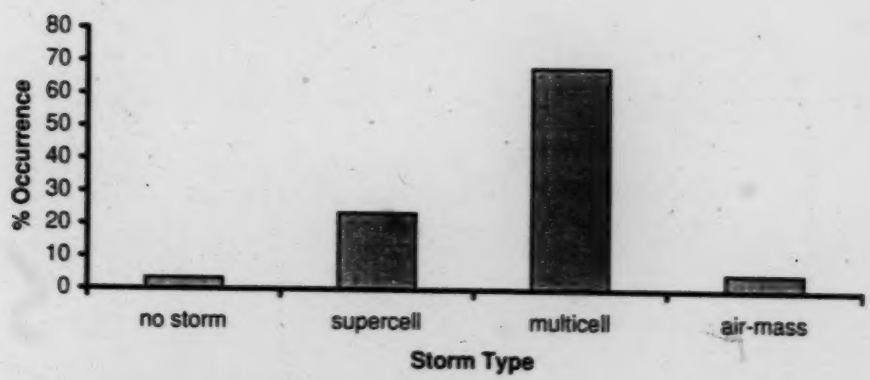

Figure 4.5: Histogram of bulk Richardson number according to storm type based on 119 mean daily R values with CAPE≥ 500 Jkg^{-1}.

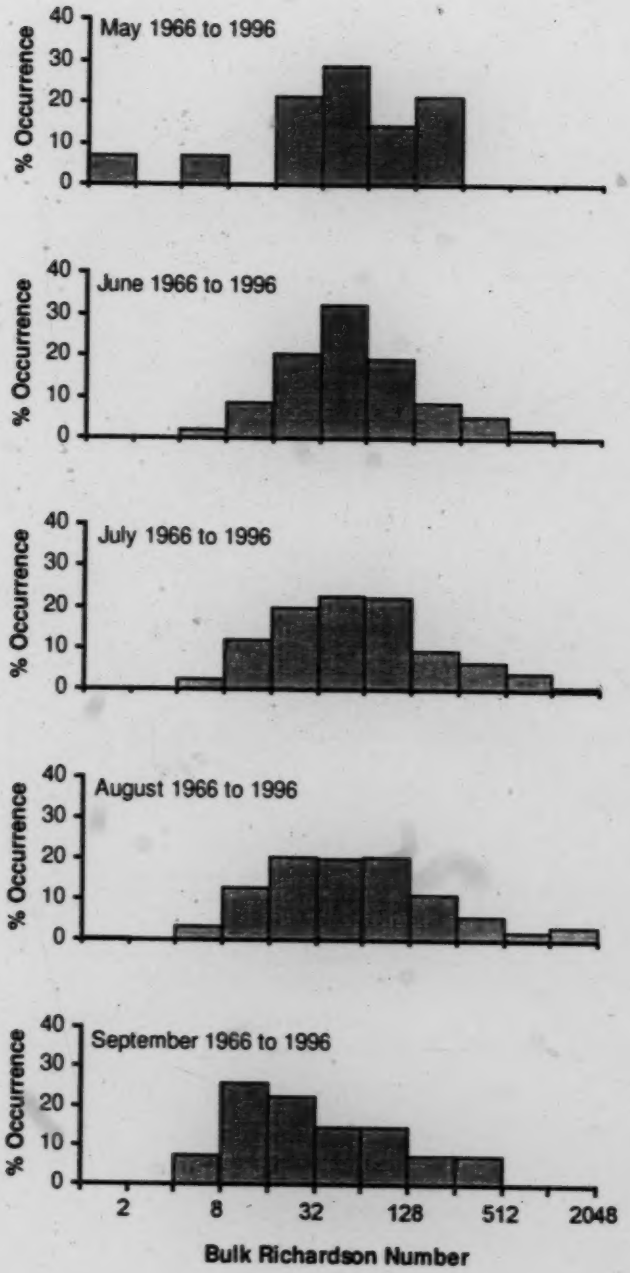

Figure 4.6: Monthly histogram distributions of bulk Richardson number.

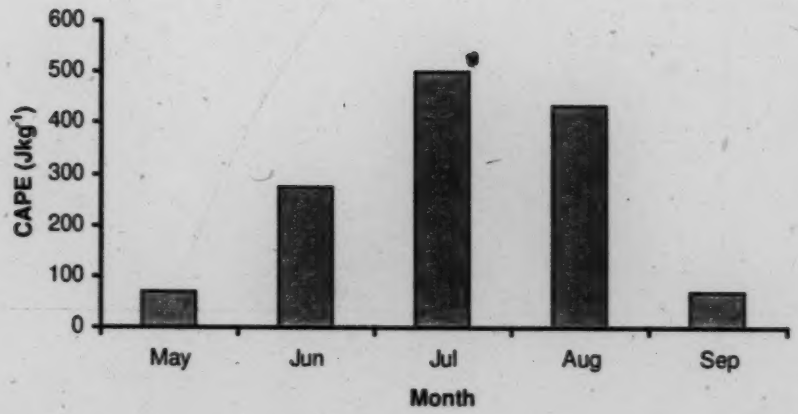

Figure 5.1: Average of daily CAPE for each month from 1990 to 1996.

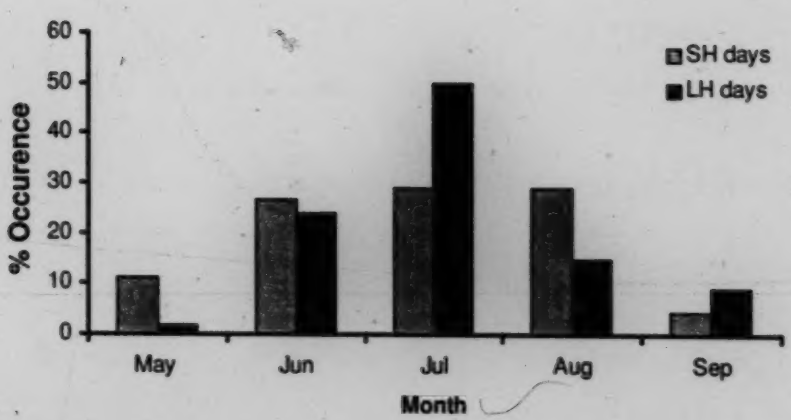

Figure 5.2: Percent occurrence of Small Hail (SH) and Large Hail (LH) days by month from 1990 to 1996.

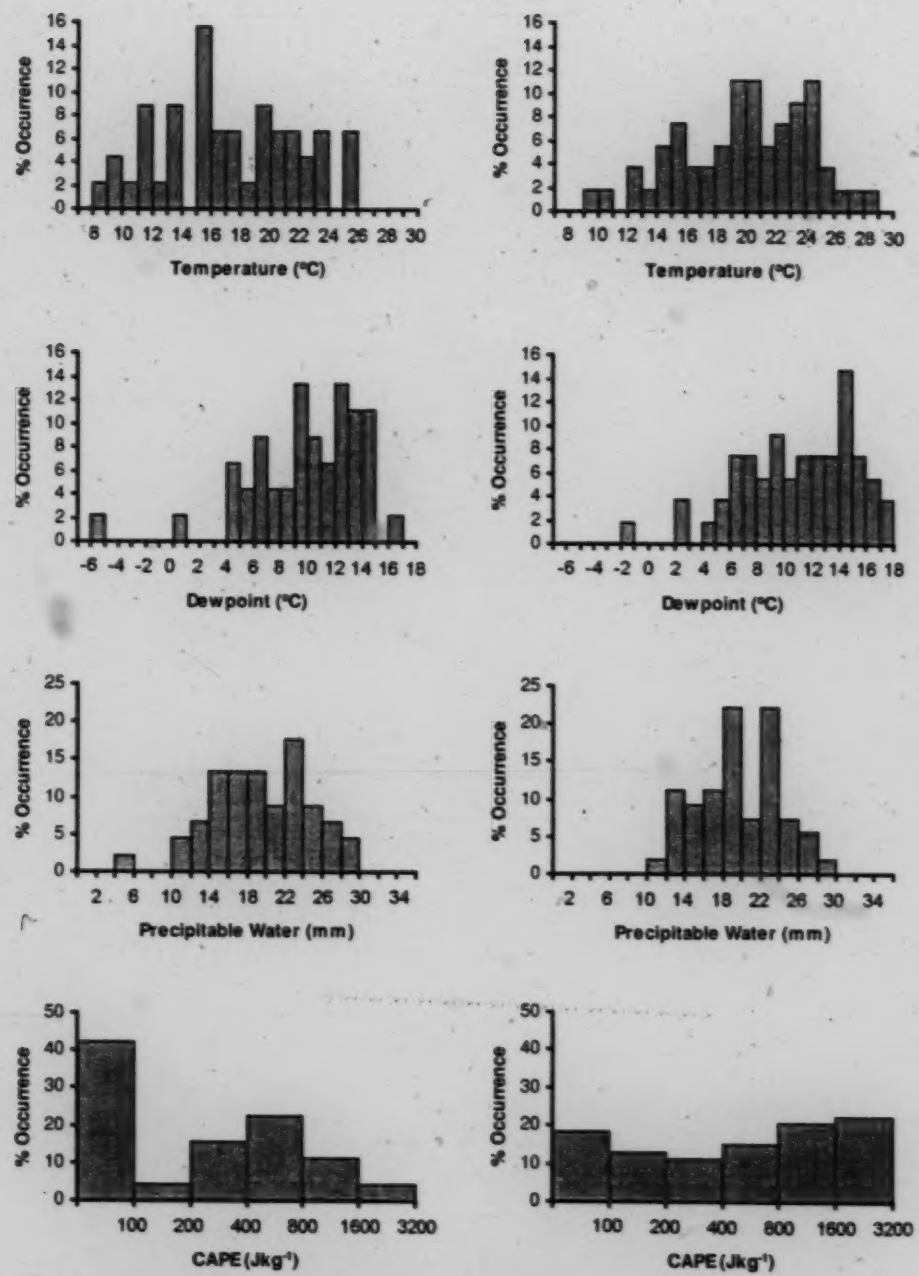

Figure 5.3: Histograms of surface temperature and dewpoint, precipitable water, and CAPE for 45 small hail (left column) and 54 large hail (right column) days from 1990 to 1996.

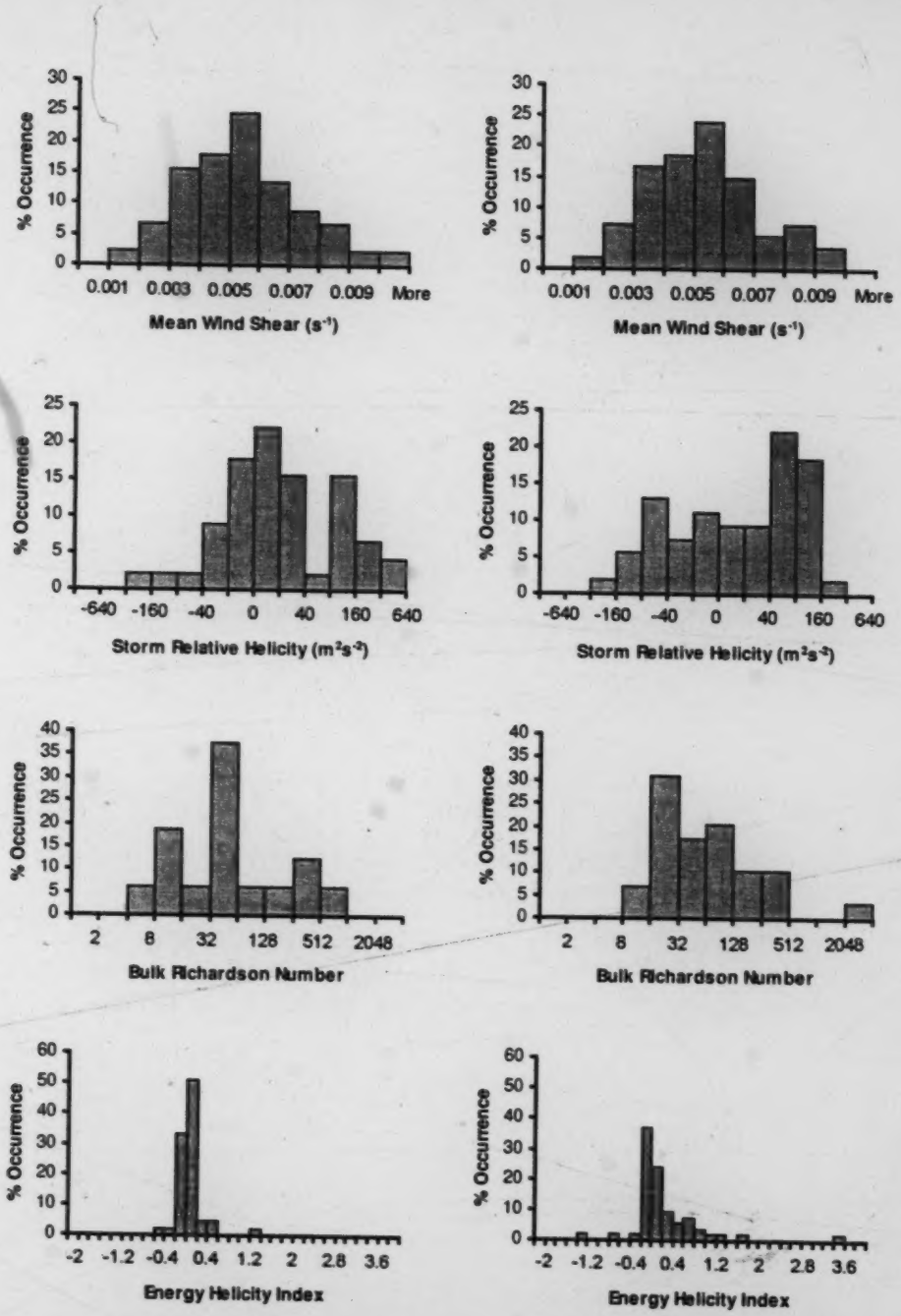
% Occurrence
Mean Wind Shear (s⁻¹)
0.001 0.003 0.005 0.007 0.009 More
Storm Relative Helicity (m²s⁻²)
-640 -160 -40 0 40 160 640
Bulk Richardson Number
2 8 32 128 512 2048
Energy Helicity Index
-2 -1.2 -0.4 0.4 1.2 2 2.8 3.6

Figure 5.4: Histograms of mean wind shear, storm relative helicity, bulk Richardson number, and energy helicity index for 45 small hail (left column) and 54 large hail (right column) days from 1990 to 1996.

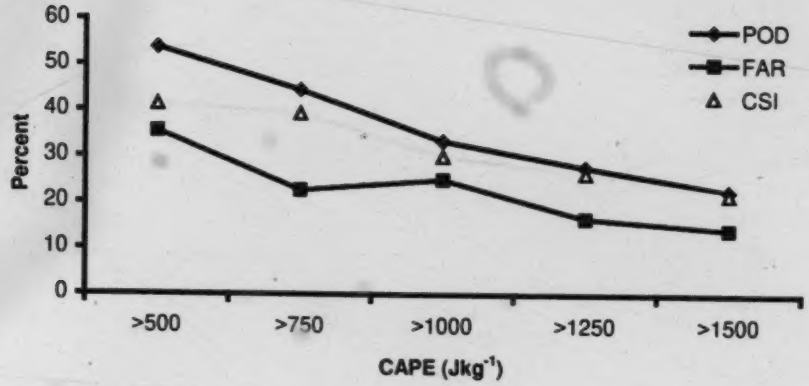

Figure 5.5: POD, FAR, and CSI (in percent) for different CAPE threshold values.

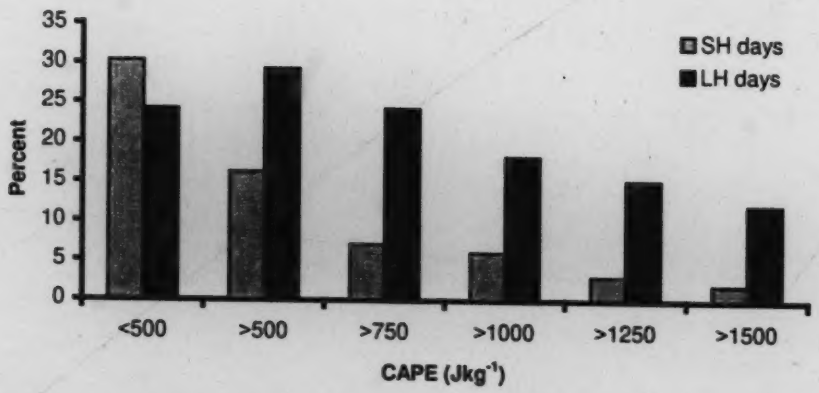

Figure 5.6: Histogram showing the percent of 99 Small Hail (SH) and Large Hail (LH) severe days detected using each CAPE threshold.

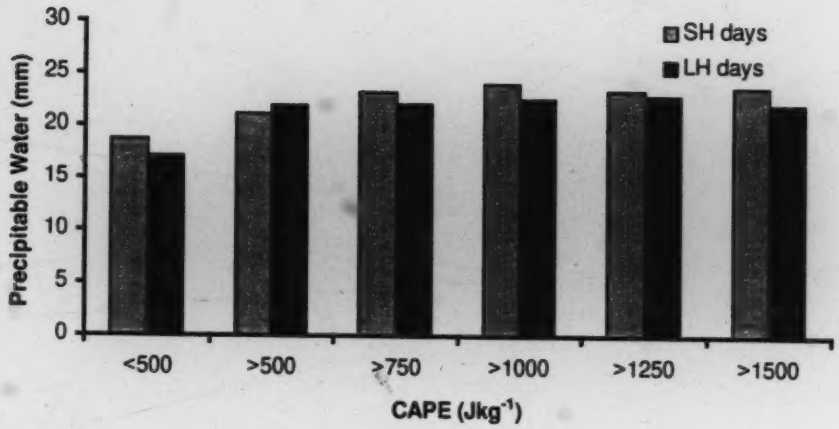

Figure 5.7: Histogram showing the distribution of precipitable water for Small Hail (SH) and Large Hail (LH) days for each CAPE threshold.

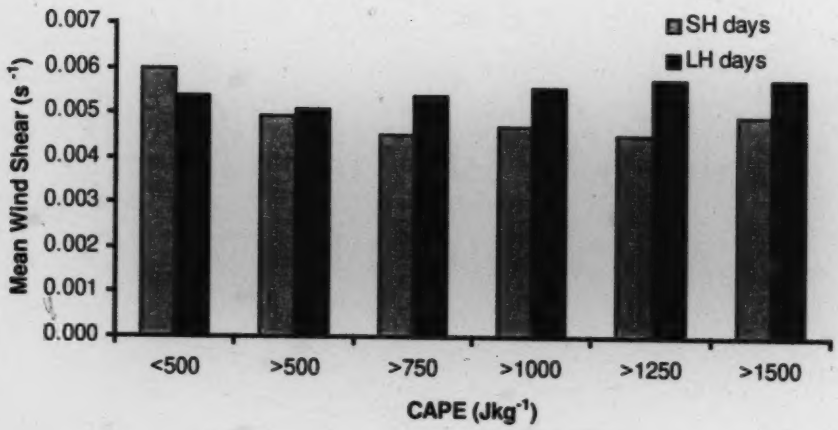

Figure 5.8: Same as Fig. 5.7 but for mean wind shear.

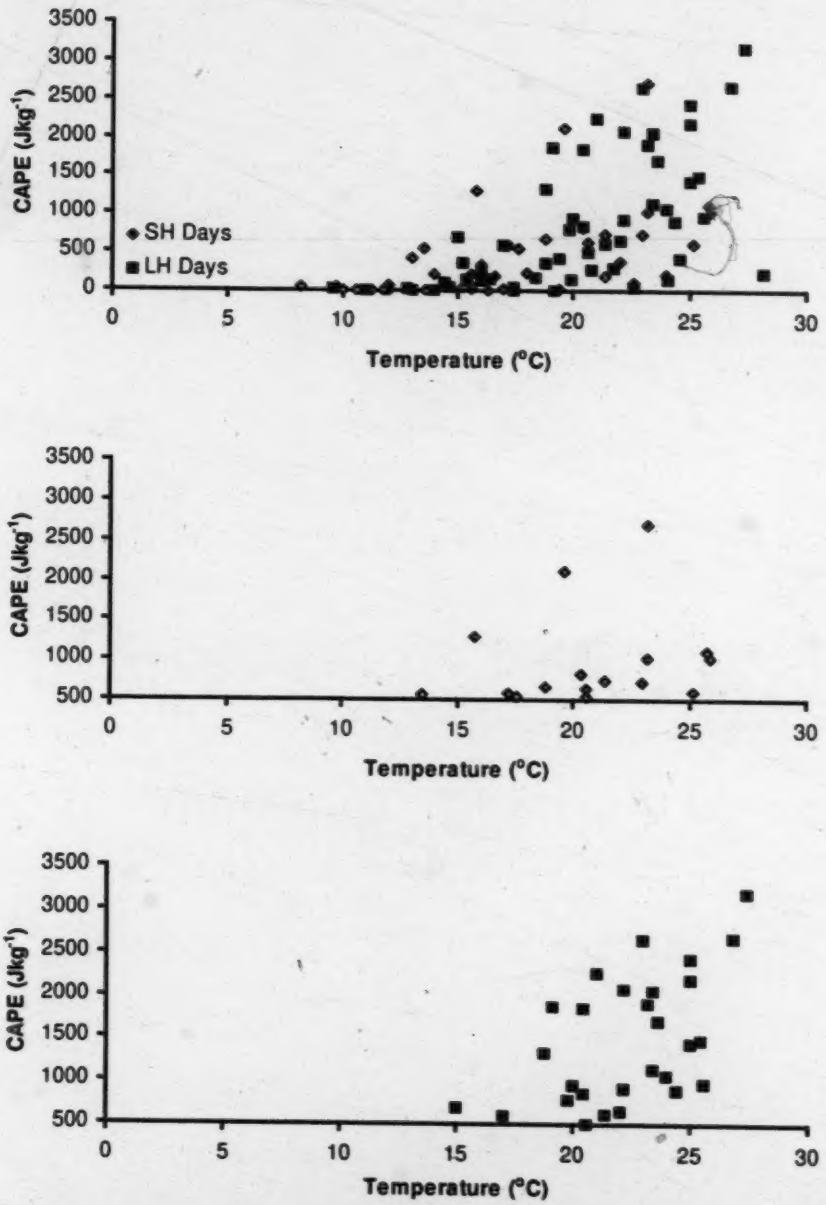

Figure 5.9: Scatter plot of CAPE and surface temperature for Small Hail (SH) and Large Hail (LH) days from 1990 to 1996 (Top). Below are plots of the same data set separated into SH and LH days for CAPE ≥ 500 Jkg^{-1}.

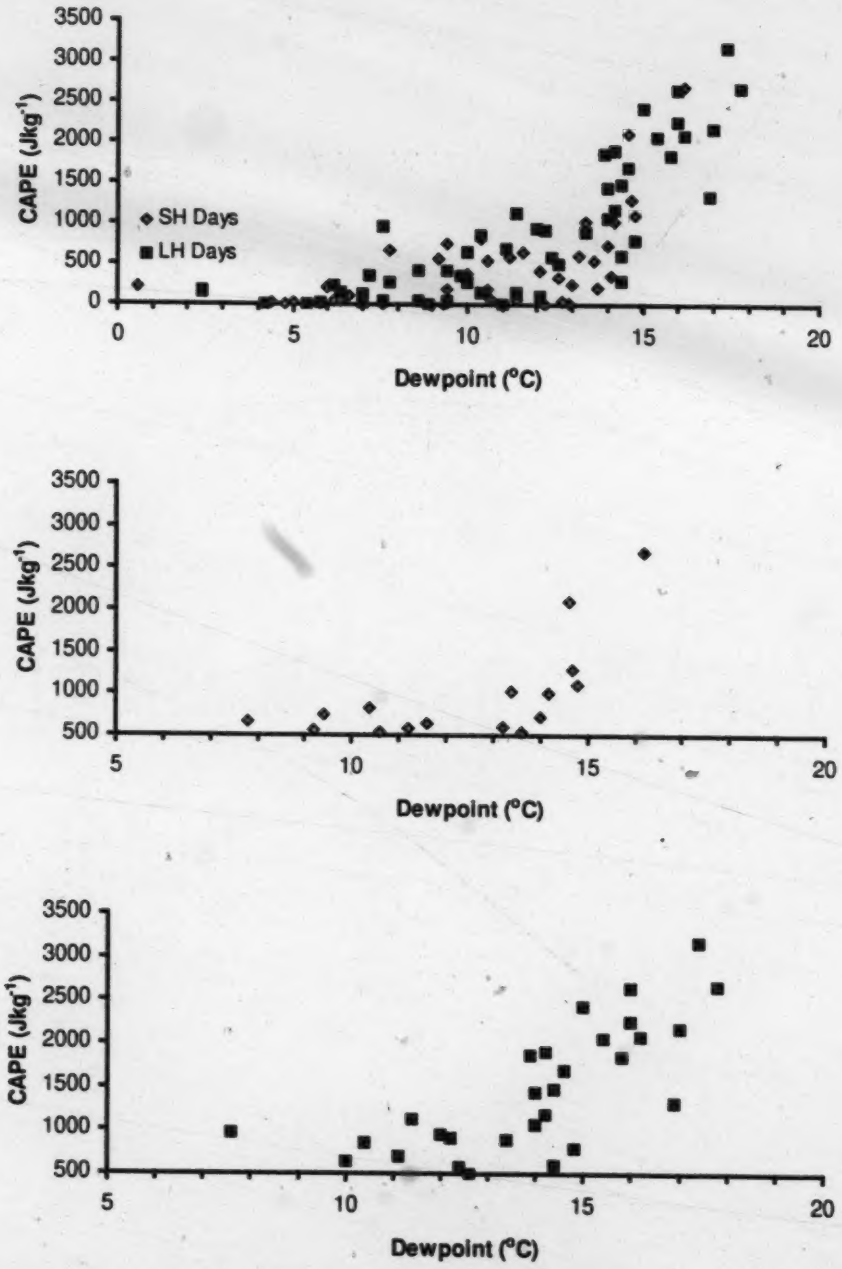

Figure 5.10: Same as 5.9 but for CAPE and surface dewpoint.

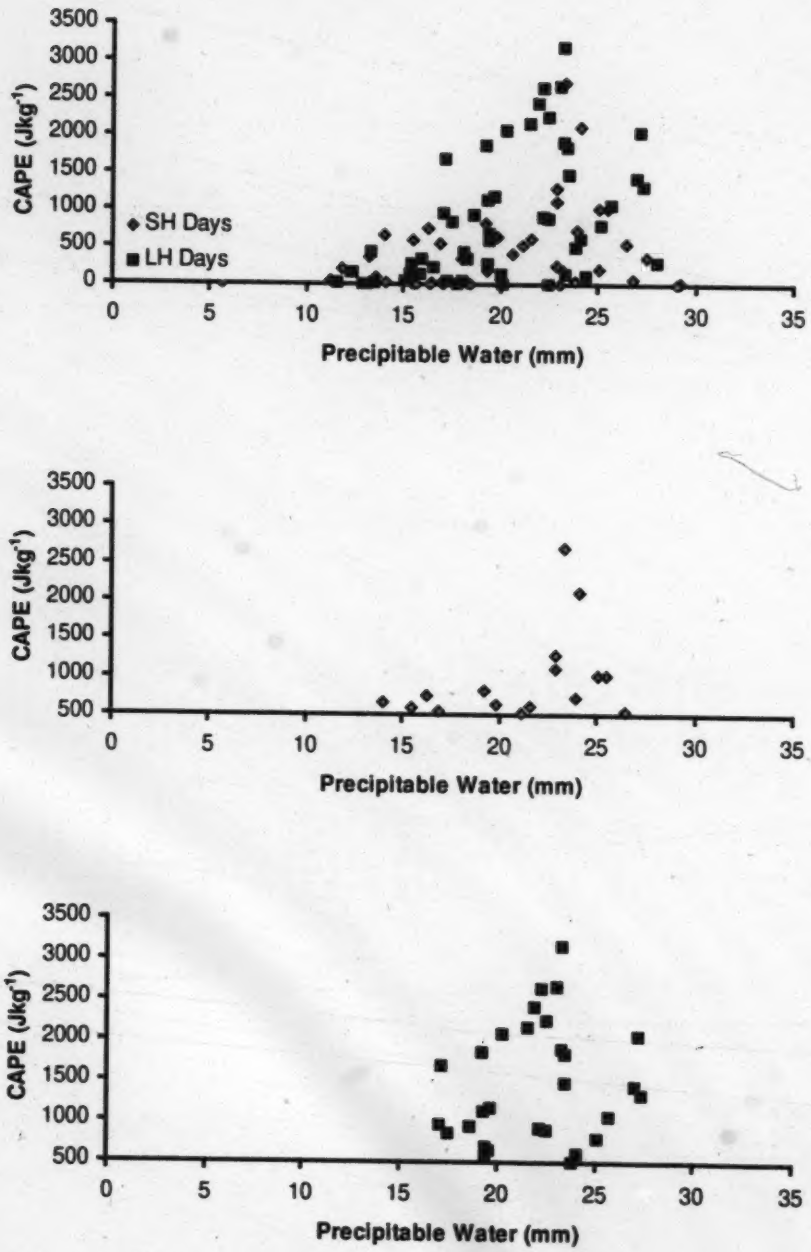

Figure 5.11: Same as 5.9 but for CAPE and precipitable water.

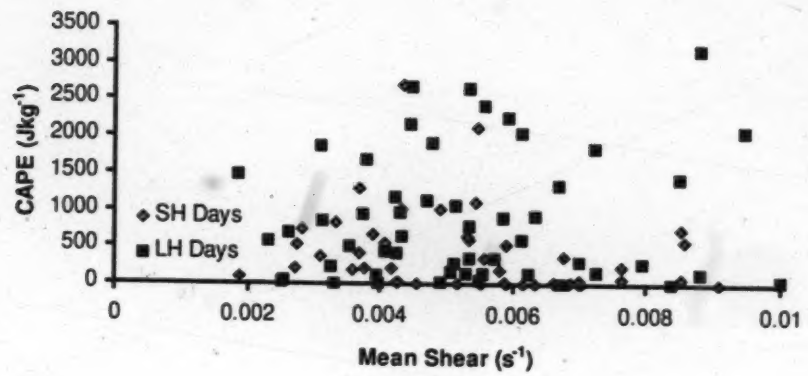

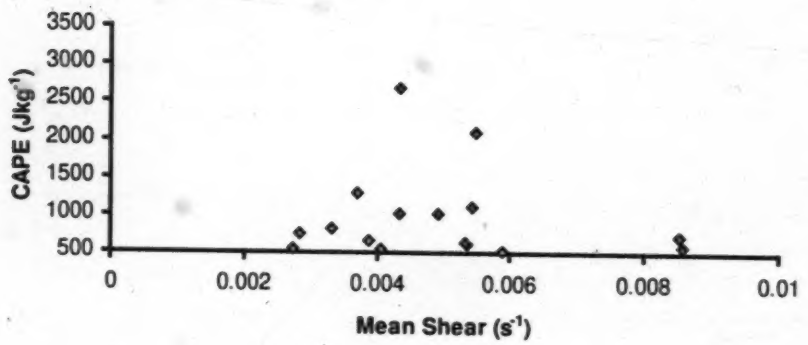

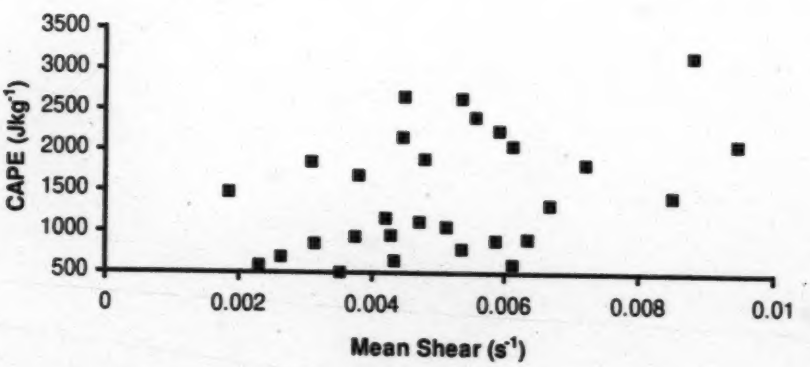

Figure 5.12: Same as 5.9 but for CAPE and mean wind shear.

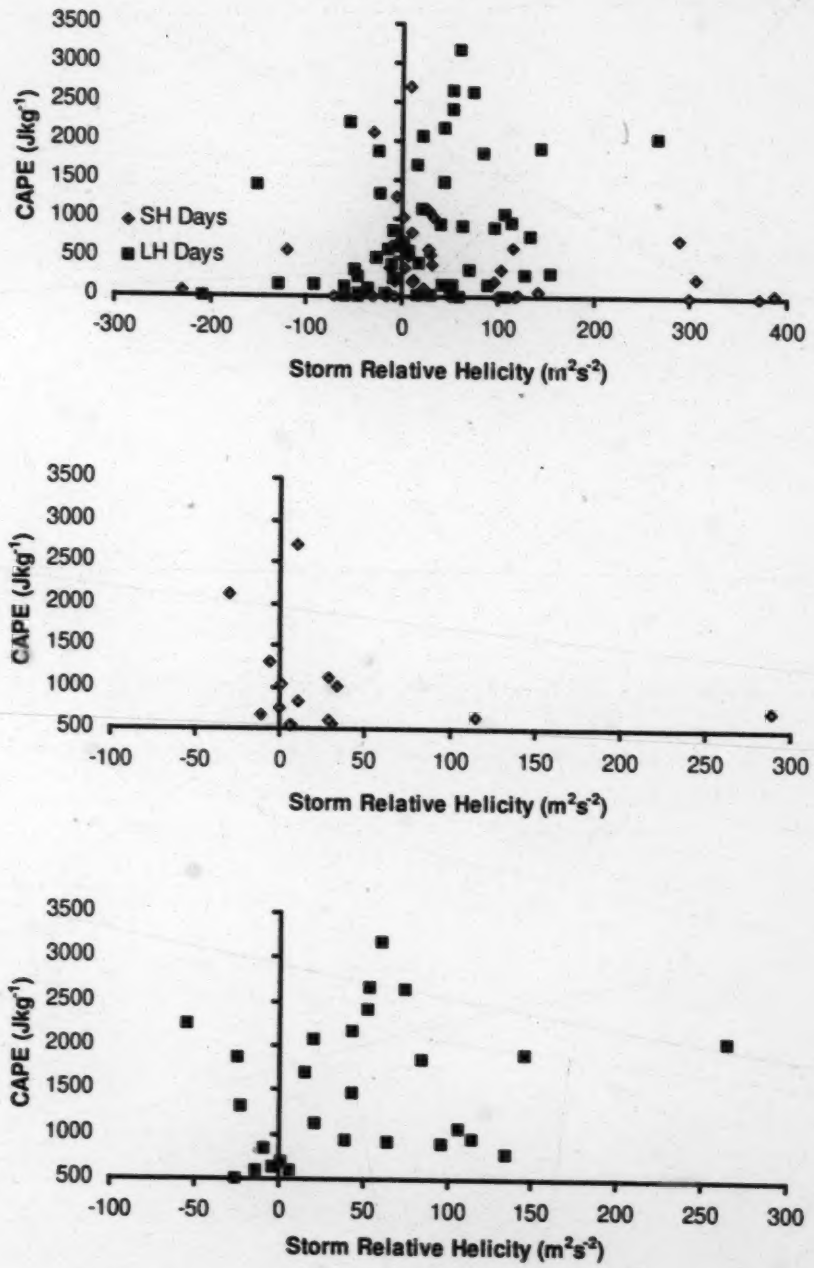

Figure 5.13: Same as 5.9 but for CAPE and storm relative helicity. The SRH axis is changed in the lower two figures to increase resolution.

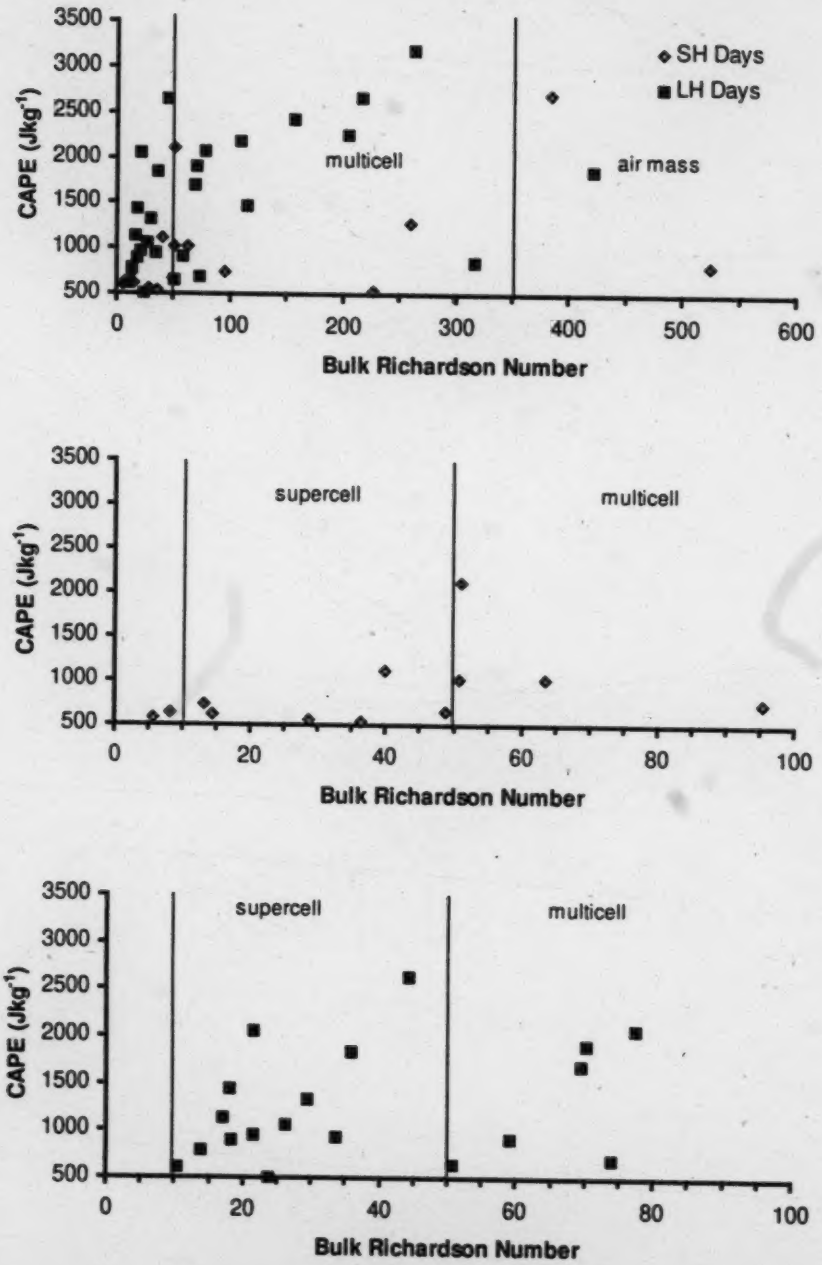

Figure 5.14: Same as 5.9 but for CAPE and bulk Richardson number derived storm type as indicated on the plots for supercell (10-50), multicell (50-350) and air mass (>350) thunderstorms. The bulk Richardson number axis is changed in the lower two figures to increase resolution.

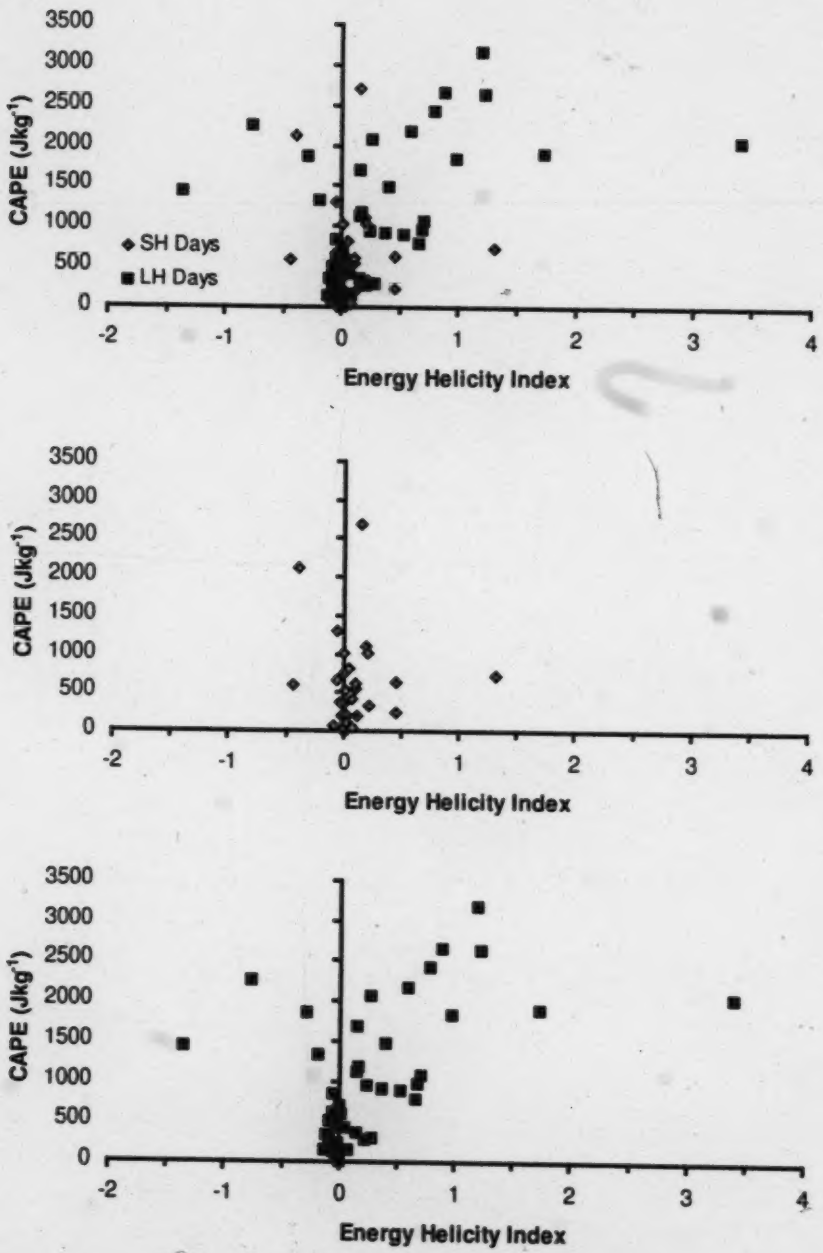

Figure 5.15: Same as 5.9 but for CAPE and energy helicity index.

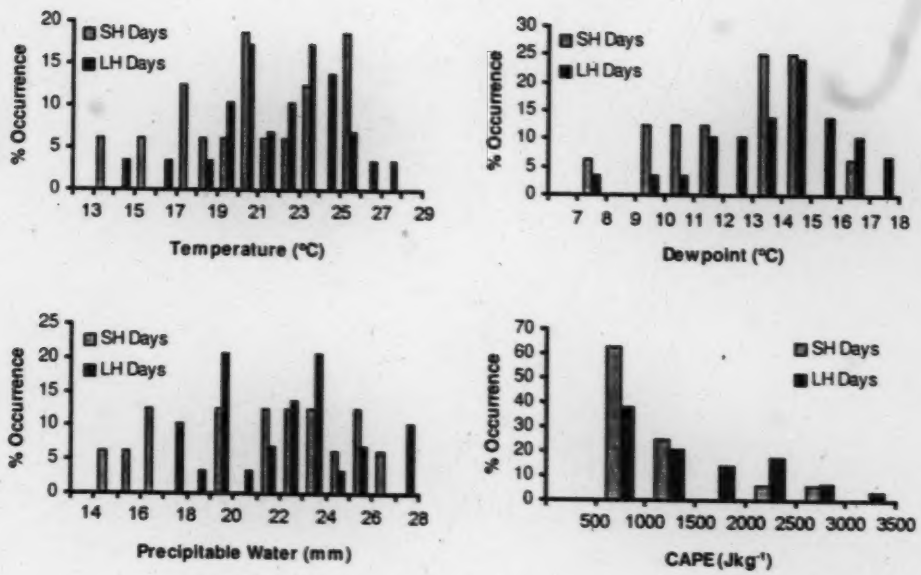

Figure 5.16:Histograms of surface temperature and dewpoint, precipitable water, and CAPE for Small Hail (SH) and Large Hail (LH) days with CAPE ≥ 500 Jkg^{-1} during 1990 to 1996.

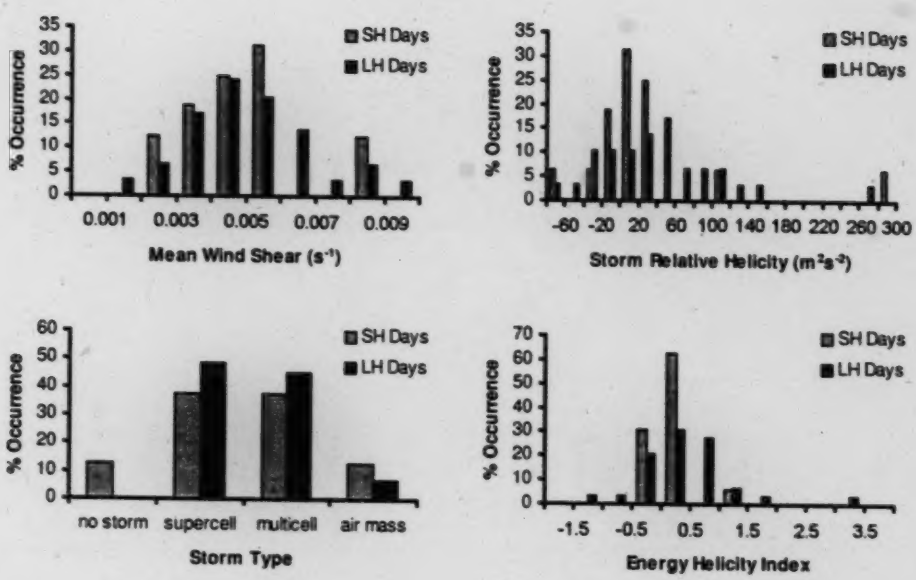
% Occurrence
SH Days
LH Days
0.001 0.003 0.005 0.007 0.009
Mean Wind Shear (s⁻¹)
-60 -20 20 60 100 140 180 220 260 300
Storm Relative Helicity (m²s⁻²)
no storm supercell multicell air mass
Storm Type
-1.5 -0.5 0.5 1.5 2.5 3.5
Energy Helicity Index

Figure 5.17: Histograms of mean wind shear, storm relative helicity, bulk Richardson number derived storm type and energy helicity index for Small Hail (SH) and Large Hail (LH) days with CAPE ≥ 500 Jkg^{-1} during 1990 to 1996.

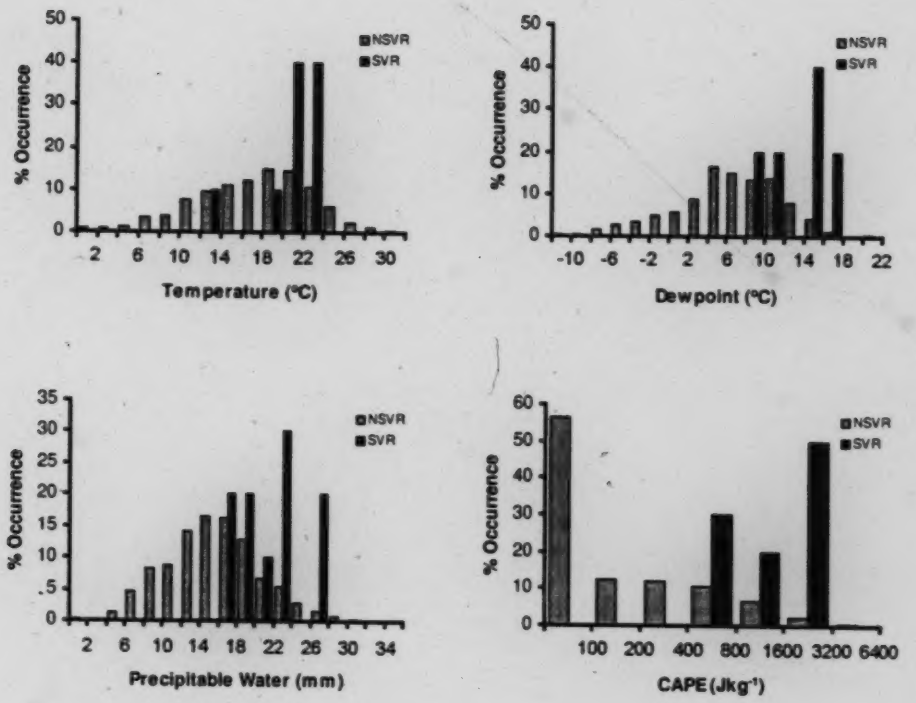

Figure 6.1: Histograms of temperature, dewpoint, precipitable water, and CAPE for severe (SVR) and non-severe (NSVR) days from 1990 to 1996.

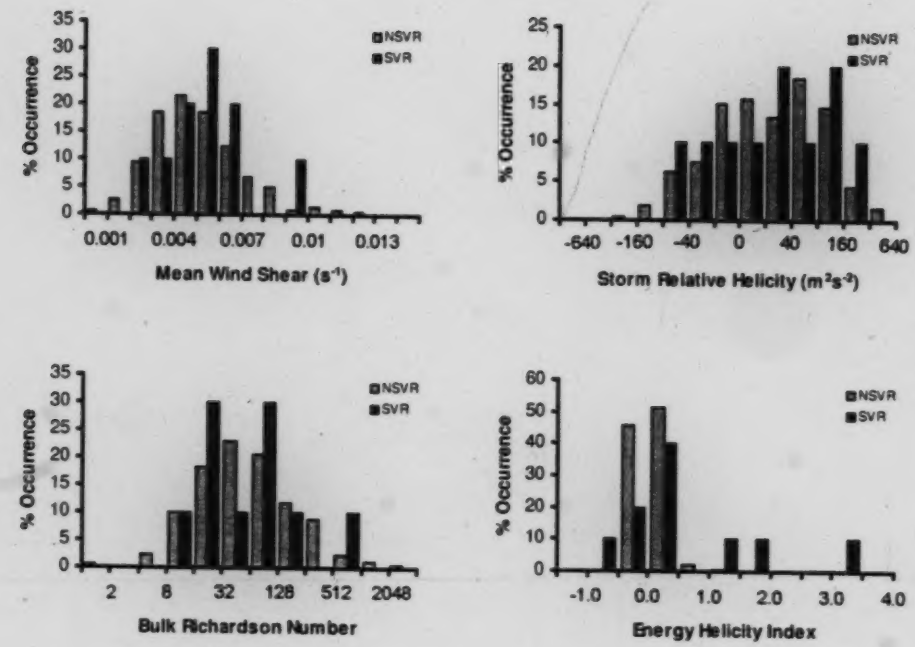

Figure 6.2: Histograms of mean wind shear, storm relative helicity, bulk Richardson number and energy helicity index for severe (SVR) and non-severe (NSVR) days from 1990 to 1996.

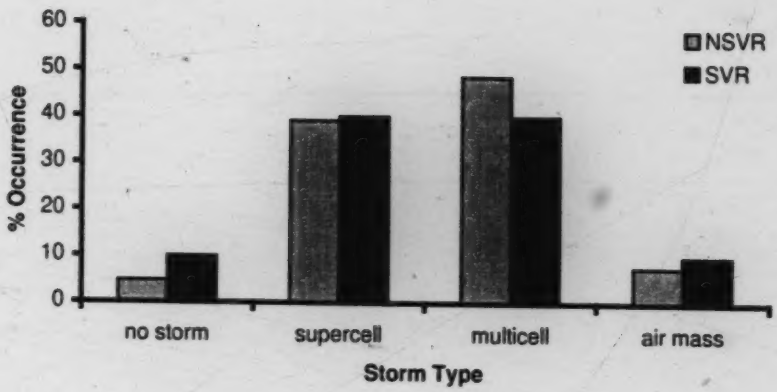

Figure 6.3: Histogram of bulk Richardson number-derived storm type for severe (SVR) and non-severe (NSVR) days from 1990 to 1996.

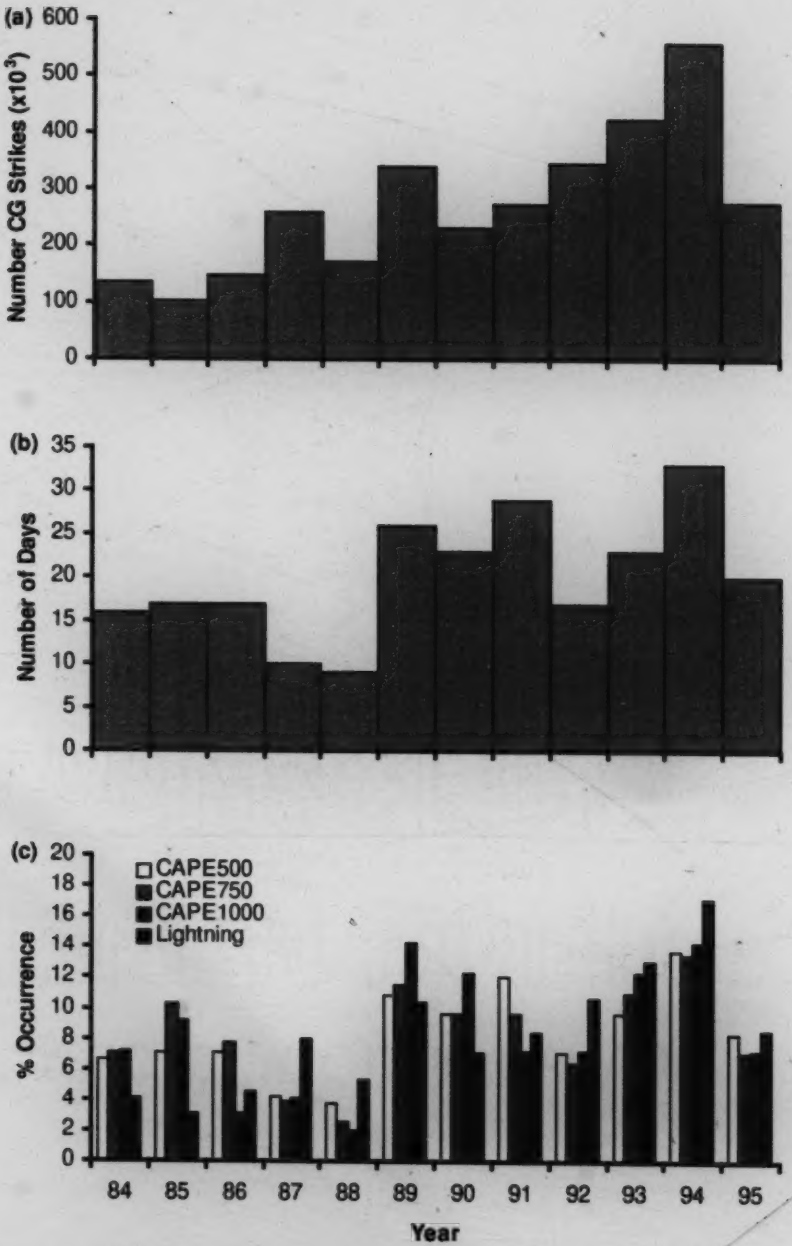

Figure 7.1: (a) Distribution of the number of cloud to ground (CG) lightning strikes from 1984 to 1995 in Alberta. (b) Number of days with CAPE ≥ 500 Jkg^{-1} for Stony Plain soundings during the same period and, (c) Number of days exceeding CAPE thresholds (500 Jkg^{-1}, 750 Jkg^{-1}, and 1000 Jkg^{-1}) and number of CG strikes as percent occurrence.

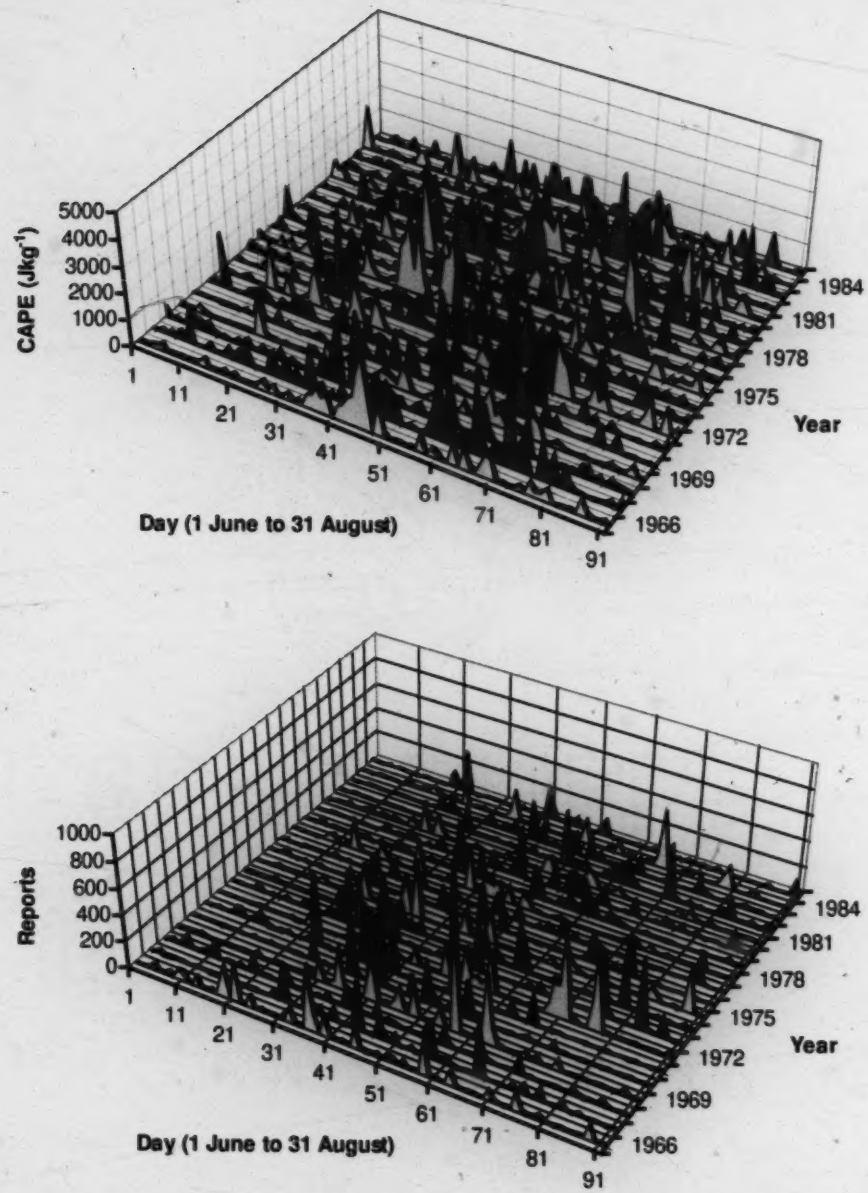

Figure 7.2: Daily CAPE from Stony Plain soundings from 1 June to 31 August for the years 1966 to 1985 (Top). Number of hail reports from Alberta Hail Project data for the same period (Bottom).

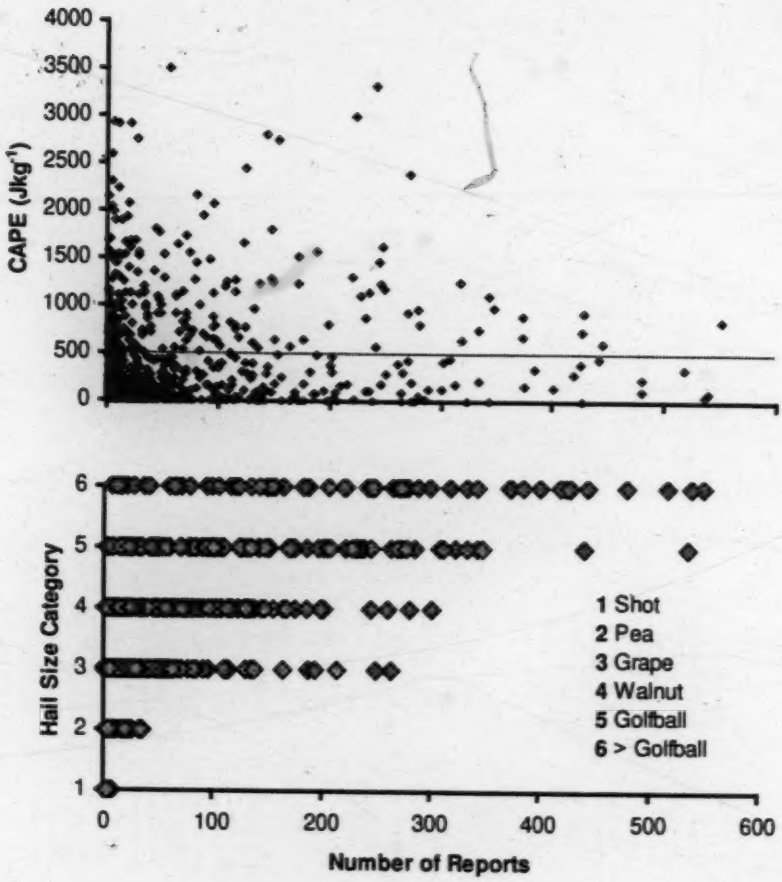

Figure 7.3: Scatter plot of CAPE and the number of hail reports (NR) for severe hail days (1 June to 31 August) during the Alberta Hail Project from 1966 to 1985 (Top). Scatter plot of maximum hail size category and the total number of hail reports for the same period (Bottom).

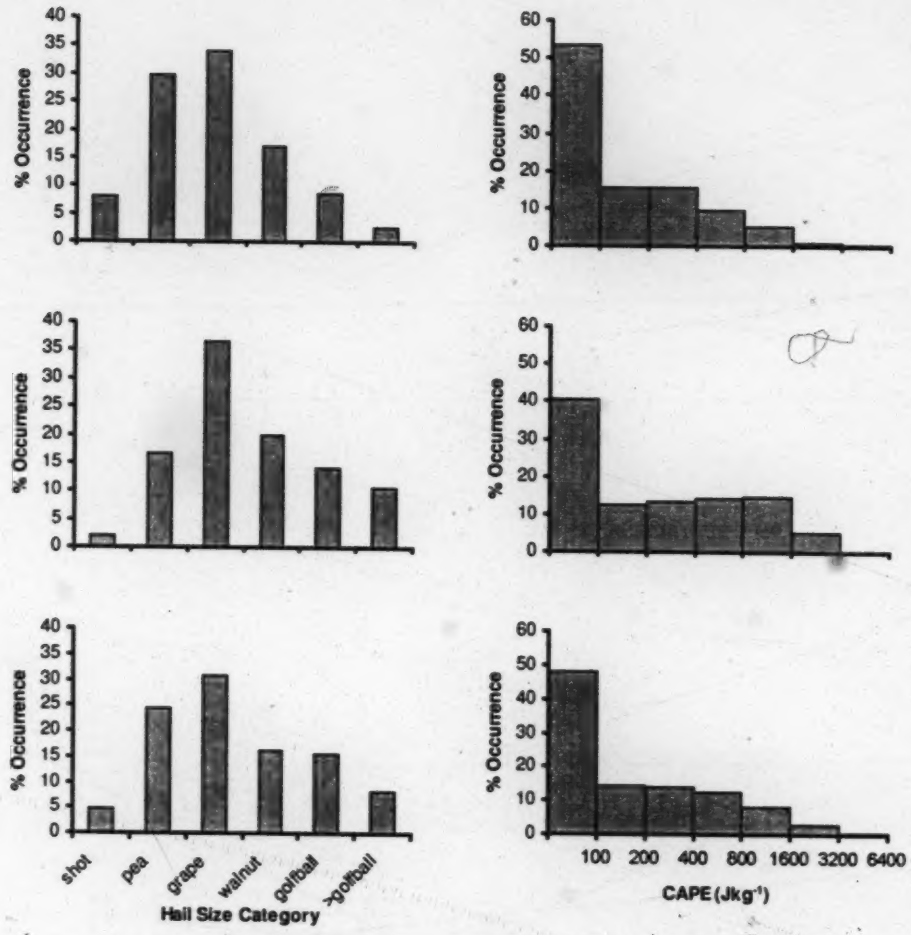

Figure 7.4: Histograms of maximum hail size category (Left) and CAPE (Right) for June (Top), July (Middle), and August (Bottom) using Alberta Hail Project data and Stony Plain soundings from 1966 to 1985.

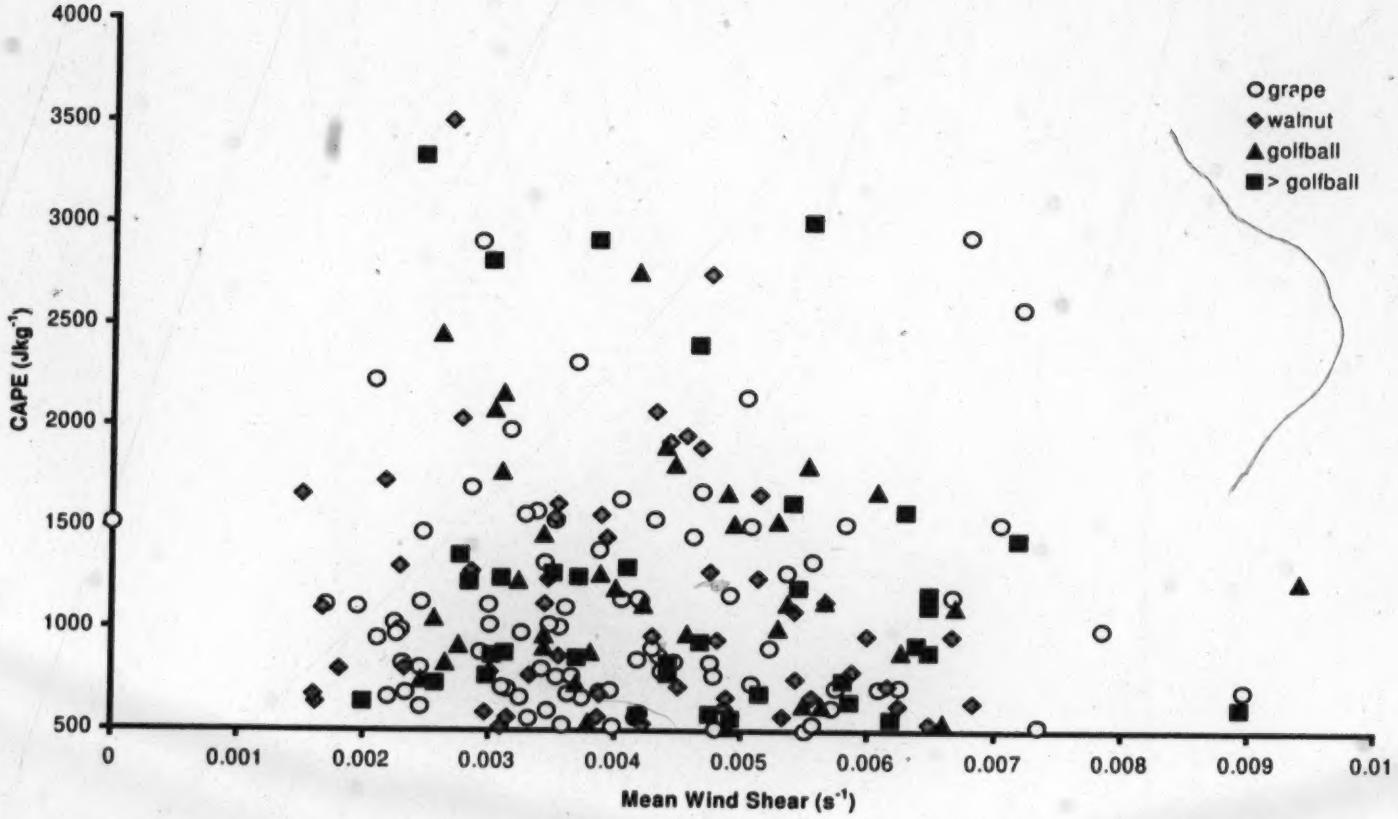

Figure 7.5: Scatter plot of CAPE and mean wind shear for each hail size category for severe hail days (1 June to 31 August) with CAPE ≥ 500 Jkg^{-1} for the years 1966 to 1985.

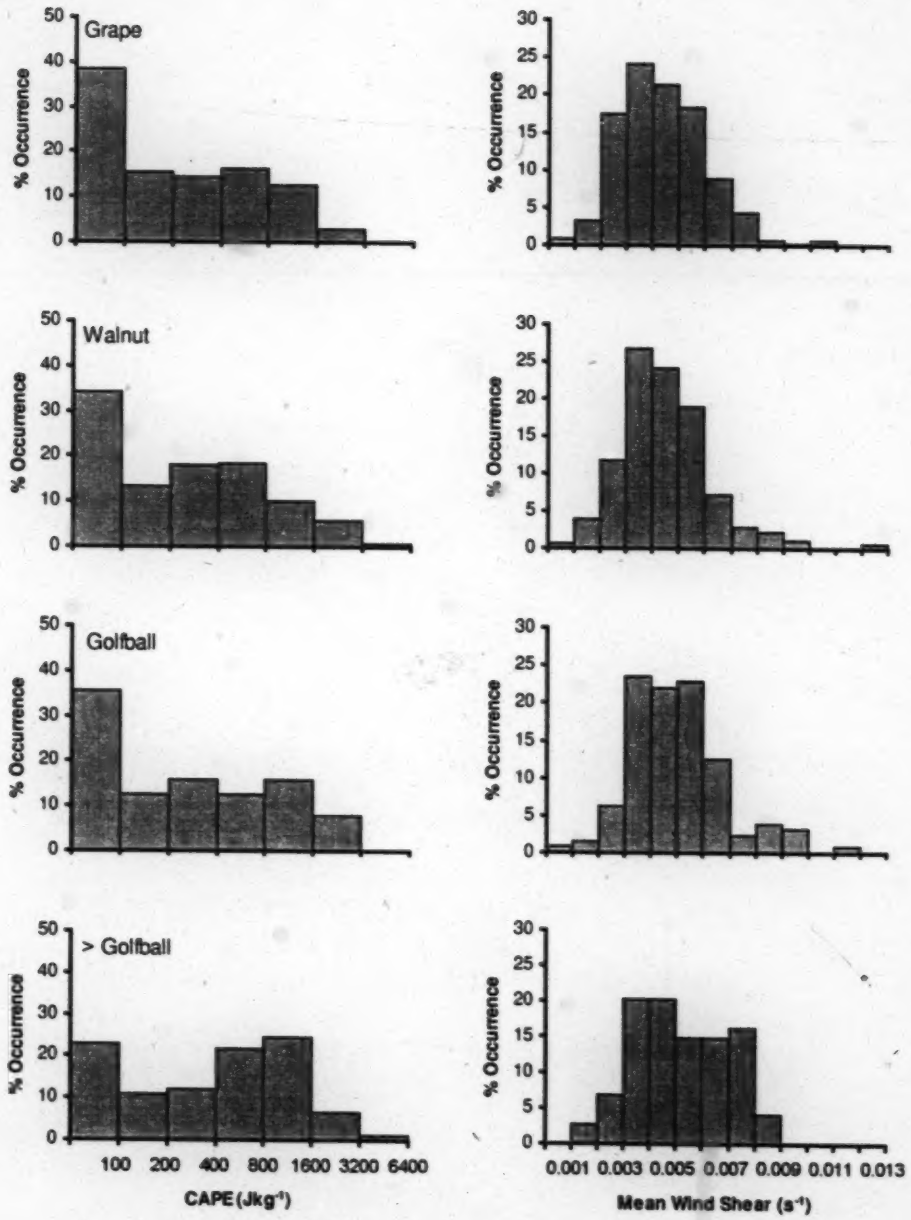

Figure 7.6: Histogram distributions of CAPE (Left column) and mean wind shear (Right column) for each severe maximum hail size category as indicated on the CAPE histograms. The data is from the Alberta Hail Project from 1 June to 31 August for the years 1966 to 1985.

Table 5.6: Evaluation statistics for detection of Large Hail (LH) days using CAPE and Precipitable Water (PW) thresholds.

PW (mm)	CAPE (Jkg^{-1})	SH	LH	HIT	MISS	FAIL	POD %	FAR %	CSI %
16	>500	14	29	29	25	14	54	33	43
	>750	7	24	24	30	7	44	23	39
	>1000	6	18	18	36	6	33	25	30
	>1250	3	15	15	39	3	28	17	26
	>1500	2	12	12	41	2	23	14	22
18	>500	12	26	26	28	12	48	32	39
	>750	7	21	21	33	7	39	25	34
	>1000	6	17	17	37	6	31	26	28
	>1250	3	14	14	40	3	26	18	25
	>1500	2	11	11	42	2	21	15	20
20	>500	10	19	19	35	10	35	34	30
	>750	6	17	17	37	6	31	26	28
	>1000	6	14	14	40	6	26	30	23
	>1250	3	13	13	41	3	24	19	23
	>1500	2	10	10	43	2	19	17	18
22	>500	8	16	16	38	8	30	33	26
	>750	6	14	14	40	6	26	30	23
	>1000	6	11	11	43	6	20	35	18
	>1250	3	10	10	44	3	19	23	18
	>1500	2	7	7	46	2	13	22	13
24	>500	4	6	6	47	4	11	40	11
	>750	3	5	5	48	3	9	38	9
	>1000	3	4	4	49	3	8	43	7
	>1250	1	3	3	50	1	6	25	6
	>1500	1	1	1	52	1	2	50	2
26	>500	1	3	3	50	1	6	25	6
	>750	0	3	3	50	0	6	0	6
	>1000	0	3	3	50	0	6	0	6
	>1250	0	3	3	50	0	6	0	6
	>1500	0	1	1	52	0	2	0	2

Table 5.7: Evaluation statistics for detection of Large Hail (LH) days using CAPE, Precipitable Water (PW), and wind shear (S) thresholds.

Shear (s^{-1})	PW (mm)	CAPE (Jkg^{-1})	SH	LH	HIT	MISS	FAIL	POD %	FAR %	CSI %
0.003	16	>500	12	26	26	27	12	49	32	40
		>750	7	23	23	30	7	43	23	38
		>1000	6	17	17	36	6	32	26	29
		>1250	3	14	14	39	3	26	18	25
		>1500	2	12	12	41	2	23	14	22
	18	>500	11	23	23	30	11	43	32	36
		>750	7	20	20	33	7	38	26	33
		>1000	6	16	16	37	6	30	27	27
		>1250	3	13	13	40	3	25	19	23
		>1500	2	11	11	42	2	21	15	20
0.004	16	>500	10	21	21	32	10	40	32	33
		>750	5	19	19	34	5	36	21	33
		>1000	5	15	15	38	5	28	25	26
		>1250	2	12	12	41	2	23	14	22
		>1500	2	10	10	43	2	19	17	18
	18	>500	9	20	20	33	9	38	31	32
		>750	5	18	18	35	5	34	22	31
		>1000	5	15	15	38	5	28	25	26
		>1250	2	12	12	41	2	23	14	22
		>1500	2	10	10	43	2	19	17	18
0.005	16	>500	6	14	14	39	6	26	30	24
		>750	2	13	13	40	2	25	13	24
		>1000	2	10	10	43	2	19	17	18
		>1250	1	9	9	44	1	17	10	17
		>1500	1	7	7	46	1	13	13	13
	18	>500	6	14	14	39	6	26	30	24
		>750	2	13	13	40	2	25	13	24
		>1000	2	10	10	43	2	19	17	18
		>1250	1	9	9	44	1	17	10	17
		>1500	1	7	7	46	1	13	13	13
0.006	16	>500	1	8	8	45	1	15	11	15
		>750	0	7	7	46	0	13	0	13
		>1000	0	6	6	47	0	11	0	11
		>1250	0	6	6	47	0	11	0	11
		>1500	0	4	4	49	0	8	0	8
	18	>500	1	8	8	45	1	15	11	15
		>750	0	7	7	46	0	13	0	13
		>1000	0	6	6	47	0	11	0	11
		>1250	0	6	6	47	0	11	0	11
		>1500	0	4	4	49	0	8	0	8